Title

Identification of Proteins Responsible for Rapid Displacement of Cas9 from DNA

Author

Wang, Alan Shyijong

Publication Date

2020

Peer reviewed|Thesis/dissertation

Identification of Proteins Responsible for Rapid Displacement of Cas9 from DNA

By

Alan S Wang

A dissertation submitted in partial satisfaction of the

requirements for the degree of

Doctor of Philosophy

in

Molecular and Cell Biology

in the

Graduate Division

of the

University of California, Berkeley

Committee in charge:

Professor Jacob Corn, Co-Chair
Professor John Dueber, Co-Chair
Professor Kathleen Ryan
Professor Xavier Darzacq
Professor Douglas Koshland

Summer 2020

Abstract

Identification of Proteins Responsible for Rapid Displacement of Cas9 from DNA

by

Alan S Wang

Doctor of Philosophy in Molecular and Cell Biology

University of California, Berkeley

Professor Jacob Corn, Co-Chair

Professor John Dueber, Co-Chair

Cas9 is a prokaryotic RNA-guided DNA endonuclease that binds substrates tightly *in vitro* but turns over rapidly when used to manipulate genomes in eukaryotic cells. Little is known about the factors that physically interact with or dislodge Cas9 from DNA and how these factors might influence genome engineering tools. I first attempted to identify Cas9 displacement factors by repurposing Cas9 as a proximity sensor in live human cells. In order to reduce the noise derived from unbound Cas9 molecules, I subsequently used cell-free *Xenopus laevis* egg extract whose lack of a plasma membrane allowed me to tightly control the ratio of Cas9 to its substrate. Label-free proteomics identified the dimeric histone chaperone facilitates chromatin transcription (FACT) as an interactor of substrate-bound Cas9. FACT is both necessary and sufficient to displace dCas9, and FACT immunodepletion converts Cas9's activity from multi-turnover to single-turnover. In human cells, FACT depletion extends dCas9 residence times, delays genome editing, and alters the balance between indel formation and homology directed repair. FACT knockdown also increases epigenetic marking by dCas9-based transcriptional effectors with a concomitant enhancement of transcriptional modulation. FACT thus shapes the intrinsic cellular response to Cas9-based genome manipulation most likely by determining Cas9 residence times.

Table of Contents

List of Figures

List of Tables

Acknowledgements

This dissertation would not have been possible without contributions from so many people to whom I am deeply indebted. To my advisor Jacob Corn – I would like to thank you for your mentorship throughout my entire graduate school career. I was thrilled to join your lab because you pushed me to think critically about the logic underlying my experiments and provided me the intellectual space to grow as a scientist. The ingenuity behind your many suggestions and your wealth of ideas undoubtedly expanded my own thinking.

To my lab mates – I struggle to imagine this experience with any other group of people. I will not forget all the coffee breaks, bubble tea excursions, and happy hours that were such an integral part of lab life. I am extremely fortunate to have had Chris Richardson as my rotation mentor in the Corn lab. To Chris – your advice during and after my rotation proved critical in me finally shaping a coherent project. Your wonderful words of wisdom – in science and life – allowed me to step back and view my struggles and successes with the proper context. To all the postdoctoral scholars Jenny Shin, Amos Liang, Beeke Wienert, Shaheen Kabir, Nicolas Bray, Pei-Chun Lin, Mark DeWitt, Rachel Valenzuela, and Benjamin Gowen – your invaluable scientific expertise, calming influence, and willingness to listen helped establish an incredible support system for all the graduate students. Often times, I could not help but admire what you all were accomplishing in and outside of lab. To my fellow graduate students Emily Lingeman and Mandy Boontanrart – your friendship and emotional support helped prop me up on more occasions that I can count. Emily, we survived as tributes! Mandy, I could not be happier you're living your best life in Switzerland! To all the lab's staff members Ron Baik, Katelynn Kazane, Gemma Curie, Jonathan Vu, Stacia Wyman, Julia Chu, and Hong Ma – you all made lab life so much more vibrant and enjoyable.

Several other labs were instrumental in my dissertation. Alex Wu and Johannes Walter taught me how to handle "frog juice." Yvonne Hao, David McSwiggen, Alec Heckert, and Xavier Darzacq were critical in completing the final experiments needed to push my project past the finish line. I would also like to thank John Dueber and the entire Dueber lab for providing a welcoming environment for me in my final two years to finish my project. Joining the lab exposed me to whole new fields of scientific research and helped me forge new friendships.

I would finally like to thank my family for their unconditional support and love throughout graduate school. My parents and brother provided unyielding encouragement and delicious food for which I will always be grateful.

Chapter 1: Introduction to CRISPR-Cas Systems and Cas9 Displacement

1.1 CRISPR-Cas Systems

Clustered Regularly Interspaced Short Palindromic Repeats (CRISPR)/CRISPR-associated (Cas) systems provide many bacteria and archaea adaptive immunity against phage infection (Barrangou et al., 2007; Brouns et al., 2008; Doudna and Charpentier, 2014; Knott and Doudna, 2018; Makarova et al., 2006; Marraffini and Sontheimer, 2008). Microbes first capture and then integrate short viral DNA fragments called protospacers as new spacer sequences into their CRISPR loci, thereby producing a genetic record of past infections (Barrangou et al., 2007; Bolotin et al., 2005; Brouns et al., 2008; Haft et al., 2005; Ishino et al., 1987; Jansen et al., 2002; Makarova et al., 2006; Marraffini and Sontheimer, 2008; Pourcel et al., 2005). Direct repeat sequences separate the unique spacers within the CRISPR loci (Ishino et al., 1987; Jansen et al., 2002). Transcription of CRISPR arrays produces precursor CRISPR RNAs (pre-crRNAs) that mature into CRISPR RNAs (crRNAs) containing both the repeat and spacer sequences (Brouns et al., 2008; Carte et al., 2010; 2008; Deltcheva et al., 2011; Haurwitz et al., 2010; Marraffini and Sontheimer, 2008). During phage infection, Cas effector proteins bind these crRNAs and cleave foreign nucleic acids containing sequences complementary to the crRNA spacers (Garneau et al., 2010; Hale et al., 2009; Marraffini and Sontheimer, 2008).

CRISPR loci also includes an operon of *cas* genes that code for these Cas effector proteins (Bolotin et al., 2005; Haft et al., 2005; Jansen et al., 2002; Pourcel et al., 2005) CRISPR-Cas systems include the Class 1 multi-subunit effector complexes and the Class 2 single-protein effectors (Koonin et al., 2017; Makarova et al., 2015; Shmakov et al., 2015). These adaptive immune systems can also be classified into six types based on how they provide the Cas nucleases targeting specificity and the architecture of the ribonucleoprotein (RNP) complexes. Class 1 systems include types I, III, and IV while Class 2 systems include types II, V, and VI (Koonin et al., 2017; Makarova et al., 2015; Shmakov et al., 2015).

The most widely used Cas protein is the Class 2 type II *Streptococcus pyogenes* Cas9, which acquires its targeting specificity through its interaction with a crRNA and a trans-activating crRNA (tracrRNA) (Deltcheva et al., 2011). These tracrRNAs contain an anti-repeat sequence with partial complementarity to the direct repeats that allows crRNAs and tracrRNAs to hybridize. The tracrRNAs also contain a set of nucleotides that form a stem-loop structure, which mediates the interaction with Cas9. Upon binding the crRNA-tracrRNA hybrid, Cas9 searches for and cleaves foreign DNA to prevent their propagation. This crRNA-tracrRNA hybrid can crucially be fused into a single guide RNA (gRNA) (Jinek et al., 2012). This two-component system consisting of a single protein and a single easily programmable RNA molecule has been widely deployed for targeted DNA cleavage in a variety of prokaryotic and eukaryotic organisms (Cong et

al., 2013; Doudna and Charpentier, 2014; Jinek et al., 2013; Knott and Doudna, 2018; Mali et al., 2013).

Cas9 RNPs first search for a short sequence downstream of the protospacer called the protospacer adjacent motif (PAM), which is required for stable binding of Cas9 to DNA (Bolotin et al., 2005; Deveau et al., 2008; Marraffini and Sontheimer, 2010; Mojica et al., 2009; Sternberg et al., 2014). The sequences of viral DNA integrated into CRISPR loci do not contain these flanking PAMs to ensure that bacterial genomes are protected from the Cas effector proteins' cleavage activity. To cleave DNA, Cas9 searches for PAMs through a process that involves random collisions with DNA and rapid dissociation from non-PAM sequences (Sternberg et al., 2014). This quick release significantly narrows the amount of DNA Cas9 needs to interrogate before finding its target.

Upon detecting a PAM, Cas9 scans for complementarity between the gRNA's spacer sequence and target DNA's protospacer sequence. Cas9 RNPs specifically first unwind the PAM adjacent sequences before extending the RNA:DNA heteroduplex (Sternberg et al., 2014). These endonucleases can tolerate some mismatches between the spacer and protospacer sequences, but perfect complementarity is typically required for the seed region that comprises the PAM-proximal 8-12 nucleotides (Pattanayak et al., 2013; Semenova et al., 2011; Sternberg et al., 2014; Wiedenheft et al., 2011). Upon finding its target, *S. pyogenes* Cas9 unwinds the duplex DNA and uses its RuvC and HNH nuclease domains to make a blunt double-stranded break (DSB) three basepairs upstream of the PAM (5'-NGG-3') (Garneau et al., 2010; Gasiunas et al., 2012; Jinek et al., 2012). The RuvC domain cleaves the non-target strand while the HNH domain cleaves the target DNA strand.

In addition, *S. pyogenes* Cas9 is a modular protein with discrete RNA-binding, DNA-binding, and nuclease domains (Jiang and Doudna, 2017; Jinek et al., 2014; Nishimasu et al., 2014). Introduction of two inactivating point mutations into the two nuclease domains (D10A and H840A) abolishes Cas9's ability to cleave DNA but preserves its capacity to bind a gRNA and target DNA. This catalytically dead Cas9 (dCas9) can act as a functional scaffold to localize different proteins to desired genomic sites without inducing DNA DSBs. For example, fusing transcriptional modulators to dCas9 has enabled the development of CRISPR interference (CRISPRi) and CRISPR activation (CRISPRa) tools in eukaryotic organisms (Gilbert et al., 2014; 2013; Hilton et al., 2015; Konermann et al., 2015a). Fusing fluorescent proteins to dCas9 enabled imaging of genomic loci in live cells (Chen et al., 2013). Other effector proteins allow one to track RNA molecules, identify proteins at genomic loci, and manipulate the three-dimensional architecture of nuclei (Gao et al., 2018; Liu et al., 2017; Myers et al., 2018; Nelles et al., 2016; Schmidtmann et al., 2016; Wang et al., 2018).

1.2 Repair of Cas9-Induced DSBs

The use of programmable nucleases for genome editing relies on cells' endogenous repair pathways, which either repair the DSBs with perfect fidelity or introduce genomic mutations. Human cells invoke non-homologous end joining (NHEJ), microhomology-

mediated end joining (MMEJ), or homology directed repair (HDR) to fix these DSBs. While the end joining pathways typically introduce short insertions and deletions (indels), HDR uses templated repair off of a separate DNA molecule to fix the lesion. Although cells occasionally use a homologous chromosome as the repair template, they predominantly rely on a sister chromatid as a template (Stark and Jasin, 2003). Cells can also use exogenously added single-stranded or double-stranded DNA molecules as HDR templates (Pawelczak et al., 2018; Yeh et al., 2019). Given the ability of HDR to introduce desired and potentially therapeutic mutations, many studies have sought to increase levels of HDR while decreasing levels of NHEJ and MMEJ (Pawelczak et al., 2018; Yeh et al., 2019). Cas9's unique interactions with DNA (Richardson et al., 2016b) and the identity of cellular factors that interact with Cas9 itself or Cas9-generated DSBs thus remain an intensive area of investigation (Yeh et al., 2019).

Several factors influence the choice of repair pathways. The end joining pathways do not require a DNA template and are not limited to specific phases of the cell cycle. HDR typically occurs during the late S and G2 phases of the cell cycle during which a sister chromatid is available (Pawelczak et al., 2018; Yeh et al., 2019). The choice of repair pathways also depends on processing of the DSB. HDR involves MRE11-RAD50-NBS1-CtIP, which initiates 5'-3' resection, and additional exonucleases such as EXO1 and DNA2 that extend the resected ends (Garcia et al., 2011; Shibata et al., 2014; Zhu et al., 2008). During canonical homologous recombination with a double-stranded template, cells coat the resected ends with RPA and RAD51, the latter of which mediates homology search and strand invasion (Chen et al., 2018a; Ciccia and Elledge, 2010). Another HDR pathway called single strand annealing uses RAD52 to bind the resected ends and anneal single-stranded homologies (Yeh et al., 2019). HDR using single-stranded templates likely involves annealing of the DNA donor to one of the resected ends and extension from that end using the DNA donor as a template. Annealing of the extended strand to the other broken end, another round of extension, and ligation ultimately resolve the DSB (Yeh et al., 2019). Unlike canonical homologous recombination, HDR with single-stranded templates does not require RAD51 but involves RAD51 paralogs and components of the Fanconi pathway (Bothmer et al., 2017; Richardson et al., 2018).

Unresected or minimally resected ends are thought to undergo end-joining pathways. During NHEJ, KU70 and KU80 bind the broken ends to physically prevents end-resecting enzymes from accessing the DSB (Ciccia and Elledge, 2010; Lieber, 2010). Limited resection after the DSB can expose small homologies that enable MMEJ (Yeh et al., 2019). Recent evidence also indicates that the Fanconi anemia (FA) pathway plays a prominent role in resolving Cas9-generated DSBs and influencing the choice of repair pathway (Richardson et al., 2018). However, the mechanistic roles that FA proteins play in DSB repair are still unclear.

1.3 Influence of Chromatin State on Cas9 Activity

Despite its widespread use in eukaryotic systems for targeted gene editing, Cas9 is a prokaryotic enzyme and thus has never seen histones in evolutionary time (Makarova et

al., 2015). Eukaryotic chromatin is both heterogenous and dynamic (Bernstein et al., 2007). Cells must constantly modify or move histones in order to allow proteins such as transcription factors, polymerases, helicases, and topoisomerase to physically interact with the DNA. Moreover, histone and higher order chromatin structures are responsible for the dense packaging of DNA that makes stretches of the genome largely inaccessible to many DNA-binding proteins. A growing body of evidence suggests that chromatin state plays a crucial role in shaping Cas9's activity (Verkuijl and Rots, 2019).

Chromatin immunoprecipitation sequencing (ChIP-Seq) of dCas9 found that chromatin accessibility is a strong indicator of dCas9 residence (Kuscu et al., 2014; O'Geen et al., 2015; Wu et al., 2014). These studies revealed that DNA hypersensitivity and protein-coding gene sequences were positively correlated with dCas9 binding while CpG methylation was negatively correlated with dCas9 binding (Kuscu et al., 2014; O'Geen et al., 2015; Wu et al., 2014). An analysis of dCas9-based genetic screens indicated that the most active gRNAs for CRISPRi bound regions with lower levels of nucleosome occupancy as measured through micrococcal nuclease-sequencing (Horlbeck et al., 2016b). Single-molecule imaging studies of Cas9 in mammalian cells similarly demonstrated that dCas9 much more readily interrogates DNA in euchromatic versus heterochromatic regions (Knight et al., 2015). This sensitivity to chromatin state may explain why several gRNAs that enable efficient editing *in vitro* do not enable efficient editing *in vivo* (Uusi-Makela et al., 2018). Chromatin state may also account for the fact that many gRNAs allow Cas9 to edit sites with mismatches more efficiently than sites that are perfectly matched (Frock et al., 2015; Tsai et al., 2015).

Several *in vitro* studies have corroborated the inhibitory effects of nucleosomes on Cas9's activity (Hinz et al., 2015; Horlbeck et al., 2016b; Isaac et al., 2016; Yarrington et al., 2018). These cell-free assays notably avoid potentially confounding effects from processes such as splicing, transcriptional pausing, and binding of transcription factors that may correlate with nucleosome occupancy. *In vitro*, nucleosomes sterically inhibit Cas9 from accessing and cleaving the DNA, and the addition of recombinant chromatin remodelers significantly increases Cas9 cleavage activity presumably by displacing histones to reveal PAMs and protospacers (Hinz et al., 2015; Horlbeck et al., 2016b; Isaac et al., 2016). One report also indicated that Cas9 can bind the linker sequences between regions directly bound by histones due to transient nucleosome breathing (Hinz et al., 2015).

Several studies indicate that chromatin state also influences Cas9's editing efficiency in live cells. For example, one report using a drug-inducible switch capable of regulating whether a single locus was open or closed demonstrated that silencing the allele inhibited Cas9 binding and cleavage (Daer et al., 2017). Another study took advantage of the differential chromatin states between maternal and paternal alleles arising from genomic imprinting to reveal that heterochromatin significantly impedes Cas9 editing rates for some but not all gRNAs (Fujita et al., 2016). A similar report that also relied on differentially methylated maternal and paternal alleles found that editing was slightly more efficient at the open alleles versus the repressed alleles (Kallimasioti-Pazi et al., 2018). This difference in editing levels between open and closed alleles was much more

pronounced when Cas9 protein levels were relatively low. The authors also noticed that heterochromatin delayed the kinetics of break repair. When Cas9 was present at relatively high levels, over 70% of the eventual set of mutations appeared within 24 hours at euchromatic sites while less than 30% of the eventual set of mutations appeared within the same time for heterochromatic sites. Surprisingly, chromatin state appeared not to influence the choice of repair pathway (Kallimasioti-Pazi et al., 2018). These results stand in contrast to many studies that have shown that local chromatin environments shape how cells engage DSB repair pathways (Aymard et al., 2014; Burman et al., 2015; Clouaire and Legube, 2015; Goodarzi et al., 2010; Lemaitre et al., 2014). However, this lack of difference could be due to the ability of Cas9 binding itself to increase chromatin accessibility (Barkal et al., 2016) and overcome any former differences in chromatin state.

1.4 *S. pyogenes* Cas9 Has a Stable Enzyme-Product State *in Vitro* but is Rapidly Displaced from DNA in Live Cells

S. pyogenes Cas9 is notable not only for its ability to efficiently edit eukaryotic genomes despite its prokaryotic origins but also for its remarkably stable enzyme-product state. Measurements of Cas9 binding *in vitro* using bio-layer interferometry indicate that Cas9 has residence times of roughly 5.5 hours (Richardson et al., 2016b). The catalytically inactive dCas9 has similar residence times, indicating that the DSB is not the critical factor determining Cas9 residence times (Richardson et al., 2016b). Total internal reflection fluorescence microscopy of Cas9 bound to DNA curtains revealed that even 0.5 M NaCl or 10 μg/ml heparin was insufficient to dislodge Cas9. Removal of Cas9 required extremely harsh chemical treatment of either 7 M urea or 2% SDS (Sternberg et al., 2014). In addition, a detailed kinetic analysis of Cas9 RNP formation, target binding, DNA cleavage, and product release using Förster resonance energy transfer revealed that the rate-limiting step in this process was by far Cas9's release from its product (Raper et al., 2018). Cas9 was able to generate a slow but linear increase in the amount of cleaved DNA In the presence of excess substrate (Raper et al., 2018). This continuous increase indicates that Cas9 is a multi-turnover enzyme whose activity on a second substrate is limited by its slow release rate. It is currently unclear how Cas9's stable enzyme-product state influences how cells engage and choose among different DSB repair pathways.

Cas9's stable enzyme-product state *in vitro* contrasts sharply with that of restriction enzymes, which also protect bacteria from viruses. Restriction enzymes undergo a process that involves substrate binding, target recognition, catalysis, and product release. After DNA cleavage, these enzymes either immediately dissociate from their product or localize to a non-specific site on the same DNA molecule before release (Pingoud and Jeltsch, 2001). Although the final step is typically the slowest step for the majority of the commonly used type II restriction enzymes, these proteins still release themselves from their products within seconds without external assistance (Joshi et al., 2006; Pingoud and Jeltsch, 2001; Robinson and Sligar, 1998).

Cas9's stable enzyme-product state *in vitro* also contrasts sharply with its much more rapid release in live cells. Editing can be detected only one hour after electroporation of Cas9 RNPs into human cells (Kim et al., 2014). NHEJ, which is significantly faster than HDR, still requires at least 30 minutes to occur (Mao et al., 2008). Cas9 thus finds its target, cleaves the DNA, and dissociates from the genome within 30 minutes. These times frames suggest that cellular factors within eukaryotic cells are capable of rapidly displacing Cas9 from the genome, but the identities of these proteins and their potential influence on DSB repair pathways remain ambiguous.

1.5 Factors Capable of Displacing Cas9

A prior study suggests that RNA polymerases can displace Cas9 from DNA (Clarke et al., 2018). The authors first conducted an *in silico* analysis of a prior dataset (Chari et al., 2015) that measured the efficacy of Cas9 when it was targeted to roughly 1400 loci. They found that higher mutation rates were positively correlated with transcription levels. Cas9 programmed with coding-strand gRNAs displayed no significant difference in editing rates between transcriptionally silent and transcriptionally active sites. However, Cas9 programmed with non-coding strand gRNAs was much more efficient at editing sites in transcriptionally active regions. *In vitro* experiments revealed that T7 Polymerase and RNA Polymerase II can dislodge Cas9 more effectively when Cas9 was programmed with a non-coding strand gRNA versus a coding-strand gRNA. This dislodged Cas9 could then cleave second DNA molecule. In live mammalian cells, Cas9 programmed with non-coding strand gRNAs edited sites somewhat more effectively than Cas9 programmed with coding-strand gRNAs. The authors claimed that this difference is due to the ability of RNA polymerases to rapidly displace Cas9 and expose the free ends to DNA repair proteins, thereby increasing overall rates of error-prone DNA repair pathways (Clarke et al., 2018).

However, this supposed strand bias cannot account for several reported differences in Cas9 editing rates (Verkuijl and Rots, 2019). For example, one study that took advantage of differences in chromatin states between maternal and paternal alleles found that the only gRNA responsible for a marked difference in editing rates between the maternal and paternal alleles bound the coding-strand and thus should be immune from the presumed Cas9-displacing ability of translocating RNA polymerases (Fujita et al., 2016). Two other gRNAs, one of which bound to the coding strand and one of which bound to the non-coding strand, showed no difference in Cas9 binding levels or editing efficiencies between the open and closed alleles.

Several additional lines of evidence suggest factors beyond polymerases are responsible for displacing Cas9. Cas9 can effectively edit many transcriptionally silent sites, indicating that DNA metabolic processes besides transcription are responsible for Cas9 eviction. In addition, the doubling time of many immortalized cell types in culture is roughly 24 hours yet Cas9-induced genomic edits can be detected one hour after electroporation of Cas9 RNPs (Kim et al., 2014). Replicative DNA polymerases thus cannot be solely responsible for Cas9 displacement. Cas9's ability to edit cells that no

longer undergo mitosis similarly suggests that factors besides replicative DNA polymerases displace Cas9 (Nishiyama et al., 2017; Suzuki et al., 2016).

1.6 Proximity Labeling in Live Eukaryotic Cells

Probing interactions between the eukaryotic cellular machinery and Cas9 would potentially reveal factors responsible for displacing Cas9. Several groups have already deployed a variety of strategies to use Cas9 to probe locus-specific protein composition. Although these tools were not designed specifically to identity Cas9 displacement factors, they may still provide insight into the displacement process.

One approach centers on a using a biotinylated dCas9 to isolate a specific genomic site and bound proteins (Liu et al., 2017). Streptavidin pulldown of dCas9 targeted to both repetitive and non-repetitive loci captured DNA and associated proteins. However, this strategy relies on chemical crosslinking and will fail to capture transient interactors. Other efforts involve fusing dCas9 to either the promiscuous biotin ligase BirA* (Arg118Gly) or the engineered pea ascorbate peroxidase APEX. BirA* generates a reactive biotin molecule that covalently attaches itself onto exposed lysine residues of nearby proteins (Roux et al., 2013; 2012). BirA*'s biotin incubation can occur over the course of several hours and thereby allow a system to accumulate biotinylated versions of even the most transiently interacting proteins. APEX uses hydrogen peroxide and biotin-phenol to likewise biotinylate nearby proteins (Lam et al., 2015; Martell et al., 2012). These marked proteins can subsequently be isolated through a streptavidin pulldown and identified through mass spectrometry.

Unfortunately, expressing dCas9 fused to BirA* or APEX in live cells generates a significant degree of background biotinylation. Cas9 expression systems typically introduce several orders of magnitude more RNPs into cells than available binding spots, and BirA* and APEX are catalytically active even when dCas9 is unbound to its target. Attempts to circumvent these signal-to-noise issues by targeting Cas9 to only highly repetitive regions such as telomeres and centromeres risk disregarding interactions beyond such specialized regions and limit the utility of these tools (Gao et al., 2018; Qiu et al., 2019; Schmidtmann et al., 2016). Efforts to capture protein-DNA interactions at non-repetitive sequence by simultaneously expressing multiple gRNAs still suffer from significant background biotinylation and capture only the most abundant proteins (Myers et al., 2018).

1.7 Cell-Free Systems Can Dissect Nuclear Dynamics

The primary obstacle to identifying interactors of substrate-bound Cas9 is the noise derived from interactors of unbound Cas9 molecules. *In vitro* cell-free systems lack of a physical barrier, and the open nature of these systems allows addition of exogenous molecules at desired concentrations and stoichiometries. Cas9 RNPs and DNA substrates can thus be introduced at specific ratios to ensure that every single Cas9 molecule has an available binding site.

These cell-free systems must faithfully recapitulate processes that occurs in live cells. However, preparing these cell-free systems typically requires detergents that disrupt the plasma membrane, break apart the intracellular architecture, enable mixing of different compartments, and threaten the solubility and integrity of proteins. Preparing cell-free systems can also change the systems' ionic aqueous environments, which must remain suitable for crucial protein-protein interactions and chemical reactions to occur. As a result, there are only a select number of extract systems appropriate for studying any given process.

The African clawed frog *Xenopus laevis* has a close evolutionary relationship with humans, and cell-free extracts derived from their eggs have become powerful tools to interrogate nuclear dynamics and DNA metabolism (Blow and Laskey, 2016; Hoogenboom et al., 2017; Lebofsky et al., 2009). Preparation of *Xenopus* egg extracts fortunately does not require harsh detergents that could potentially inhibit protein activity. Disrupting the plasma membrane to lyse the cells requires spinning mature eggs at 100000g to produce a cytoplasmic extract containing membranes called low speed supernatant (LSS) (Hoogenboom et al., 2017; Lebofsky et al., 2009). Centrifuging these samples with an additional spin at 260000g removes membranes to produce high speed supernatant (HSS) (Hoogenboom et al., 2017; Lebofsky et al., 2009).

These two types of *Xenopus* extracts have been used to study a number of processes such as mitosis, nuclear assembly, nuclear import, membrane trafficking, and apoptosis. Moreover, these extracts are currently the only cell-free system capable of replicating DNA and have become valuable tools for interrogating DNA synthesis (Almouzni and Wolffe, 1993; Arias and Walter, 2004; Blow, 2001). While LSS is capable of promoting a single round of DNA replication upon addition of sperm chromatin, HSS requires addition of a nucleoplasmic extract (NPE) and ATP to initiate a complete round of DNA replication (Hoogenboom et al., 2017; Lebofsky et al., 2009).

Both LSS and HSS are also efficient at conducting DNA repair (Cupello et al., 2016). These cell-free systems possess all the factors necessary to efficiently perform mismatch repair, NHEJ, and inter-strand crosslink repair. *Xenopus* extracts can also respond to replication stress. Addition of aphidicoidin, which stalls replication forks, triggers phosphorylation of CHK1 and has facilitated investigation of the ATR-CHK1 pathway (Cupello et al., 2016; Michael et al., 2000; Van et al., 2010). *Xenopus* extracts have also proved useful in interrogating signaling through the ATM kinase (Costanzo et al., 2004; Hoogenboom et al., 2017).

In addition, *X. laevis* extracts can efficiently promote nucleosome assembly (Blow and Laskey, 2016; Earnshaw et al., 1980; Laskey et al., 1978; 1977). These extracts contain the protein nucleoplasmin, which is a histone chaperone that directs assembly of nucleosome cores (Earnshaw et al., 1980; Laskey et al., 1977; 1978). Given the potential role of chromatin in shaping Cas9-DNA interactions, the ability of these extracts to chromatinize DNA may be critical in dissecting interactions between Cas9 and chromatin-modifying proteins.

1.8 Identification of Cas9 Displacement Factors

Here, we take multiple strategies to identify eukaryotic factors responsible for rapid displacement of Cas9 from DNA. We first target BirA*-dCas9 to the repetitive centromeric repeats within live human cells to capture interactors of DNA-bound Cas9. In order to reduce the noise from unbound Cas9 molecules and enable identification of proteins at non-repetitive sequences, we then split BirA* into two inactive halves and fused each half onto two separate dCas9 molecules. We attempted to assemble the BirA* halves into a catalytically active enzyme by targeting the dCas9 fusion proteins in close proximity to one another.

We next used *X. laevis* HSS to identify Cas9 displacement factors. Addition of DNA and recombinant Cas9-BirA* or dCas9-BirA* RNPs at desired ratios enabled an unbiased proteomics strategy that identified the dimeric histone chaperone facilitates chromatin transcription (FACT) as an interactor of substrate-bound Cas9. FACT is both necessary and sufficient to displace Cas9 *in vitro*. In human cells, FACT depletion enhanced dCas9 residence times, altered Cas9 editing outcomes, and increased the potency of dCas9-based transcriptional effectors. These results reveal that the eukaryotic machinery can functionally interact with the prokaryotic Cas9 and plays a critical role in shaping Cas9-based interventions.

Chapter 2: Identification of Proteins at Genomic Loci

2.1 Connection to Overall Dissertation

Cas9 is widely used to edit eukaryotic genomes, but little is known about the factors that physically interact with genome-bound Cas9 and how these factors shape Cas9's interaction with DNA. In order to identity interactors of Cas9 in live cells, we engineered multiple dCas9-proximity sensors and deployed them to both repetitive and non-repetitive sequences. These proximity sensors would not only provide a tool to identify proteins at genomic loci but also potentially uncover interactions between the eukaryotic machinery and Cas9 responsible for rapid displacement of Cas9 from DNA.

2.2 Introduction

Protein-DNA interactions are critical for regulating a variety of fundamental processes, including transcription, replication, recombination, and DNA repair. Proteins are also responsible for packaging DNA and shaping the three-dimensional architecture of chromosomes within nuclei. Several assays are currently available to interrogate these protein-DNA interactions.

ChIP involves first crosslinking proteins to DNA and then using an antibody to isolate a protein of interest and the genomic sites it binds. ChIP thus requires *a priori* knowledge of the target protein's identity and an antibody with a sufficiently high affinity. Electrophoretic mobility shift assays (EMSAs) provide a readout of the degree of affinity between a protein and a DNA sequence and the specificity of these protein-DNA interactions *in vitro*. EMSAs take advantage of the fact that DNA bound by proteins migrates through a gel more slowly than free DNA molecules. *In vitro* DNA footprinting assays assess the sequence specificity of DNA-binding proteins by taking advantage of the inability of a non-specific DNase to access DNA already bound by a protein.

Several studies have also reported different strategies to identify proteins at genomic loci in live cells. One approach relies on formaldehyde to stabilize protein-DNA interactions and a biotinylated locked nucleic acid probe to isolate a specific sequence and any bound proteins (Dejardin and Kingston, 2009). Such a strategy crucially relies on crosslinking, which cannot capture transient protein-protein interactions. This study also targeted the highly repetitive telomeric repeats yet still required three billion cells to generate a detectable level of peptides for mass spectrometry. These limitations have likely prevented this tool from being applied to non-repetitive sequences.

Attempts to interrogate locus-specific protein composition at a single site required first inserting a LexA, LacI, or TetR-binding sequence into a genomic locus (Byrum et al., 2012; Fujita and Fujii, 2011; Hoshino and Fujii, 2009; McCullagh et al., 2010; Pourfarzad et al., 2013). Expression of LexA, LacI, or TetR fused to an affinity tag or fluorescent protein followed by chemical crosslinking allowed immunoprecipitation of the integrated binding site using antibodies against the fused affinity tag or fluorescent protein. Any bound proteins could then be identified through mass spectrometry.

However, these techniques involve arduous engineering of cell lines to stably integrate LexA, LacI, or TetR-binding sequences at desired loci.

Other groups have taken advantage of the ability of programmable nucleases to bind to specific genomic sites. Directly immunoprecipitating tagged versions of dCas9 or transcription activator-like effector nucleases (TALENs) enabled isolation of the target site as well as any bound proteins (Fujita and Fujii, 2013; Fujita et al., 2013; Waldrip et al., 2014). A similar approach involves directly biotinylating dCas9 in live cells and using streptavidin beads to isolate dCas9, bound DNA, and associated proteins (Liu et al., 2017). This strategy takes advantage of the high affinity between biotin and streptavidin to permit harsher wash conditions to decrease noise. However, these techniques still suffer from a significant amount of background biotinylation due to unbound dCas9 or TALENs. All of these techniques also involve chemical crosslinking, which can capture only relatively stable protein-DNA interactions.

Additional strategies involve fusing dCas9 to either BirA* or APEX (Gao et al., 2018; Lam et al., 2015; Martell et al., 2012; Myers et al., 2018; Roux et al., 2012). Both of these enzymes biotinylate nearby proteins for subsequent isolation and identification. The BirA* system in particular does not require any toxic chemicals and can thus tolerate extended incubation times that allows cells to accumulate tagged versions of even transient interactors. Unfortunately, a significant amount of noise derived from unbound dCas9 molecules obscures identification of proteins at unique loci.

Here, we first express BirA*-dCas9 in live human cells and target this fusion protein to the highly repetitive centromeric repeats to optimize this technique. In order to reduce the noise from unbound dCas9 molecules, we next engineered a split BirA* and fused complementary halves to dCas9. We targeted these fusion molecules in close proximity in an attempt to drive assembly of the split BirA* into a catalytically active enzyme only at a single genomic site.

2.3 Results

2.3.1 Identification of Proteins at Repetitive Sequences

To develop and validate a dCas9-based proximity sensor in live human cells, we expressed and targeted BirA*-dCas9 to human centromeres. Human centromeres comprise roughly 5% of the human genome, spanning anywhere between 250 and 5000 kilo basepairs (Aldrup-Macdonald and Sullivan, 2014). The primary alpha satellite repeat is 171 bp, but the DNA sequence is often heterogeneous even within the same organism. Despite these sequence differences, the set of proteins that localize to centromeres is very consistent and well-established (Aldrup-Macdonald and Sullivan, 2014). We chose to target BirA*-dCas9 to centromeric repeats because the repetitive nature of this genomic region allows multiple dCas9 molecules to bind simultaneously, thereby increasing the signal to noise ratio.

The proteomics enrichment data set revealed several sets of factors that were preferentially enriched when dCas9 was targeted to the centromeric repeats (Figure 1). Relative to cells without a gRNA, cells expressing the centromere-targeting gRNA were enriched in proteins involved in centromere assembly and maintenance (CENPV, INCENP, and CENPF) and sister chromatid cohesion (SMC3, STAG2, SMC1A, PDS5, NIPBL, RAD21, PDS5A, STAG1, CDCA5, and MAU2). Cells expressing the centromere-targeting gRNA were also enriched in proteins that play crucial roles in DNA repair (PRKDC, XRCC5, RAD50, MDC1, XPC, XRCC6, and MRE11A) and DNA replication (MCM2, MCM7, MCM2, MCM5, MCM6, and MCM3). We also notably detected factors involved in chromatin remodeling (CHD4, BAZ1B, BPTF, CHD7, CHAF1A, CHD2, SRCAP, CHD6, CHD5, CHD3, CHD8, CHD1, CHD9, SMARCA5, and SMARCD1). Given their roles in displacing and reorganizing histones, these chromatin remodeling proteins may also be capable of displacing Cas9. These results indicate that BirA*-dCas9 can effectively biotinylate proteins at repetitive loci in live human cells with a signal to noise ratio that is sufficiently high for their enrichment to be detected through mass spectrometry.

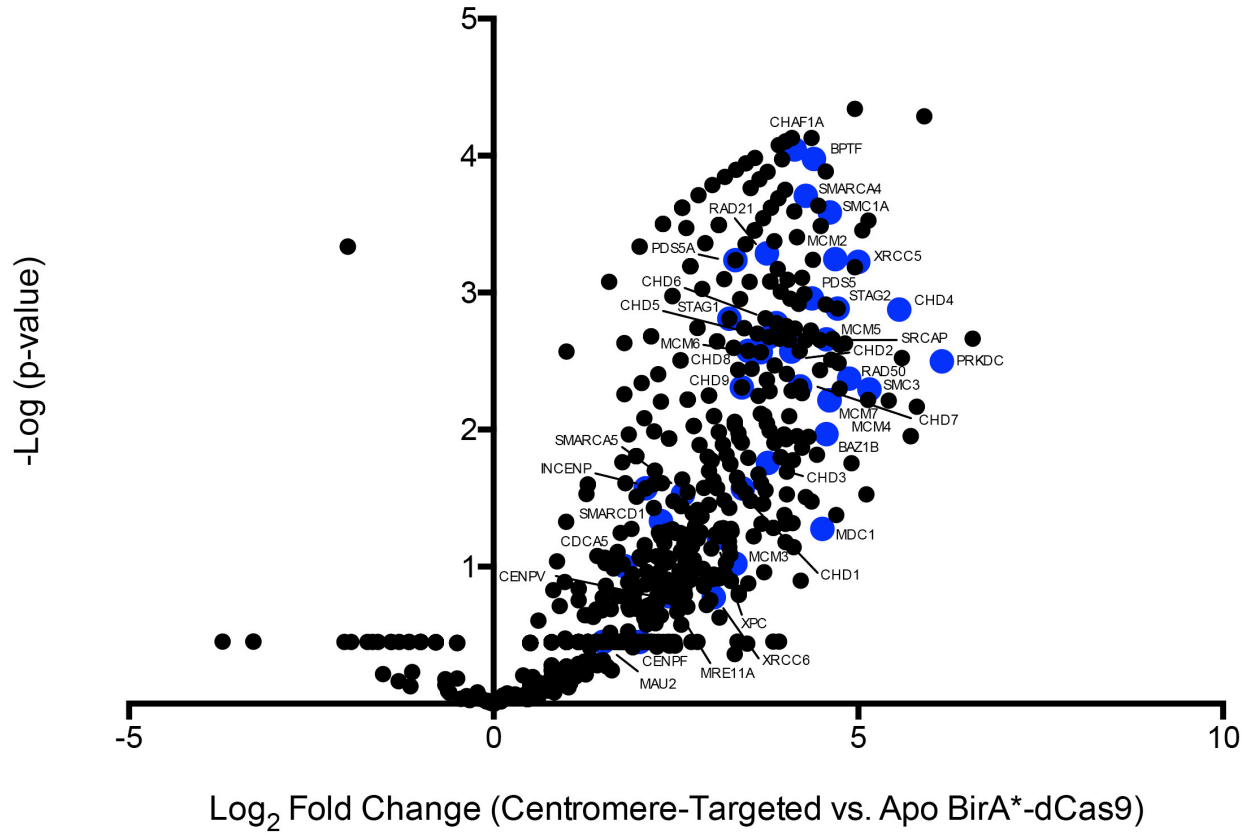

Figure 1: Identification of Proteins at Centromeres Using BirA*-dCas9
Volcano plot of biotinylated proteins in BirA*-dCas9-centromere gRNA samples (n = 2 biological replicates) versus apo BirA*-dCas9 samples (n = 2 biological replicates).

2.3.2 Design of a Split BirA*

Targeting BirA*-dCas9 to highly repetitive alpha repeats allowed multiple BirA*-dCas9 molecules to simultaneously bind the genome. However, even these conditions produced a significant amount of background biotinylation from free BirA*-dCas9 molecules. Identifying proteins at single loci cells thus requires a strategy to significantly reduce this background biotinylation. We therefore engineered a split BirA* whose two halves are inactive in isolation but assemble into a catalytically active enzyme when brought into close proximity.

Prior split systems typically cut a protein at a flexible site that separates well-defined secondary structures (Romei and Boxer, 2019). The X-ray crystallography structure of BirA (PDB: 1HXD) omits a short stretch of amino acids presumably because that region of the protein was too flexible to be crystallized (Weaver et al., 2001). We thus split the protein at this site (residues 215/216). In order to determine whether this cut site would produce two inactive peptides that reconstitute into a catalytically active enzyme when brought into close proximity, we fused the complementary halves of BirA* onto complementary halves of split GFP. Split GFP fragments readily reassemble and have been widely used to drive protein-protein interactions (Romei and Boxer, 2019).

In contrast to full-length BirA*, each split BirA* fragment on its own did not generate any detectable biotinylation of itself or other proteins (Figure 2). Fusing the split GFP tether to only one of the split BirA* fragments also failed to reconstitute a catalytically active BirA* enzyme. However, fusing both split BirA* fragments to the split GFP tether generated a detectable auto-biotinylation signal, which indicates that the split BirA* assembled into an active enzyme. Given how full-length BirA* can generate a high degree of biotinylation, we also developed split BirA* mutants with reduced activity. We screened through a series of alanine mutants of residues that lie at the interface of the two halves. Introduction of these point mutations reduce the amount of auto-biotinylation to varying degrees (Figure 2).

2.3.3 Attempts to Identify Proteins at Non-Repetitive Loci

We next fused the split BirA* halves onto dCas9 with the flexible XTEN linker used to fuse FokI monomers to dCas9 (Guilinger et al., 2014). We targeted these split BirA*-dCas9 constructs to a site several dozen basepairs downstream of the *ACTB* TATA box containing conveniently placed PAMs that separated pairs of gRNAs by either 14, 15, or 16 basepairs. Biotinylated proteins were isolated through a streptavidin pulldown and identified through mass spectrometry (Figures 3-5). For all three pairs of gRNAs, we did not detect significant enrichment of any factors that are known localize to the TATA box of a highly expressed gene.

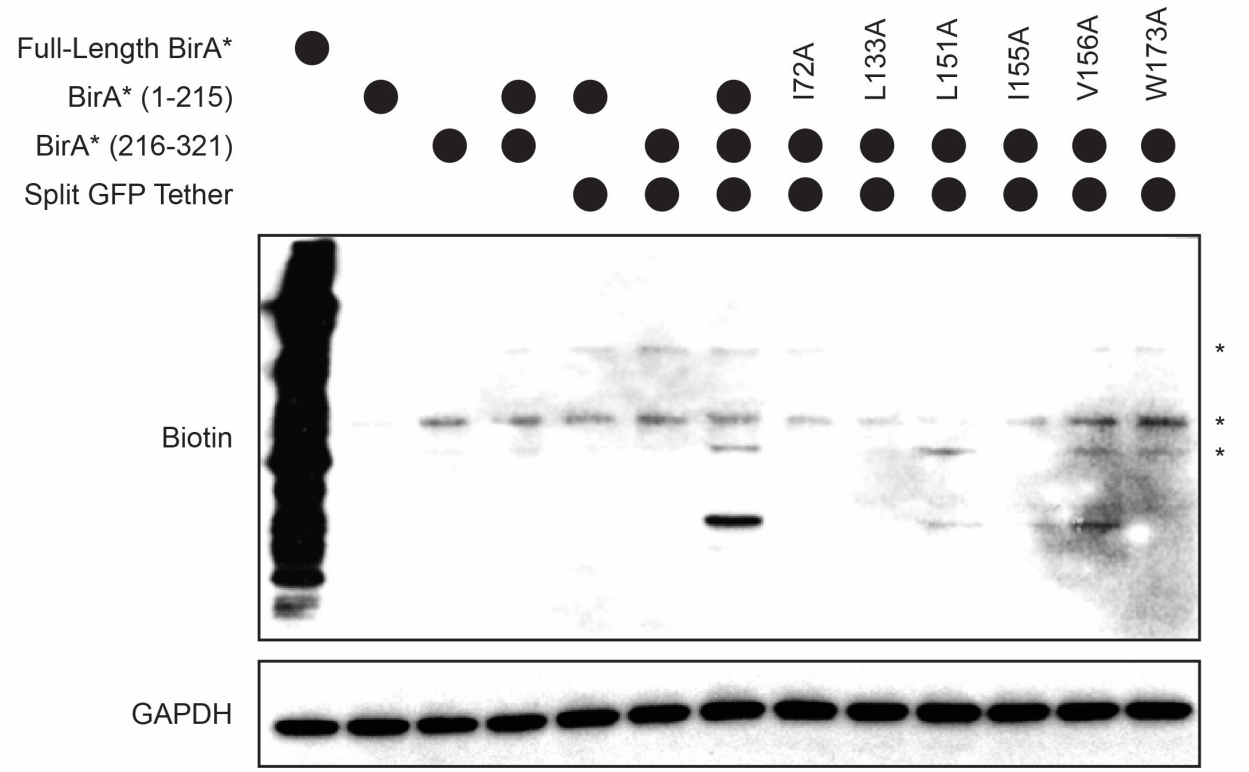

Figure 2: Engineering a Novel Split BirA*
Transfection of full-length and split BirA* either fused or unfused to a split GFP tether. Asterisks refer to endogenously biotinylated proteins.

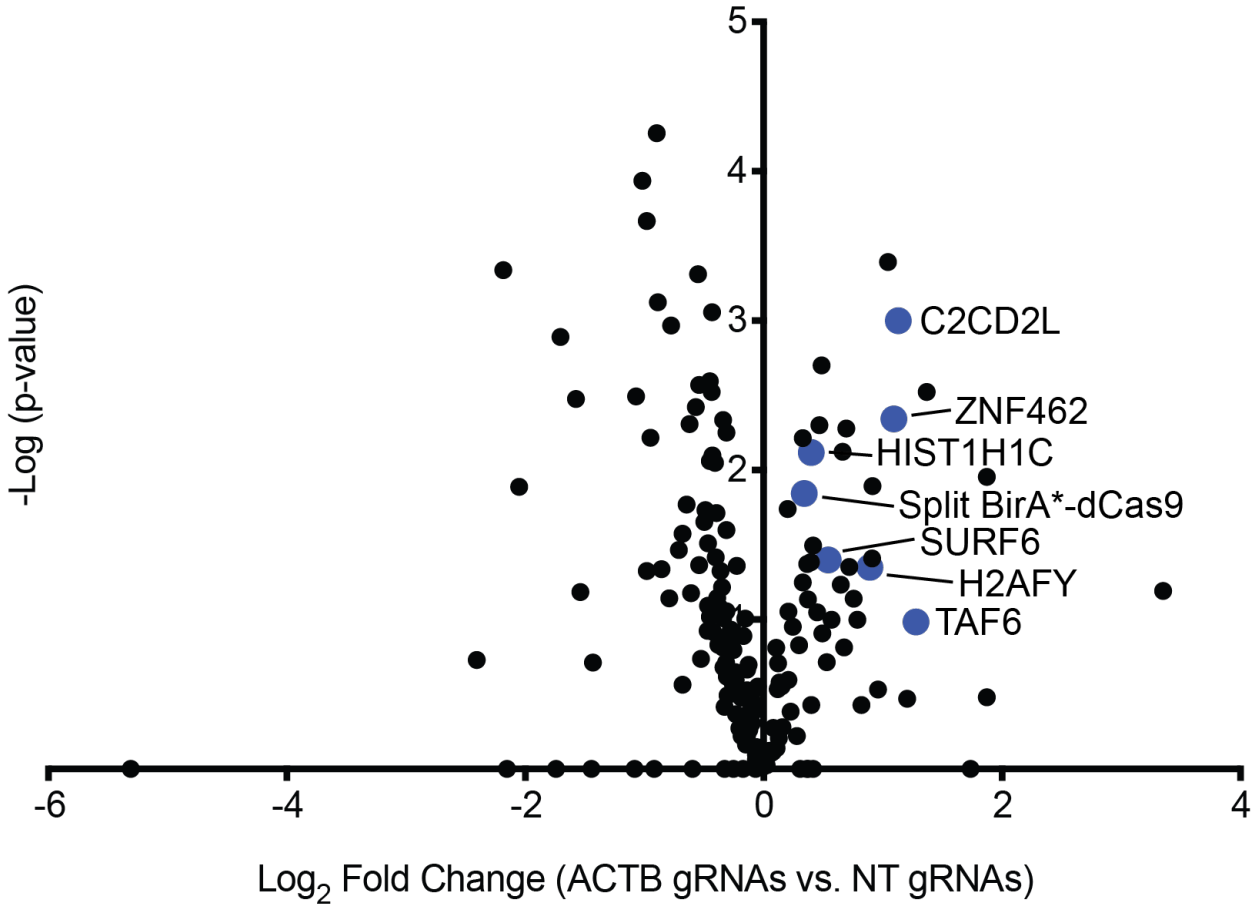

Figure 3: Targeting Split BirA*-dCas9 to *ACTB* with gRNAs Separated by 14 Basepairs
Volcano plot of biotinylated proteins from samples with *ACTB* gRNAs separated by 14 basepairs (n = 2 biological replicates) versus non-targeting gRNAs (n = 2 biological replicates). Selected hits are shown in blue.

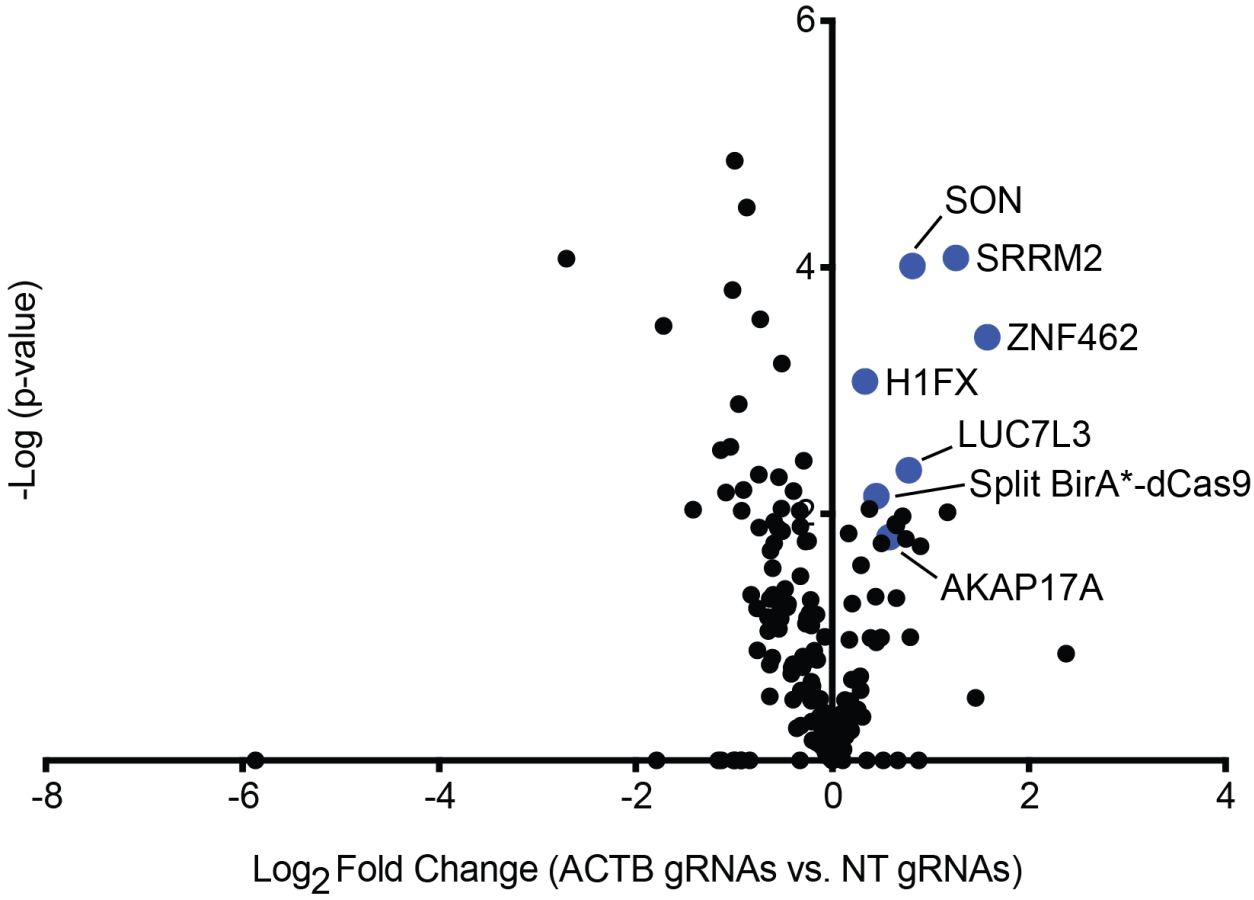

Figure 4: Targeting Split BirA*-dCas9 to *ACTB* with gRNAs Separated by 15 Basepairs

Volcano plot of biotinylated proteins from samples with *ACTB* gRNAs separated by 15 basepairs (n = 2 biological replicates) versus non-targeting gRNAs (n = 2 biological replicates). Selected hits are shown in blue.

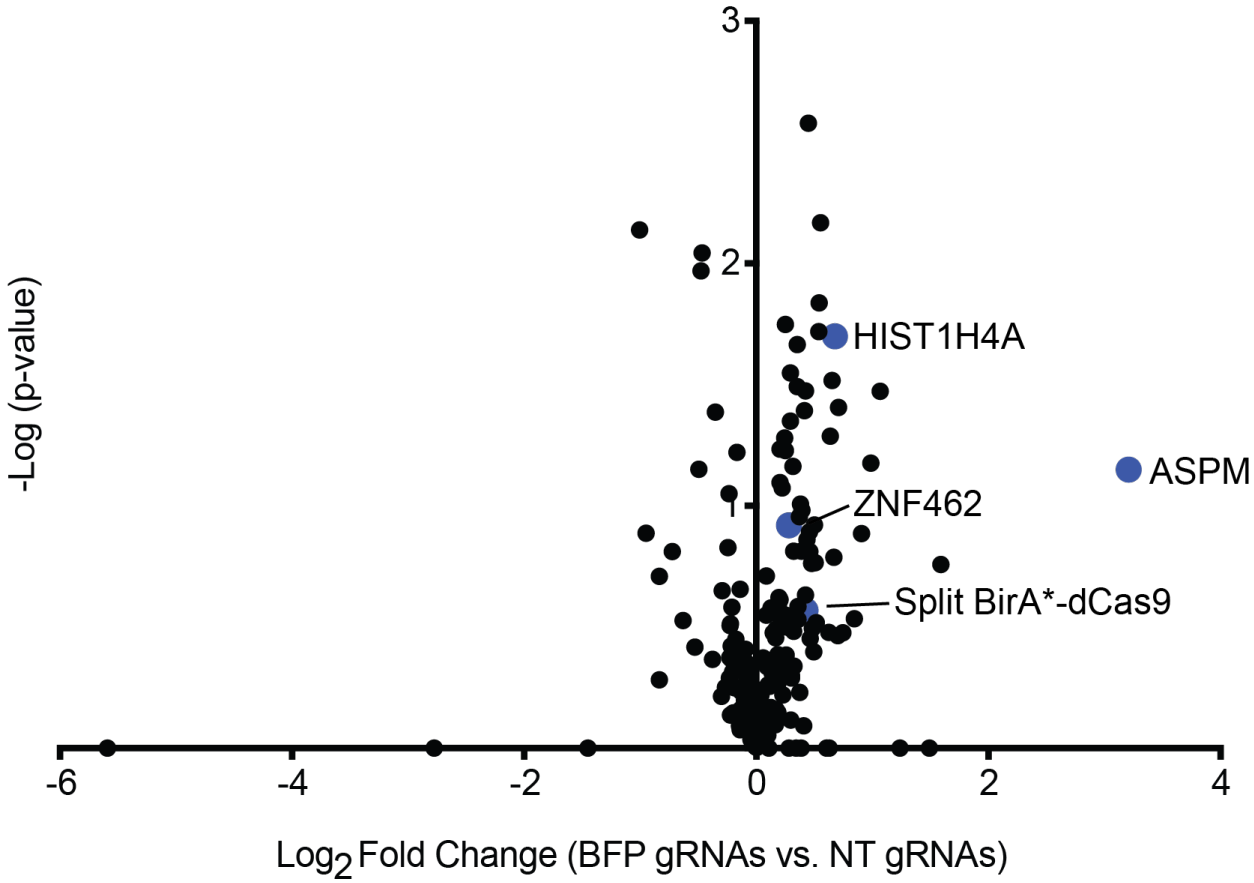

Figure 5: Targeting Split BirA*-dCas9 to *ACTB* with gRNAs Separated by 16 Basepairs
Volcano plot of biotinylated proteins from samples with *ACTB* gRNAs separated by 16 basepairs (n = 2 biological replicates) versus non-targeting gRNAs (n = 2 biological replicates). Selected hits are shown in blue.

2.4 Discussion

Here we deployed a dCas9-based proximity sensor to both repetitive and non-repetitive sequences in live human cells. BirA*-dCas9 successfully biotinylated several factors known to bind centromeric repeats, including almost the entirety of the cohesin complex. We also detected several DNA repair factors. Prior reports indicate that some repair proteins localize to centromeres (Aze et al., 2016), but it is currently unclear if the specific DNA repair factors we identified are naturally present at centromeres or localized there only in response to dCas9 binding. We also detected several chromatin-modifying proteins at centromeres. Their potential ability to displace not only histones but also Cas9 warrants further investigation.

Prior reports fusing dCas9 to APEX have taken varying strategies to combat the noise derived from unbound dCas9 molecules. Targeting this fusion protein to centromeres and telomeres enabled enrichment of proteins bound to highly repetitive sites (Gao et al., 2018). We were similarly able to capture proteins bound to centromeres with our BirA*-dCas9 proximity sensor. Simultaneously expressing multiple gRNAs targeting either the *hTERT* or *MYC* promoter enabled only a very modest enrichment of select proteins known to bind gene promoters (Myers et al., 2018). Efficient and selective assembly of a split system at unique loci would potentially provide a much more sensitive means of detecting proteins at non-repetitive loci.

Targeting our engineered split BirA*-dCas9 proteins to *ACTB*, however, did not significantly enrich for any factors known to localize around a transcription start site of a highly transcribed gene. There are several possible reasons for this result. The protein linker between the split BirA* and dCas9 may not be optimal for BirA* assembly. The initial design of the split BirA*-dCas9 system employed the same linker between BirA* halves and dCas9 used to fuse FokI monomers to dCas9 (Guilinger et al., 2014). It is plausible that the linker that allowed dimerization of FokI monomers does not efficiently promote assembly of the split BirA*. Future experiments can also interrogate the optimal distance between the two gRNAs. In addition, the cut site within BirA* may not enable efficient assembly when the complementary halves are fused to dCas9. A previous report identified a separate cut site within BirA* (Schopp et al., 2017) that may allow more effective assembly. Another study also identified a cut site within TurboID, a mutant form of BirA* that enables faster proximity ligation, that may also allow more effective assembly (Cho et al., 2020). Moreover, transiently overexpressing the split BirA*-dCas9 constructs may be producing so many molecules that the split system is assembling away from the specific *ACTB* locus, thereby generating a substantial degree of`` noise. Additional experiments are thus required to optimize the design of the split system and expression levels of individual components.

2.5 Methods

2.5.1 gRNA and BirA* Constructs

For centromere-targeting experiments, full-length BirA*-dCas9 was cloned into a Tet-On vector. gRNAs were cloned into the lentiviral pLG1-library vector (Addgene #84832) as previously described (Horlbeck et al., 2016a). To test the split BirA* design, the first half of BirA* (1-215) fused to the second half of superfolder GFP (213-236) was cloned into the pRK5 backbone. Similarly, the second half of BirA* (216-2321) fused to the first half of superfolder GFP (1-212) was cloned into the pRK5 backbone. For ACTB experiments, BirA* (1-215)-dCas9 and BirA* (216-321)-dCas9 were cloned into the pRK5 backbone. gRNAs were cloned into versions of the lentiviral pLG1-library vector modified to express either puromycin resistance and GFP or hygromycin resistance and BFP.

2.5.2 Cell Culture

Parental HEK293 and HEK293T cells were acquired from the UC Berkeley Cell Culture Facility. All cells were regularly tested for mycoplasma contamination. HEK293 and HEK293T cells were maintained in DMEM with glutamax (Gibco) supplemented with 10% fetal bovine serum, 1% sodium pyruvate (Gibco), and 100 U/ml penicillin-streptomycin (Gibco).

2.5.3 Lentiviral Packaging and Transduction

Lentiviral packaging of all constructs was performed in HEK293T cells. Plasmids were transfected using TransIT®-LT1 Transfection Reagent (Mirus) at a ratio of 1 μg of total DNA to 3 μl of the transfection reagent. The plasmid mixture consisted of 50% lentiviral transfer plasmid, 40% ΔVPR plasmid, and 10% VSVG plasmid. Virus was harvested at 48 and 72 hours after transfection, passed through a 0.45 μM filter, and added to target cells for transduction

For centromere-targeting experiments, cells were transduced to express BirA*-dCas9. 48 hours after transduction, HEK293 cells were exposed to puromycin at 1 μg/ml. Cells were maintained in media containing puromycin for at least two passages to ensure complete selection. For ACTB experiments, cells were transduced to express two separate gRNAs. 48 hours after transduction, HEK293 cells were exposed to puromycin at 1 μg/ml and hygromycin at 250 μg/ml. Cells were maintained in media containing puromycin and hygromycin for at least two passages to ensure complete selection.

2.5.4 Transient Plasmid Transfection

For centromere-targeting experiments, cells were maintained in the absence of tetracycline or doxycycline. Levels of BirA*-dCas9 was dependent on leaky expression off of the Tet-On promoter. The gRNA vector was transfected into using TransIT®-LT1 (Mirus). To test the split BirA* design, the split BirA*-split GFP construct(s) were transfected either alone or in equivalent amounts using TransIT®-LT1 (Mirus). For ACTB experiments, equivalent amounts of each split BirA*-dCas9 vector were co-transfected using TransIT®-LT1 (Mirus). For all conditions, biotin was added 24 hours after transfection to a final concentration of 50 μM.

2.5.5 Cellular Fractionation

Cells were fractionated 24 hours after biotin addition as previously described (Holden and Horton, 2009). Cells were first resuspended in digitonin buffer (150 mM NaCl, 50 mM HEPES pH 7.4, and 25 μg/ml digitonin) with protease inhibitors and incubated for 10 minutes with rotation at 4°C. Samples were then centrifuged at 2000g for 5 minutes at 4°C, and the supernatant was collected and stored as the cytoplasmic fraction. The pellet was then resuspended in NP-40 buffer (150 mM NaCl, 50 mM HEPES pH 7.4, and 1% NP-40) with protease inhibitors and incubated for 30 minutes at 4°C. Samples were then centrifuged at 2000g for 5 minutes at 4°C, and the supernatant was collected and stored as the membrane fraction. The pellet was then resuspended in RIPA buffer (150 mM NaCl, 50 mM HEPES pH 7.4, 0.5% sodium deoxycholate, 0.1% sodium

dodecyl sulfate, and 10 U/ml benzonase) with protease inhibitors and incubated overnight with rotation at 4°C. Samples were centrifuged at 15000g for 15 minutes at 4°C, and the supernatant was collected as the nuclear fraction.

2.5.6 Streptavidin Pulldown

Streptavidin pulldowns were conducted on the nuclear fractions to isolate biotinylated proteins. For Western blots, 100 μl of Dynabeads MyOne Streptavidin C1 (Life Technologies) were used for each sample. For mass spectrometry, 300 μl of beads were used for each sample. The beads were brought to room temperature and washed three times with lysis buffer (50 mM Tris pH 7.4, 500 mM NaCl, 0.4% SDS, 5 mM EDTA, 1 mM DTT). For Western blots, beads were then resuspended in 1000 μg of the nuclear fraction. For mass spectrometry, beads were resuspended in 3000 μg of the nuclear fraction. Samples were incubated overnight with rotation at 4°C. Tubes were then transferred to the magnetic rack, and beads were washed twice in wash buffer 1 (2% SDS), once in wash buffer 2 (0.1% sodium deoxycholate, 1% Triton X-100, 500 mM NaCl, 1 mM EDTA, and 50 mM Hepes pH 7.5), once in wash buffer 3 (250 mM LiCl, 0.5% NP-40, 0.5% sodium deoxycholate, 1 mM EDTA, and 10 mM Tris pH 8.1), and twice in wash buffer 4 (50 mM Tris pH 7.4 and 50 mM NaCl).

2.5.7 Western Blot

Beads were resuspended in 30 μl of 1X Laemmli Buffer (Bio-Rad) containing 50 μM biotin, transferred to a new tube, and then heated at 99°C for 5 minutes. Tubes were then transferred to a magnetic rack, and the supernatant was retained as the eluate.

Protein samples were resolved on Mini-PROTEAN® TGX™ 4-20% gels (Bio-Rad), and resolved proteins were transferred (TransBlot Turbo, Bio-Rad) to nitrocellulose membranes. Membranes were blocked in 5% milk in TBST for 30 min at room temperature and incubated with primary antibodies in blocking buffer overnight at 4°C. Membranes were washed three times in TBST, incubated with secondary antibodies (LI-COR Biosciences) in blocking buffer for 45 min, and then exposed on an Odyssey® CLx Imaging System (LI-COR Biosciences). Protein levels were probed using the following antibodies: Biotin (Cell Signaling #5597 1:1000) and GAPDH (Cell Signaling #2118 1:1000).

2.5.8 Mass Spectrometry

Beads were washed five times with 1 ml of 50 mM ammonium bicarbonate and then resuspended in 100 μl of 50 mM ammonium bicarbonate containing 0.01% ProteaseMAX (Promega) and 3 μg of sequencing-grade trypsin (Promega). Samples were incubated with mixing at 37°C for 4 hours after which the supernatant was collected and transferred to a new tube. Beads were washed again with 50 μl of 50 mM ammonium bicarbonate, and supernatants were pooled. 2 μl of formic acid (Fisher Scientific) was added to acidify the samples to a pH of ~3.0. Samples were then spun

down to dryness in a speedvac and submitted to the University of California, Davis Proteomics Core for Multi-Dimension Protein Identification Technology mass spectrometry. Trypsinized peptides were mapped to the human proteome, and protein enrichment levels were analyzed by the Limma Bioconductor package.

Chapter 3: The Histone Chaperone FACT Induces Cas9 Multi-turnover Behavior and Modifies Genome Manipulation in Human Cells

A portion of the material in this chapter was previously published as:

Wang, A.S., Chen, L.C., Wu, R.A., Hao, Y., McSwiggen, D.T., Heckert, A.B., Richardson, C.D., Gowen, B.G., Kazane, K.R., Vu, J.T., et al. (2020). The Histone Chaperone FACT Induces Cas9 Multi-turnover Behavior and Modifies Genome Manipulation in Human Cells. Mol Cell *79* (2), 221-233.e5.

The work has been adapted here with permission from co-authors.

3.1 Connection to Overall Dissertation

Attempts to identify proteins at genomic loci using a dCas9-based proximity sensor were successful at highly repetitive sequences. However, background biotinylation derived from unbound dCas9 molecules inhibited application of this tool to identify Cas9 interactors at non-repetitive sequences. In order to increase the signal to noise ratio, we turned to a cell-free system whose lack of a physical barrier allows tight of control over the ratios of Cas9 RNPs and DNA substrates. This *in vitro* system enabled identification of FACT as a Cas9 displacement factor, and additional experiments demonstrated that FACT plays a critical role in shaping dCas9 residence times and Cas9-based interventions in live human cells.

3.2 Introduction

Cas9 is a CRISPR-associated RNA-guided DNA endonuclease that is directed to a target DNA molecule by forming a ribonucleoprotein (RNP) complex with a guide RNA (gRNA) (Doudna and Charpentier, 2014; Hsu et al., 2014; Jinek et al., 2012; Knott and Doudna, 2018). After unwinding its duplex substrate, Cas9 uses two nuclease domains to generate a double-stranded break (DSB) (Doudna and Charpentier, 2014; Hsu et al., 2014; Jinek et al., 2012; Knott and Doudna, 2018; Sternberg et al., 2015). Subsequent break repair relies on a cell's endogenous machinery to either incorporate sequences using a DNA template through homology-directed repair (HDR) or introduce insertions or deletions (indels) during non-homologous end joining (NHEJ) (Maggio and Goncalves, 2015). The ease of programming Cas9 to generate targeted DSBs and initiate break repair has enabled its widespread use as a genome-editing agent (Cong et al., 2013; Jinek et al., 2012; 2013; Mali et al., 2013).

Mutations that inactivate Cas9's nuclease activity preserve its capacity to bind a gRNA and target DNA (Qi et al., 2013). Catalytically inactive Cas9 (dCas9) has dramatically expanded the CRISPR toolbox. Fusing various effector proteins to dCas9 has enabled CRISPR-based methods to activate or repress gene expression, manipulate the three-dimensional architecture of nuclei, image genomic loci, track RNA molecules, and

identify proteins at specific loci (Chen et al., 2013; Gao et al., 2018; Gilbert et al., 2013; Hilton et al., 2015; Konermann et al., 2015; Liu et al., 2017; Myers et al., 2018; Nelles et al., 2016; Qi et al., 2013; Schmidtmann et al., 2016; Wang et al., 2018).

The relationship between the efficacy of the CRISPR-Cas9 toolbox and Cas9's lifetime on a genomic target site is unclear. For example, CRISPR transcriptional effectors localize histone acetyltransferases or methyltransferases around a transcription start site (TSS) to manipulate expression of endogenous genes (Gilbert et al., 2013; Hilton et al., 2015). Such transcriptional engineering presumably relies on providing these histone modifiers sufficient time at the TSS to deposit the appropriate epigenetic marks. Conversely, Cas9's utility as a targeted nuclease may be predicated on its removal from the genome because Cas9 itself masks the DSB from cellular repair enzymes (Clarke et al., 2018; Richardson et al., 2016b). Cas9 residence times and unloading might thus play crucial roles in Cas9-based interventions.

While some Cas9 molecules behave as multi-turnover enzymes (Yourik et al., 2019), the widely used *Streptococcus pyogenes* Cas9 and dCas9 exhibit extremely stable protein-DNA interactions and possess residence times of over 5 h *in vitro* (Raper et al., 2018; Richardson et al., 2016b; Sternberg et al., 2014). Estimates of residence times in live cells vary (Ma et al., 2016; Shao et al., 2016), but some experiments indicate that *S. pyogenes* Cas9 stays bound to its target in mammalian cells for as little as 5 min (Knight et al., 2015) and imply that cellular factors promote turnover. Given that DNA repair requires at least 30 min to occur (Mao et al., 2008), the ability to detect resolved genomic edits only 1 h after electroporation of Cas9 RNPs (Kim et al., 2014) further suggests that cells actively remove Cas9 from the genome either purposefully or as a byproduct of normal genome metabolism.

Prior work has suggested that RNA polymerases can dislodge Cas9 from DNA *in vitro* when the gRNA anneals to the non-coding DNA strand, but not to the coding strand (Clarke et al., 2018). Targeting the non-coding strand with a gRNA roughly correlated with increased editing rates in human cells and an increased ability of a bacterially-encoded CRISPR system to fight phage infection. However, the ability to edit non-transcribed regions of the human genome implies that RNA polymerases are not solely responsible for Cas9 eviction. Moreover, the ability to edit post-mitotic cells, such as neurons, suggests that replicative DNA polymerases are also not solely responsible for unloading Cas9 (Nishiyama et al., 2017; Suzuki et al., 2016).

Here, we find that metazoan cellular extracts contain a factor responsible for rapid multi-turnover activity of Cas9 on DNA substrates. An unbiased proteomics approach to mark proteins transiently associating with substrate-bound Cas9 and dCas9 identified both components of the heterodimeric facilitates chromatin transcription (FACT) histone chaperone complex, SPT16 and SSRP1. In *Xenopus* extracts, immunodepletion of FACT subunits prevented dCas9 displacement and converted Cas9's activity from multi-turnover to single-turnover. In a minimal buffer system, recombinant FACT was sufficient to displace dCas9. In living human cells, FACT promoted dCas9 unbinding, modified Cas9 editing outcomes, and played a strand-independent role in determining

the extent of epigenetic marking and transcriptional regulation from dCas9-based effectors. These results reveal an unanticipated functional interaction between Cas9 and the eukaryotic machinery responsible for regulating nucleosome assembly.

3.3 Results

3.3.1 Cell-free *X. laevis* Egg Extract Promotes Rapid Turnover of Cas9 from DNA Substrates

Xenopus egg extracts have a long track record of dissecting nuclear dynamics and interrogating processes, such as DNA replication, chromosome segregation, and DNA repair (Heald et al., 1996; Hoogenboom et al., 2017; Kalab et al., 2006; Knipscheer et al., 2009; Lebofsky et al., 2009). We therefore used high-speed supernatant (HSS) of total *Xenopus laevis* egg lysate (Lebofsky et al., 2009) to look for cellular factors that promote the dissociation of a pre-formed Cas9 RNP-DNA complex.

We first tested the ability of HSS to promote the dissociation of *S. pyogenes* Cas9 RNPs from linear and plasmid DNA substrates harboring a single on-target site. We incubated RNPs with twice as many moles of DNA for 45 min before adding buffer or HSS. With excess substrate, complete cleavage would occur only if Cas9 possesses multi-turnover activity. Consistent with prior *in vitro* data (Richardson et al., 2016b; Sternberg et al., 2014), a Cas9 RNP targeting linear double-stranded DNA in buffer failed to cleave the excess substrate and thus behaved as a single-turnover enzyme, even under these multi-turnover conditions (Figure 6A). However, incubation of RNP and target DNA in HSS and ATP yielded a steady conversion of substrate to product that was consistent with multi-turnover behavior (Figure 6A). Pre-depleting HSS ATP levels using calf intestinal phosphatase (CIP) and adding an excess of the non-hydrolysable analogue ATPγS reverted Cas9's behavior to single-turnover (Figure 6A). We observed similar results when targeting Cas9 to a circular plasmid under multi-turnover conditions (Figure 6B).

We next developed a competition assay to determine whether factors in HSS induce dCas9 removal from a circular DNA substrate under single-turnover conditions (Figure 6C). We allowed a dCas9 RNP to equilibrate in buffer with a plasmid containing a single on-target site and then incubated this RNP-plasmid complex with buffer alone, HSS containing an ATP-regenerating system (ARS) (see STAR Methods), or HSS pre-incubated with CIP and excess ATPγS. Finally, we added a 10-fold molar excess of catalytically active Cas9 programmed with the identical on-target gRNA. Persistent binding of dCas9 should prevent binding of Cas9 and preclude cleavage, whereas dCas9 unloading would grant Cas9 access to the target site. The presence of linearized DNA thus provides a readout of dCas9 unloading. Consistent with our data using multi-turnover conditions, buffer alone did not promote dCas9 dissociation from the plasmid (Figure 6D, lanes 3-5). By contrast, HSS containing the ARS rapidly removed dCas9 to allow the catalytically active Cas9 to cleave the plasmid within 45 min (Figure 6D, lanes 6-8). Conversely, ATP-depleted HSS supplemented with ATPγS did not evict the majority of dCas9 molecules, thereby preventing Cas9 from cleaving the plasmid

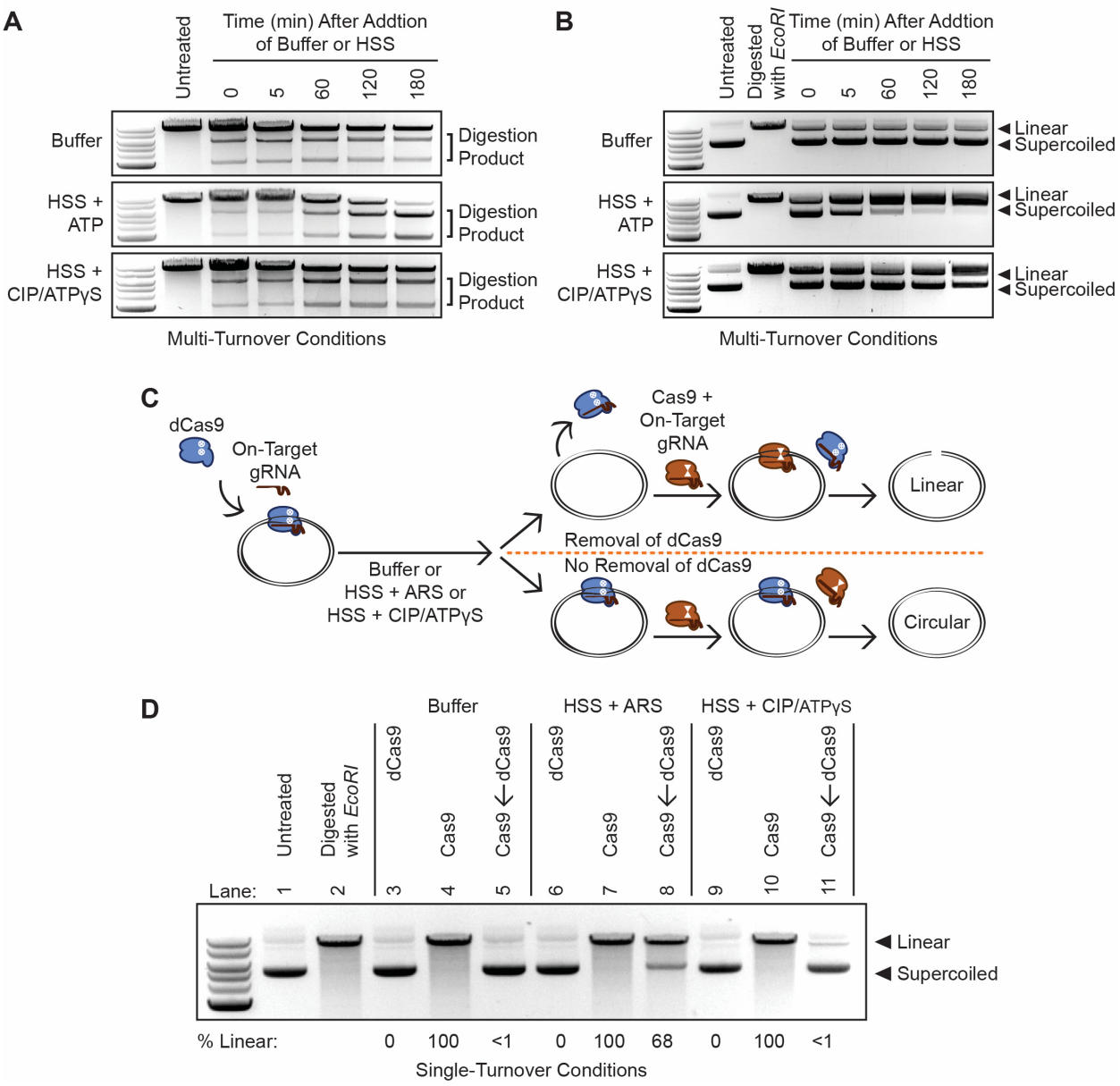

Figure 6: Energy-Dependent Release of Cas9 and dCas9 from DNA in HSS
(A) Time course of Cas9 RNPs programmed against a linear DNA substrate in a 1:2 molar ratio in buffer, HSS with ATP, or HSS with CIP and ATPγS. (B) Time course of Cas9 RNPs programmed against a plasmid substrate in a 1:2 molar ratio in buffer, HSS with ATP, or HSS with CIP and ATPγS. (C) Schematic of the single-turnover competition assay. (D) ATP-dependent unloading of dCas9 off a plasmid substrate in *X. laevis* HSS. Presence of linearized DNA after addition of a 10-fold molar excess of Cas9 indicates removal of dCas9, although persistence of circular DNA indicates stable binding of dCas9. See also Figure 7.

(Figure 6D, lanes 9-11). Overall, our data with linear and circular DNA substrates indicate that HSS contains at least one factor capable of dislodging Cas9 from its target, enabling re-binding to uncleaved molecules and multi-turnover behavior.

3.3.2 Unbiased Cas9 Interaction Marking Identifies the FACT Histone Chaperone as Required for Cas9 Removal and Multi-turnover Activity in HSS

To identify factors that remove Cas9 from DNA in HSS, we fused Cas9 and dCas9 to the promiscuous biotin ligase BirA* (Arg118Gly). BirA* covalently labels nearby proteins, which can then be isolated with streptavidin-coupled beads and identified through mass spectrometry proteomics (Gao et al., 2018; Roux et al., 2012; Schmidtmann et al., 2016). BirA*'s utility for our purposes is derived from our ability to extend the labeling time beyond a few minutes, thereby allowing the system to accumulate biotinylated versions of transient yet repeated interactors (Roux et al., 2013). BirA*-dCas9 fusions expressed in living cells have helped identify DNA interactors at repetitive genomic regions (Schmidtmann et al., 2016), but excess BirA*-dCas9 unbound to the genomic target has complicated its use at non-repetitive loci. We reasoned that the ability to form a defined Cas9-BirA* RNP-DNA or dCas9-BirA* RNP-DNA species in HSS could enable identification of Cas9 and dCas9 removal factors.

We expressed and purified recombinant Cas9-BirA* and dCas9-BirA* in and from bacterial cells (Data S1; Figure 7A). The fused biotin ligase neither compromised Cas9's nuclease activity nor hindered rapid dislodging of dCas9 in HSS (Figures 7B and 7C). We programmed Cas9-BirA* with an on-target gRNA, dCas9-BirA* with the same on-target gRNA, or dCas9-BirA* with a non-targeting (NT) gRNA. We added a 10-fold molar excess of plasmid substrate relative to each RNP in buffer and then added this mixture to HSS containing ARS and biotin (Figure 8A). Streptavidin pulldown and label-free proteomic mass spectrometry (Wuhr et al., 2014) identified biotinylated *X. laevis* proteins that were specifically enriched by gRNA-mediated binding of Cas9 or dCas9 to the plasmid relative to non-specific biotinylation when dCas9 was complexed with the NT gRNA. Cas9-BirA* and dCas9-BirA* programmed with the on-target gRNA had nearly identical interactors (Figure 7D), consistent with prior *in vitro* data indicating that Cas9 obscures the DSB so that repair factors are not preferentially enriched around Cas9 (Clarke et al., 2018; Richardson et al., 2016b).

Three major sets of DNA-bound Cas9 interactors were apparent by comparing the on-target samples in which Cas9 was bound to the plasmid to the NT background control in which Cas9 was unbound to the target: PIP4K2C; H/ACA-associated proteins DKC1, NHP2, and GAR1; and both components of the FACT heterodimer, SPT16 and SSRP1 (Figure 8B; Table S1). PIP4K2C is a lipid kinase that converts phosphatidylinositol-4-phosphate to phosphatidylinositol-4,5-bisphosphate. PIP4K2C is not explicitly linked to DNA metabolism, but it has recently been found that phosphoinositides accumulate at sites of double-stranded DNA damage (Wang et al., 2017). H/ACA RNPs are involved in pseudouridylation of RNA, maintenance of telomere integrity, and ribosome biogenesis (Kiss et al., 2010). The ability of H/ACA-associated proteins to interact with unique RNA secondary structures and preserve genomic integrity could imply roles in the cellular

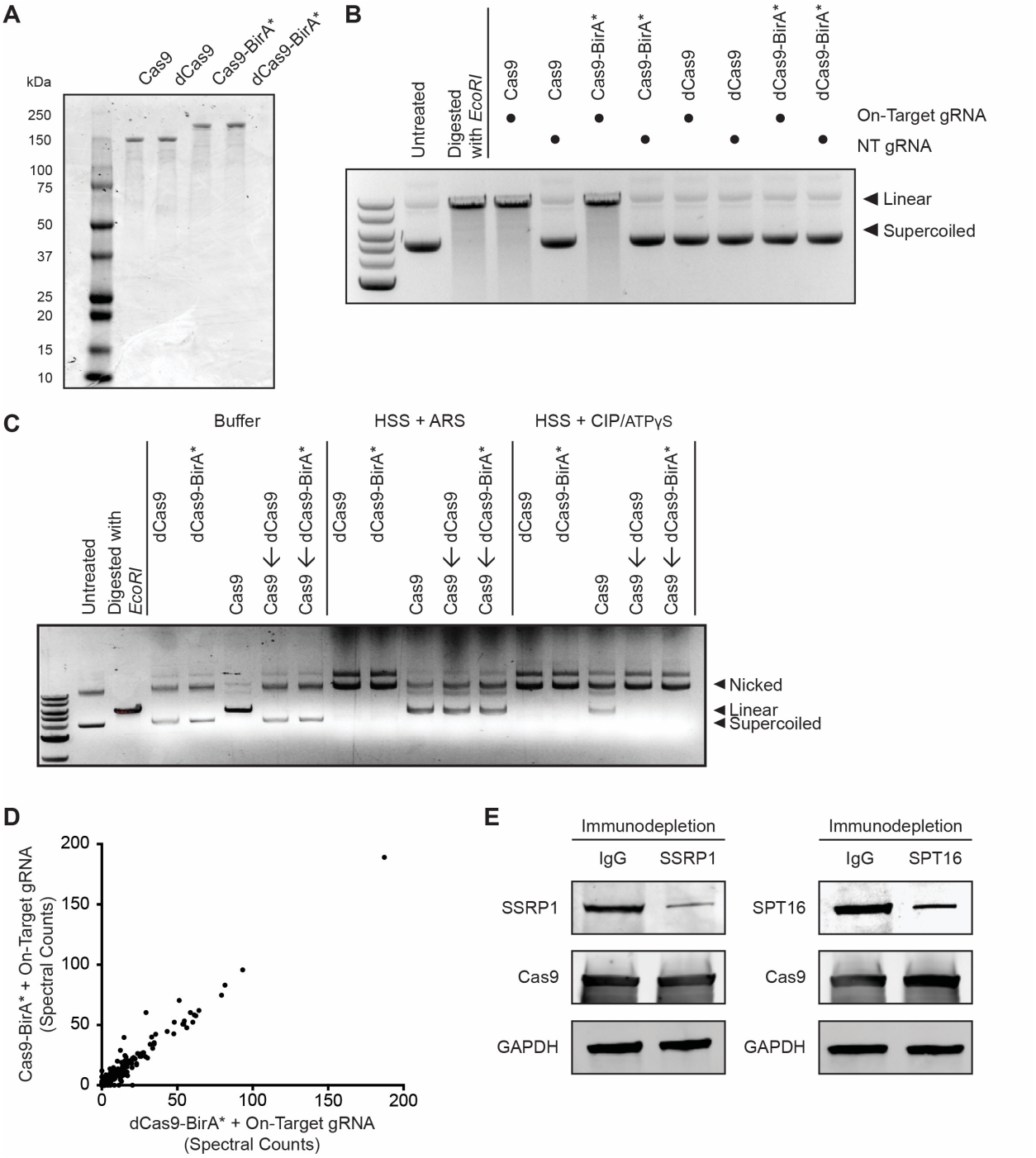

Figure 7: Deployment of Recombinant Cas9-BirA* and dCas9-BirA* in HSS
(A) Coomassie of purified Cas9, dCas9, Cas9-BirA*, and dCas9-BirA*. (B) BirA* fusion does not compromise gRNA-targeting of Cas9 or Cas9's cleavage ability in vitro. (C) BirA* fusion does not impede energy-dependent removal of Cas9 from plasmid substrates in HSS. (D) Proteins identified by mass spectrometry plotted according to average number of spectral counts in Cas9-BirA*–on-target gRNA samples (n = 3

biological replicates) versus dCas9-BirA*–on-target gRNA samples (n = 3 biological replicates). (E) Immunodepletion of SSRP1 or SPT16 from HSS.

---

response to Cas9 binding. However, PIP4K2C and H/ACA proteins are not known to destabilize protein-DNA interactions and thus were not top candidates for being the Cas9 release factors in HSS.

The FACT complex is a histone chaperone with established roles in nucleosome assembly and remodeling and thus represented an attractive candidate to mediate Cas9 removal in HSS. FACT is a heterodimer consisting of SSRP1 and SPT16, both of which were strongly enriched by proximity biotinylation and unbiased proteomics. FACT promotes chromosomal transactions by removing the H2A-H2B dimer specifically or generally weakening histone contacts within chromatin (Okuhara et al., 1999; Orphanides et al., 1998; Winkler and Luger, 2011). Individual testing by streptavidin pull-down and western blotting confirmed that binding of dCas9-BirA* to a plasmid leads to increased biotinylation of SSRP1 and SPT16 (Figure 8C).

To determine whether FACT is necessary to displace Cas9 in HSS, we immunodepleted either SSRP1 or SPT16 from HSS and ensured that immunodepletion of either FACT subunit did not affect Cas9 degradation (Figure 7E). In the single-turnover competition assay, immunodepletion of either FACT component prevented even a 10-fold molar excess of Cas9 from accessing a DNA target that was pre-bound by dCas9 (Figure 8D). Add-back of recombinant human FACT to SSRP1 or SPT16-immunodepleted extracts rescued the ability of HSS to dislodge dCas9 (Figure 8D). Notably, under multi-turnover conditions, we found that immunodepletion of SSRP1 from HSS was sufficient to convert Cas9's activity from multi-turnover to apparently single turnover (Figure 8E). FACT is therefore necessary to displace Cas9 from DNA substrates in a cell-free system. To determine whether FACT is also sufficient to displace Cas9, we incubated recombinant human FACT with a DNA target pre-bound by dCas9 under single-turnover conditions in a minimal buffer system (Figure 8F). Even in buffer alone, FACT was capable of displacing dCas9 to expose the target site to Cas9 (Figure 8F).

3.3.3 FACT Depletion Increases dCas9 Residence Times in Human Cells

To directly monitor FACT's ability to displace Cas9 in live human cells, we conducted fluorescence recovery after photobleaching (FRAP) microscopy. To generate visible foci of Cas9 bound to the genome, we stably expressed dCas9-HaloTag in a U2OS cell line containing tandem arrays of *lacO* and *tetO* sites in a single locus (Janicki et al., 2004) (Figure 9A and Figure 10A). Each array contained roughly 50,000 repeats of *lacO* and 75,000 repeats of *tetO*. We then co-transfected a *tetO* gRNA plasmid (Table S2) and either a NT or SPT16 small interfering RNA (siRNA). Depletion of SPT16 led to a concomitant reduction in SSRP1 levels (Figure 10B), consistent with prior reports that levels of the two FACT subunits are interdependent (Safina et al., 2013). 48 h after transfection, we labeled HaloTag with the dye JF_{549}, photobleached dCas9-HaloTag

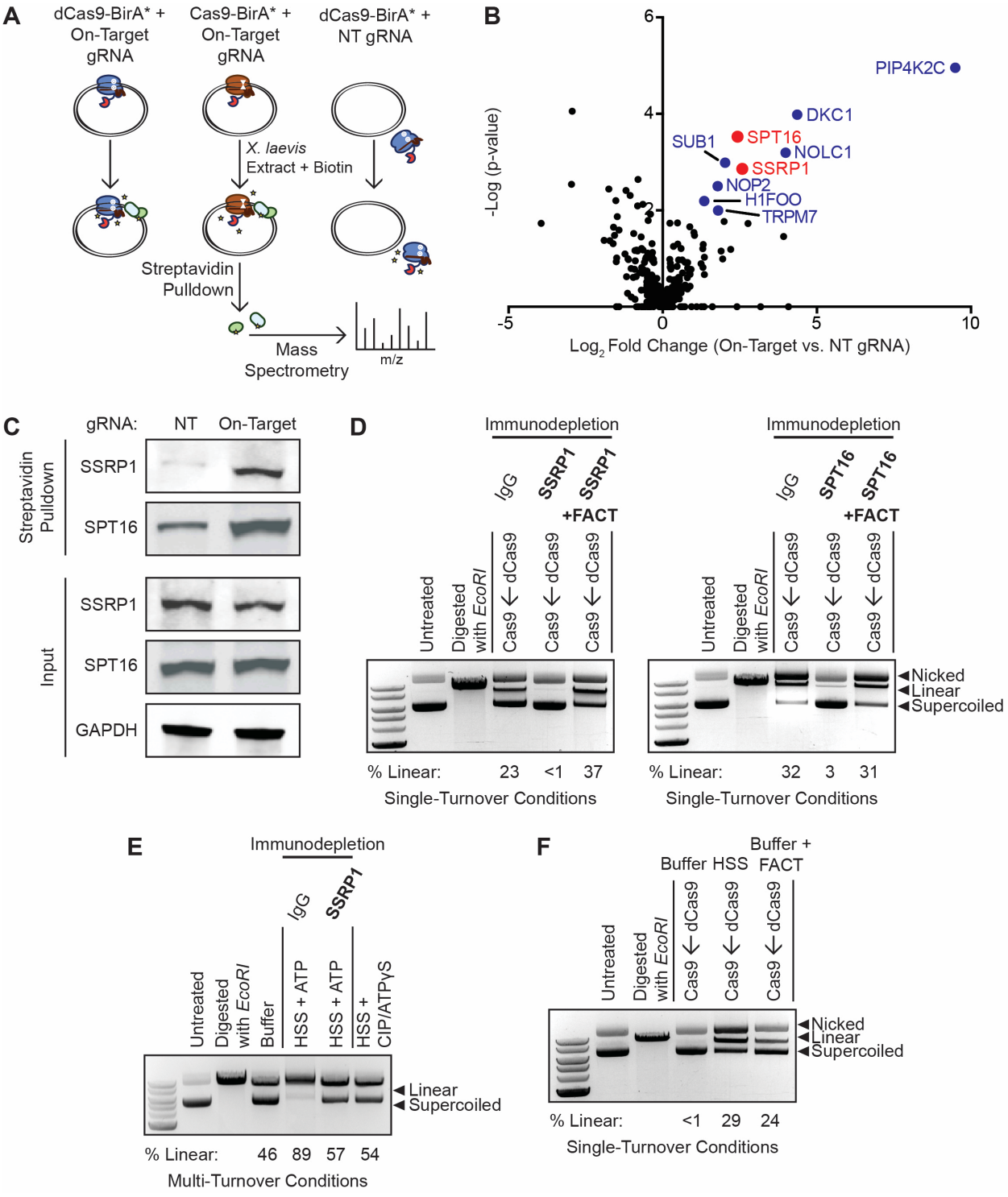

Figure 8: FACT Complex Interacts with DNA-Bound Cas9 and dCas9 to Promote Eviction and Multi-Turnover Behavior

(A) Schematic of samples prepared for mass spectrometry. dCas9-BirA* programmed with the on-target gRNA, Cas9-BirA* programmed with the on-target guide, and dCas9-

BirA* programmed with a NT sgRNA were incubated with a 10-fold molar excess of plasmid and then added to HSS containing the ARS and biotin. Biotinylated proteins were isolated with streptavidin-coupled beads and identified through mass spectrometry. (B) Volcano plot of biotinylated proteins in Cas9-BirA*–on-target gRNA samples (n = 3 biological replicates) versus dCas9-BirA*–NT gRNA samples (n = 3 biological replicates). Colored circles correspond to factors that were significantly enriched ($p < 0.05$) according to a limma analysis. Red circles correspond to the two components of the FACT complex. See also Figure 7D and Table S1. (C) Enrichment of biotinylated SSRP1 and SPT16 in HSS containing dCas9-BirA*–on-target gRNA versus dCas9-BirA*–NT gRNA. (D) FACT immunodepletion inhibits dCas9 eviction in HSS. A 10-fold molar excess of Cas9 was added to dCas9 RNP-plasmid complexes incubated in SSRP1 or SPT16-immunodepleted extract either in the presence or absence of recombinant FACT. See also Figure 7E. (E) FACT promotes Cas9's multi-turnover activity. Cas9 RNPs were incubated with a plasmid substrate in a 1:2 molar ratio with either buffer, mock-immunodepleted HSS with ATP, SSRP1-immunodepleted HSS with ATP, or HSS with CIP and ATPγS for 180 min. (F) Recombinant FACT displaces dCas9 pre-loaded on a plasmid in a minimal buffer system.

---

molecules bound to the synthetic arrays, and monitored fluorescence recovery with confocal imaging.

Three-dimensional FRAP imaging at the arrays revealed that dCas9-HaloTag within cells containing wild-type levels of FACT (n = 27) recovered to roughly half of their original fluorescence levels 500 s after photobleaching (Figures 9B-9D). dCas9-HaloTag within cells treated with SPT16 siRNAs (n = 31) on average recovered less than a third of their original fluorescence levels after the same time period (Figures 9B-9D), indicating that FACT is likely responsible for displacing Cas9 from the genome in live cells. FACT knockdown extended the mean dCas9-HaloTag residence times at the arrays by approximately 30% from 183.5 to 238.3 s (Figure 10C).

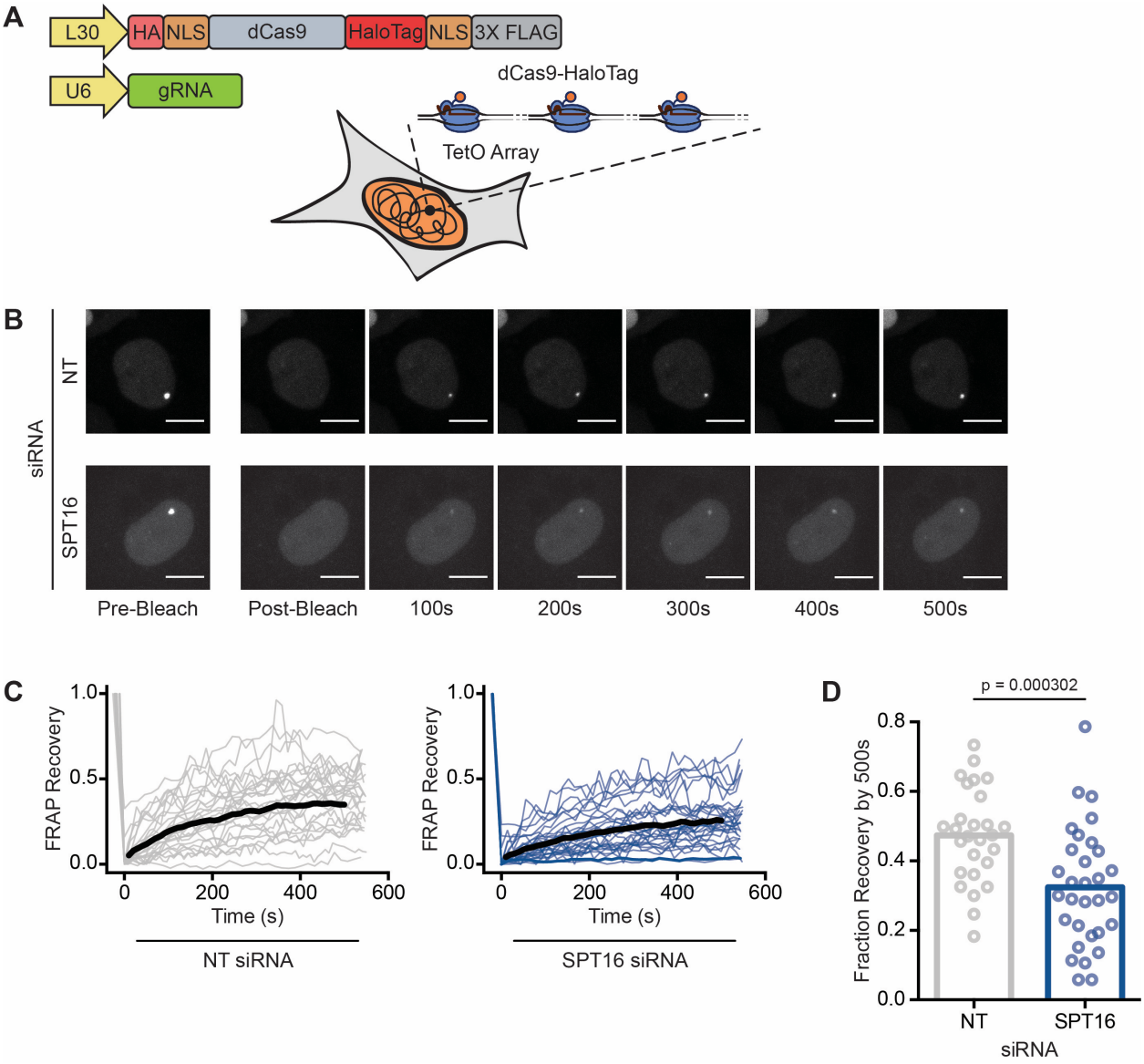

Figure 9: FACT Depletion Enhances dCas9 Binding Times in Human Cells
(A) Schematic of synthetic arrays bound by dCas9-HaloTag. See also Figure 10A. (B) Representative FRAP images of dCas9-HaloTag targeted to arrays in U2OS cells treated with either NT (top) or SPT16 (bottom) siRNAs. Scale bars represent 10 μm. (C) Compiled FRAP curves for cells treated with either NT (n = 27) or SPT16 (n = 31) siRNAs. Black lines are the average recovery curves for each condition. See also Figure 10C. (D) Quantification of fraction recovery 500 s after photobleaching for cells transfected with NT or SPT16 siRNAs. Statistical significance was calculated via a Mann-Whitney U Test.

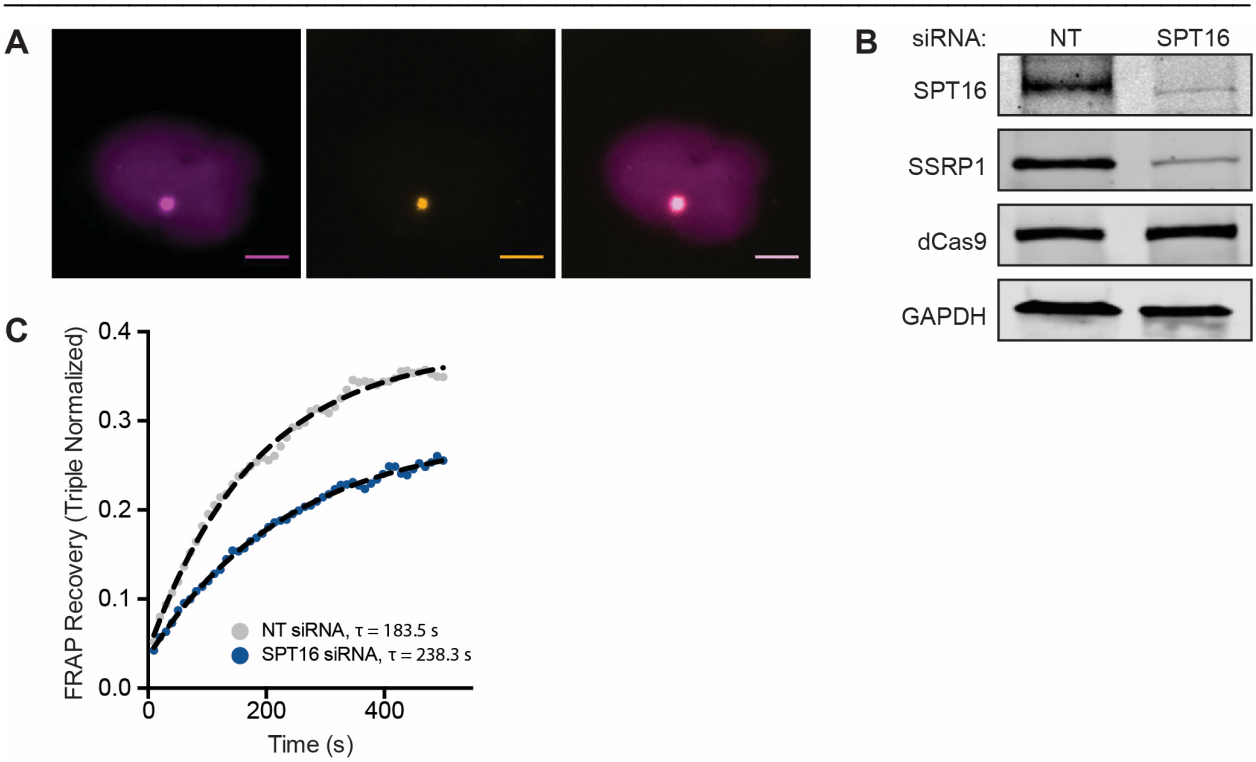

Figure 10: FRAP Imaging of dCas9-HaloTag after FACT Depletion
(A) Colocalization of dCas9-HaloTag labeled with JF_{646} and programmed with a tetO gRNA (left panel) and mOrange-LacI-NLS (middle panel) at synthetic arrays. The right panel is an overlay of the two channels. Scale bars = 10 μm. (B) Western blot of SPT16, SSRP1, dCas9, and GAPDH in U2OS cells transfected with either NT or SPT16 siRNAs. (C) Mean FRAP recoveries with single component exponential fits.

3.3.4 Knockdown of FACT Alters Cas9 Genome Editing Outcomes in Human Cells

To determine how FACT knockdown affects phenotypic outcomes of Cas9-based interventions, we first asked whether FACT influences Cas9-based genome editing in intact human cells. We specifically measured editing rates and outcomes via amplicon next-generation sequencing (amplicon-NGS) after FACT knockdown (Tables S2-S4). 60 h after transfecting K562 cells with either NT or SPT16 siRNAs (Figure 11A), we electroporated separate cultures of cells with Cas9 RNPs targeted to eight different loci, including a non-transcribed gene desert. For each locus, we performed editing reactions with and without a matched single-stranded oligodeoxynucleotide (ssODN) HDR donor that programs a protospacer adjacent motif (PAM) mutation at the appropriate locus.

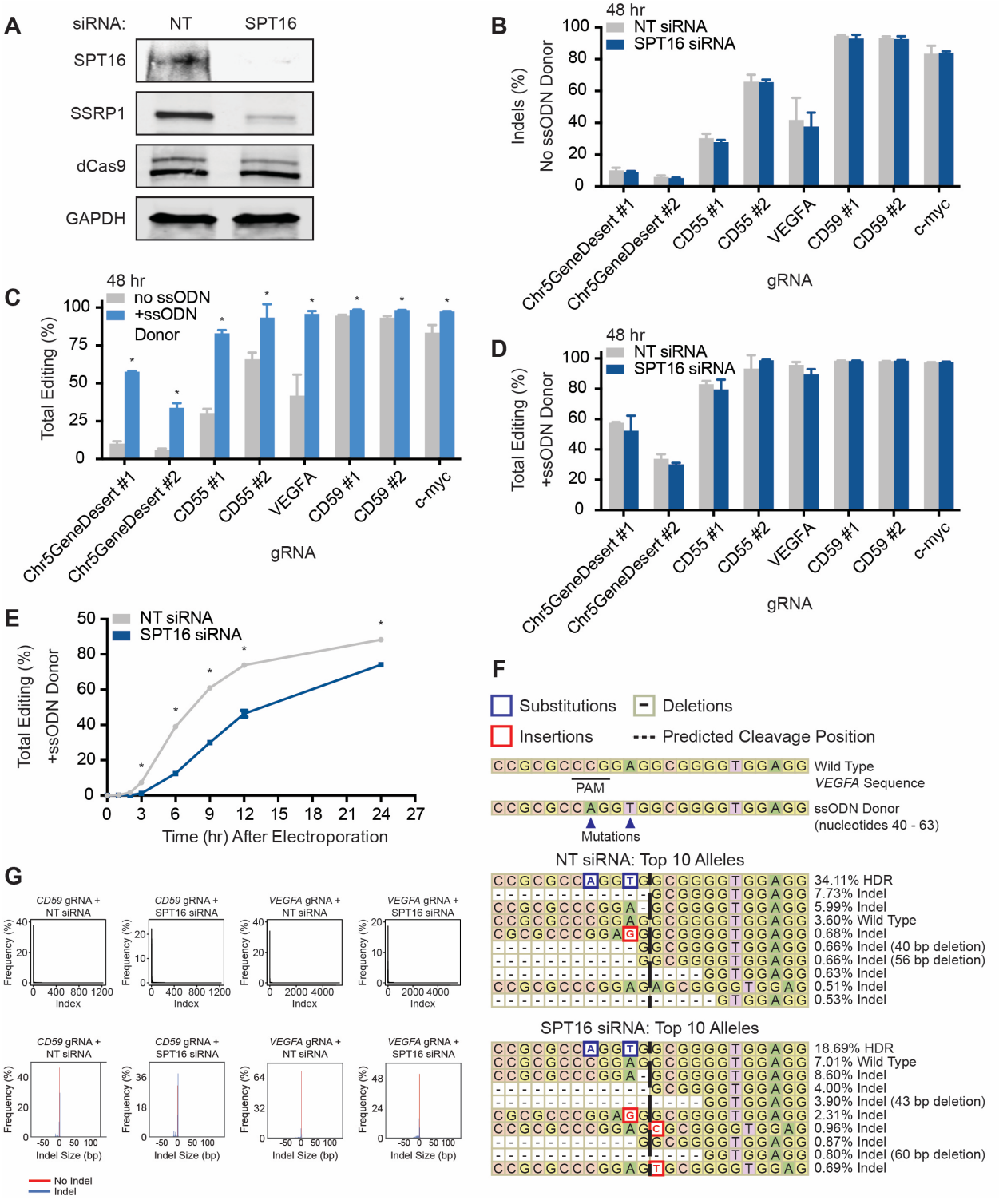
A
siRNA:
NT
SPT16
SPT16
SSRP1
dCas9
GAPDH
B
48 hr
NT siRNA
SPT16 siRNA
Indels (%)
No ssODN Donor
Chr5GeneDesert #1
Chr5GeneDesert #2
CD55 #1
CD55 #2
VEGFA
CD59 #1
CD59 #2
c-myc
gRNA
C
48 hr
no ssODN
+ssODN Donor
Total Editing (%)
gRNA
D
48 hr
NT siRNA
SPT16 siRNA
Total Editing (%)
+ssODN Donor
gRNA
E
NT siRNA
SPT16 siRNA
Total Editing (%)
+ssODN Donor
Time (hr) After Electroporation
F
Substitutions
Deletions
Insertions
Predicted Cleavage Position
Wild Type
VEGFA Sequence
PAM
ssODN Donor
(nucleotides 40 - 63)
Mutations
NT siRNA: Top 10 Alleles
34.11% HDR
7.73% Indel
5.99% Indel
3.60% Wild Type
0.68% Indel
0.66% Indel (40 bp deletion)
0.66% Indel (56 bp deletion)
0.63% Indel
0.51% Indel
0.53% Indel
SPT16 siRNA: Top 10 Alleles
18.69% HDR
7.01% Wild Type
8.60% Indel
4.00% Indel
3.90% Indel (43 bp deletion)
2.31% Indel
0.96% Indel
0.87% Indel
0.80% Indel (60 bp deletion)
0.69% Indel
G
CD59 gRNA + NT siRNA
CD59 gRNA + SPT16 siRNA
VEGFA gRNA + NT siRNA
VEGFA gRNA + SPT16 siRNA
Frequency (%)
Index
Indel Size (bp)
No Indel
Indel

Figure 11: Effects of FACT Depletion and ssODN Inclusion on Cas9 Editing Outcomes

(A) Western blot of SPT16, SSRP1, dCas9, and GAPDH in K562 cells transfected with either NT or SPT16 siRNAs. (B) Indel rates from amplicon-NGS sequencing of eight different loci after electroporation of Cas9 RNPs in the absence of an HDR donor (n = 3 biological replicates). Data are represented as mean ± standard deviation ($p < 0.05$). (C) Total editing rates from amplicon-NGS sequencing of eight different loci after electroporation of Cas9 RNPs in the absence or presence of an HDR donor (n = 3 biological replicates). Data are represented as mean ± standard deviation ($p < 0.05$). (D) Total editing rates from amplicon-NGS sequencing of eight different loci after electroporation of Cas9 RNPs in the presence of an HDR donor (n = 3 biological replicates). Data are represented as mean ± standard deviation ($p < 0.05$). (E) Total editing rates from amplicon-NGS sequencing of VEGFA 0, 1, 2, 3, 6, 9, 12, and 24 hours after electroporation of Cas9 RNPs in the presence of an HDR donor (n = 3 biological replicates). Data are represented as mean ± standard deviation ($p < 0.05$). (F) Representative alleles from cells edited with Cas9 programmed with the VEGFA gRNA and a PAM-out ssODN HDR donor. (G) Histograms of indel distributions for CD59 and VEGFA plotted by indel abundance (top) or indel size (bottom).

Knockdown of FACT did not significantly alter indel frequencies measured after 48 h in the absence of an HDR donor (Figure 11B). Consistent with previous reports (Richardson et al., 2016a), inclusion of an ssODN donor increased total editing (indels plus HDR; Figure 11C). This increase in editing was consistent across all eight gRNAs tested and rescued otherwise relatively ineffective gRNAs.

In the presence of an ssODN, siRNA-mediated depletion of SPT16 did not affect total editing frequencies relative to the NT siRNA control 48 h after Cas9 RNP electroporation (Figure 11D). However, a time course of editing rates at one site (*VEGFA*; Figure 11E) revealed that SPT16 knockdown significantly impeded the rate of HDR (Figure 12A). HDR levels for SPT16-depleted cells was approximately 50% of that in NT siRNA-treated cells 12 h after electroporation of Cas9 RNPs (Figure 12A). Indels in SPT16-depleted cells were somewhat reduced at early timepoints but caught up to that of NT siRNA-treated cells within 24 h (Figure 12B). Measurements taken 48 h after electroporation indicate that SPT16 knockdown ultimately increased indel frequencies and concomitantly reduced HDR frequencies by up to 50% at multiple loci (Figures 12C and 12D). At the eight loci tested, we observed no marked difference in the effect of SPT16 knockdown on gRNAs that targeted the coding or non-coding strand (Figure 12C and 12D). Although knockdown of SPT16 did not alter the relative abundance of the five most common edited alleles containing indels for a *CD59* locus, depletion of FACT altered their absolute frequencies and the relative abundance of several alleles, each comprising less than 1% of all editing outcomes (Figure 12E). We found similar conservation of the most frequent allele but re-ordering of minor alleles after editing the *VEGFA* locus (Figure 11F). Both *CD59* and *VEGFA* loci possessed a long tail of rare editing outcomes that were mostly deletions (Figure 11G).

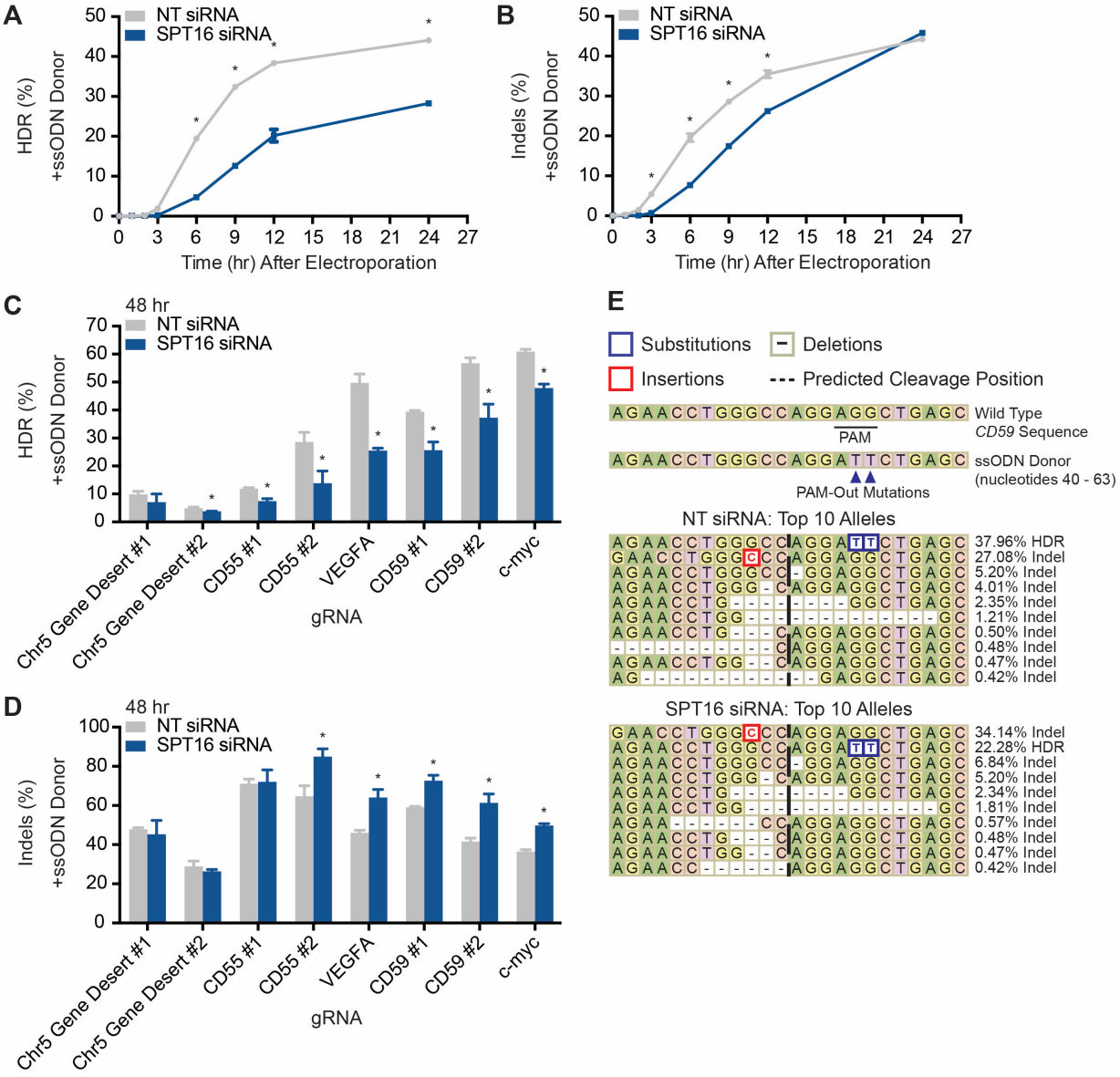

Figure 12: FACT Alters Cas9 Genome Editing Outcomes in Human Cells
(A) HDR rates from amplicon-NGS sequencing of *VEGFA* 0, 1, 2, 3, 6, 9, 12, and 24 h after electroporation of Cas9 RNPs in the presence of an HDR donor (n = 3 biological replicates). Data are represented as mean ± standard deviation ($p < 0.05$). See also Figure 11E. (B) Indel rates from amplicon-NGS sequencing of *VEGFA* 0, 1, 2, 3, 6, 9, 12, and 24 h after electroporation of Cas9 RNPs in the presence of an HDR donor (n = 3 biological replicates). Data are represented as mean ± standard deviation ($p < 0.05$). See also Figure 11E. (C) HDR rates from amplicon-NGS sequencing of eight different loci 48 h after electroporation of Cas9 RNPs in the presence of an HDR donor (n = 3 biological replicates). Data are represented as mean ± standard deviation ($p < 0.05$). See also Figure 11D. (D) Indel rates from amplicon-NGS sequencing of eight different loci 48 h after electroporation of Cas9 RNPs in the presence of an HDR donor (n = 3

biological replicates). Data are represented as mean ± standard deviation ($p < 0.05$). See also Figure 11D. (E) Representative alleles from cells edited with Cas9 programmed with a *CD59* gRNA and a PAM-out ssODN HDR donor. See also Figure 11G.

3.3.5 Knockdown of FACT Increases Epigenetic Marking and Transcriptional Phenotypes from dCas9-based Effectors in Human Cells

We next interrogated whether increased Cas9 residence times after FACT depletion influences the potency of dCas9-based transcriptional effectors that rely on the recruitment of epigenetic modifying enzymes to a target site. We specifically investigated whether FACT influences the deposition of chromatin marks by two different modifiers that can be fused to dCas9. The histone acetyltransferase p300 directly deposits H3K27ac marks on chromatin to upregulate transcription and has been deployed for CRISPR activation (CRISPRa) (Hilton et al., 2015). The Krüppel-associated box (KRAB) domain is a transcriptional repressor that recruits other factors to methylate histones and has been used for CRISPR interference (CRISPRi) (Gilbert et al., 2013).

We began by interrogating the role of FACT in dCas9-based histone acetylation. We generated HEK293T cells that stably express both dCas9-p300 and a gRNA targeting the *CD25* TSS on either the coding or non-coding strand (Figure 13A; Table S2). Also known as *IL2RA*, *CD25* encodes a subunit of the interleukin-2 receptor and is poorly expressed under basal conditions (Uhlen et al., 2015), but its expression can be induced using CRISPRa (Simeonov et al., 2017). We transfected NT or SPT16 siRNAs into dCas9-p300 cells expressing either a coding or non-coding strand gRNA (Figure 13B). Relative to the NT siRNA control, SPT16 depletion induced a significant increase in H3K27ac levels with either targeted gRNA according to qPCR using primers (Table S5) that amplified either a region upstream (Figure 14A) or inclusive (Figure 13C) of the protospacer. Knockdown of SPT16 did not increase basal histone acetylation when dCas9-p300 was paired with a NT gRNA (Figures 13C and 14A). siRNA knockdown of SSRP1 in the dCas9-p300 cell lines yielded similar increases in H3K27ac levels as knockdown of SPT16 (Figure 13D).

We used a similar approach to interrogate the role of FACT in dCas9-based histone methylation with K562 cells stably expressing dCas9-KRAB. We took advantage of conveniently located PAMs to target dCas9-KRAB to either the coding or non-coding strand of an identical location at the *CD55* TSS (Figure 13E). *CD55* is a ubiquitously and highly expressed gene (Uhlen et al., 2015) that encodes a cell surface glycoprotein involved in the complement system. Transfection of SPT16 siRNAs increased levels of H3K9 methylation when dCas9-KRAB was targeted with a gRNA to either the coding or non-coding strand (Figures 13F and 14B; Table S5). Knockdown of SPT16 did not increase basal histone methylation when dCas9-KRAB was paired with a NT gRNA (Figures 13F and 14B). We found similar increases in H3K9me2 using an siRNA against SSRP1 (Figure 13G).

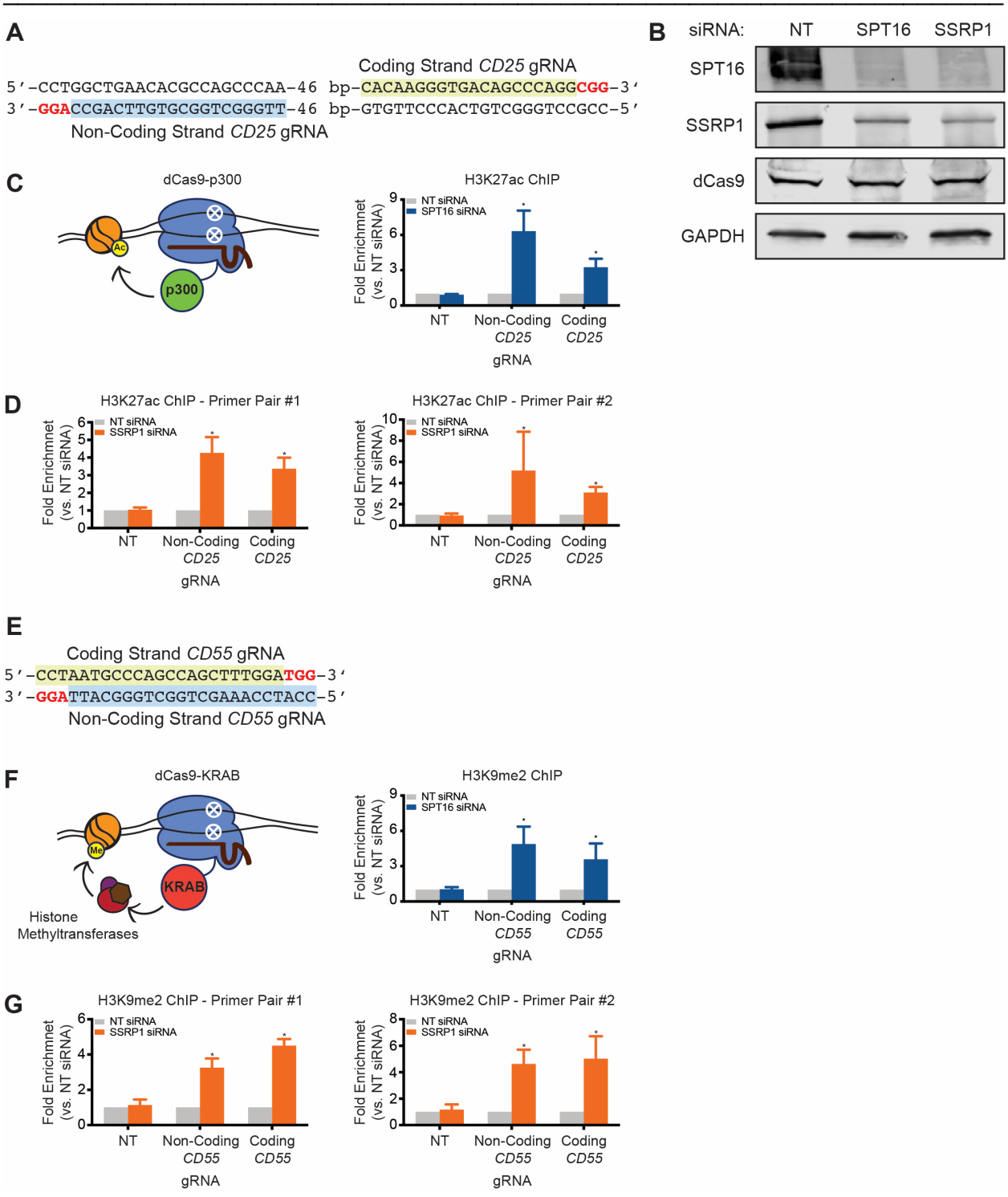

Figure 13: FACT Depletion Enhances Chromatin Marking by dCas9-p300 and dCas9-KRAB

(A) Schematic of coding and non-coding strand CD25 gRNAs. (B) Western blot of SPT16, SSRP1, dCas9, and GAPDH in HEK293T cells transfected with either NT,

SPT16, or SSRP1 siRNAs. (C) Knockdown of SPT16 increases H3K27 acetylation in HEK293T dCas9-p300 cells (n = 3 biological replicates). Fold enrichment is the amount of H3K27ac after SPT16 depletion normalized to the amount of H3K27ac after treatment with a NT siRNA. qPCR primers amplified regions that include the corresponding protospacer. Data are represented as mean ± standard deviation ($p < 0.05$). (D) Knockdown of SSRP1 increases H3K27 acetylation in HEK293T dCas9-p300 cells (n = 3 biological replicates). Fold enrichment is the amount of H3K27ac after SSRP1 depletion normalized to the amount of H3K27ac after treatment with a NT siRNA. qPCR primers amplified regions 9 base pairs upstream of the non-coding-strand gRNA protospacer and 46 base pairs upstream of the coding strand gRNA protospacer (Primer Pair #1) or regions that include the corresponding protospacers (Primer Pair #2). Data are represented as mean ± standard deviation ($p < 0.05$). (E) Schematic of coding and non-coding strand CD55 gRNAs. (F) Knockdown of SPT16 increases H3K9 methylation in K562 dCas9-KRAB cells (n = 3 biological replicates). Fold enrichment is the amount of H3K9me2 after SPT16 depletion normalized to the amount of H3K9me2 after treatment with a NT siRNA. qPCR primers amplified a region that include the protospacers. Data are represented as mean ± standard deviation ($p < 0.05$). (G) Knockdown of SSRP1 increases H3K9 methylation in K562 dCas9-KRAB cells (n = 3 biological replicates). Fold enrichment is the amount of H3K9me2 after SSRP1 depletion normalized to the amount of H3K9me2 after treatment with a NT siRNA. qPCR primers amplified a region 66 base pairs upstream of both the coding and non-coding strand gRNA protospacers (Primer Pair #1) or a region that includes the protospacers (Primer Pair #2). Data are represented as mean ± standard deviation ($p < 0.05$).

We asked whether increased epigenetic marking by dCas9-based effectors during knockdown of FACT translates into increased transcriptional phenotypes. Targeting dCas9-p300 to the *CD25* TSS with gRNAs at varying distances from the TSS (Table S2) generated cell populations that were between 12% and 95% CD25 positive, but knockdown of SPT16 did not further increase *CD25* expression for any gRNA tested (Figures 15A and 16).

Targeting dCas9-KRAB to the *CD55* TSS with gRNAs at varying distances from the TSS (Table S2) generated cell populations that were between 8% and 77% CD55-positive (Figures 14C, 14D, and 16). Notably, siRNA knockdown of SPT16 potentiated the degree of CRISPRi as measured by a decrease in CD55-positive cells (Figures 14C, 14D, and 16), with some CRISPRi cell populations exhibiting more than a 60% drop in CD55-positive cells upon SPT16 depletion. This transcriptional phenotype was observed regardless of the strand to which the gRNA bound. We found similar potentiation of CRISPRi transcriptional phenotypes after SPT16 knockdown when targeting *CD59* (Figures 14E, 14F, and 16), which is even more highly expressed on the cell surface than *CD55* (Uhlen et al., 2015). Increased CRISPRi was still dependent on proper targeting of dCas9-KRAB to the typical CRISPRi window around each gene's TSS (Gilbert et al., 2013), as targeting dCas9-KRAB several kilobase pairs downstream of the TSS was ineffective even during knockdown of FACT (Figures 15B and 16).

Similarly, localizing dCas9 unattached to an effector at various distances from the *CD55* or *CD59* TSSs did not affect transcription even after SPT16 knockdown (Figures 15C, 15D, and 16).

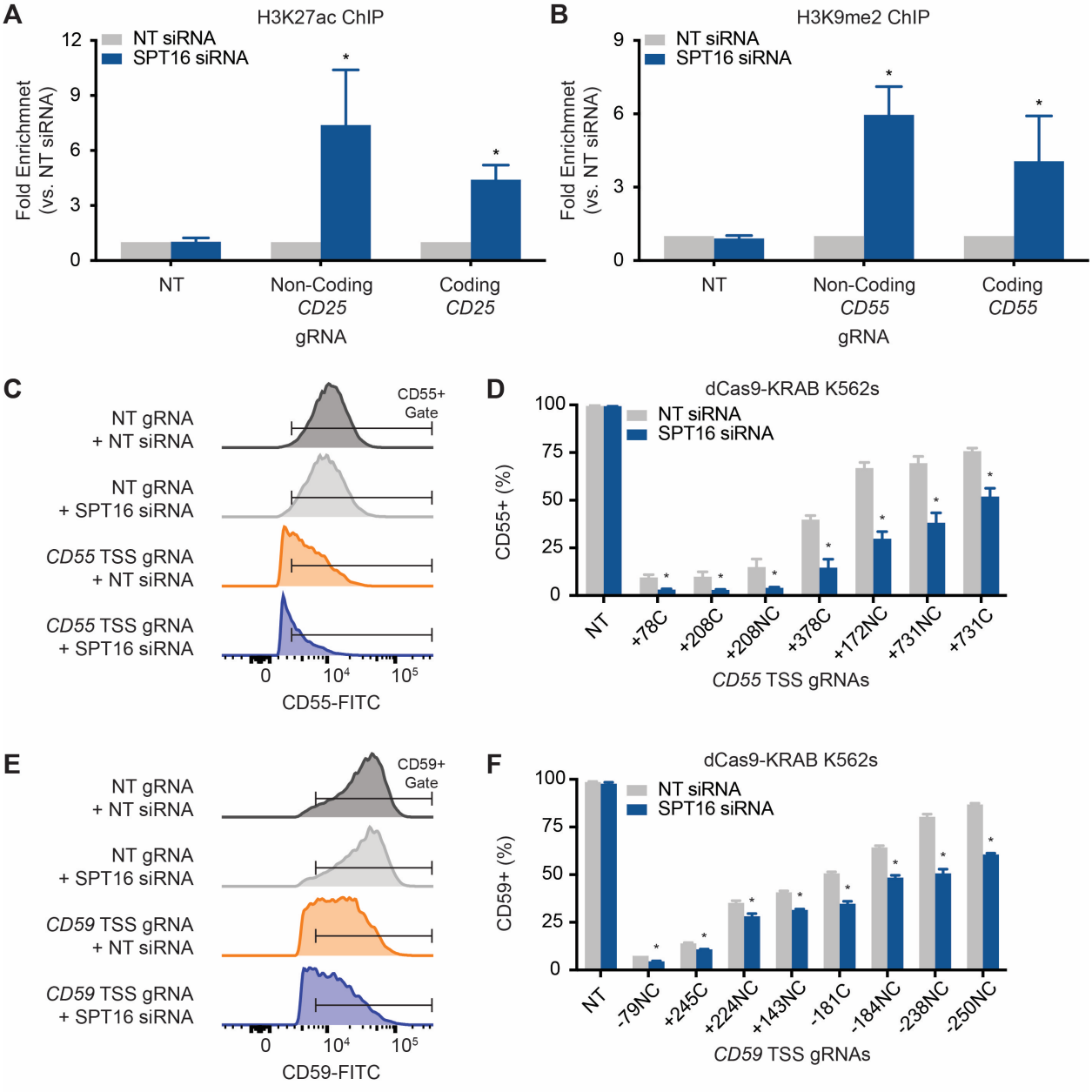

Figure 14: FACT Depletion Increases Epigenetic Marking and Transcriptional Phenotypes From dCas9-based Effectors in Human Cells

(A) Knockdown of SPT16 increases H3K27 acetylation in HEK293T dCas9-p300 cells (n = 3 biological replicates). Fold enrichment is the amount of H3K27ac after SPT16 depletion normalized to the amount of H3K27ac after treatment with a NT siRNA. qPCR primers amplified a region 9 bp upstream of the non-coding-strand gRNA protospacer and 46 bp upstream of the coding strand gRNA protospacer. Data are represented as

mean ± standard deviation ($p < 0.05$). See also Figure 13. (B) Knockdown of SPT16 increases H3K9 methylation in K562 dCas9-KRAB cells (n = 3 biological replicates). Fold enrichment is the amount of H3K9me2 after SPT16 depletion normalized to the amount of H3K9me2 after treatment with a NT siRNA. qPCR primers amplified a region 66 bp upstream of both the non-coding and coding strand gRNA protospacers. Data are represented as mean ± standard deviation ($p < 0.05$). See also Figure 13. (C) Representative histograms of CD55 levels in CRISPRi cells after treatment with NT or SPT16 siRNAs. (D) FACT depletion enhances dCas9-KRAB-mediated knockdown of *CD55* in K562 cells expressing *CD55* TSS gRNAs (n = 3 biological replicates). CRISPRi cells were stained with fluorescein isothiocyanate (FITC) anti-CD55 after transfection of either NT or SPT16 siRNAs. gRNAs bind to either the coding (C) or non-coding (NC) strand and are labeled according to their distance in base pairs from the TSS. Data are represented as mean ± standard deviation ($p < 0.05$). See also Figure 15. (E) Representative histograms of CD59 levels in CRISPRi cells after treatment with NT or SPT16 siRNAs. (F) FACT depletion enhances dCas9-KRAB-mediated knockdown of *CD59* in K562 cells expressing *CD59* TSS gRNAs (n = 3 biological replicates). CRISPRi cells were stained with FITC anti-CD59 after transfection of either NT or SPT16 siRNAs. gRNAs are labeled as in (D). Data are represented as mean ± standard deviation ($p < 0.05$). See also Figure 15.

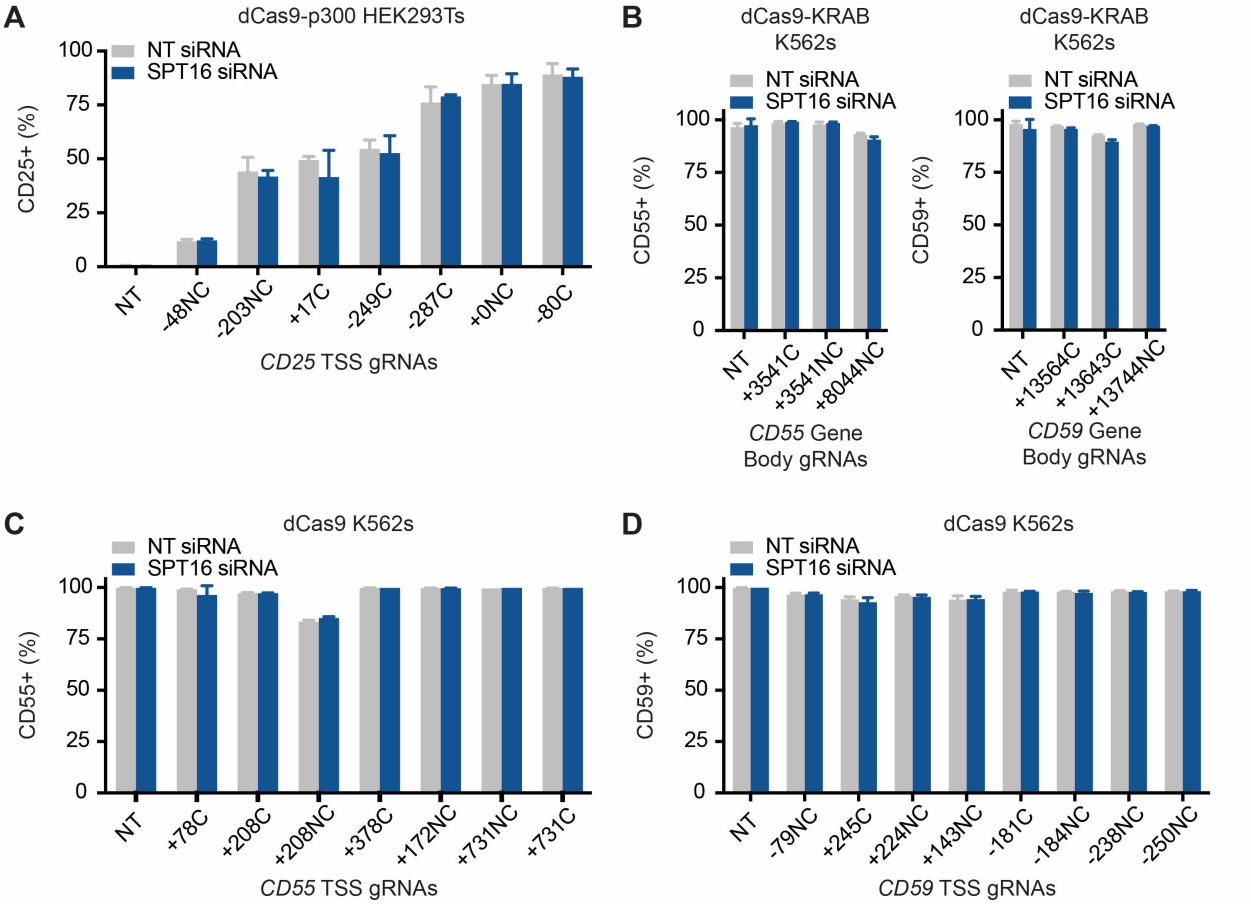

Figure 15: Enhancement of Transcriptional Engineering After FACT Depletion Requires Localizing KRAB Domain to TSSs

(A) FACT depletion does not affect *CD25* expression in HEK293T dCas9-p300 cells expressing *CD25* TSS gRNAs (n = 3 biological replicates). CRISPRa cells were stained with PE anti-CD25 after transfection of either NT or SPT16 siRNAs. gRNAs are labeled as in Figure 14D. Data are represented as mean ± standard deviation ($p < 0.05$). (B) Knockdown of FACT does not affect *CD55* (left) or *CD59* (right) expression in K562 dCas9-KRAB cells expressing *CD55* or *CD59* gene body gRNAs (n = 3 biological replicates). gRNAs are labeled as in Figure 14D. Data are represented as mean ± standard deviation ($p < 0.05$). (C) Knockdown of FACT does not affect *CD55* expression in K562 dCas9 cells expressing *CD55* TSS gRNAs (n = 3 biological replicates). gRNAs are labeled as in Figure 14D. Data are represented as mean ± standard deviation ($p < 0.05$). (D) Knockdown of FACT does not affect *CD59* expression in K562 dCas9 cells expressing *CD59* TSS gRNAs (n = 3 biological replicates). gRNAs are labeled as in Figure 14D. Data are represented as mean ± standard deviation ($p < 0.05$).

Figure 16: Histograms of CD25, CD55, and CD59 Levels After SPT16 Knockdown

The ability of FACT to displace Cas9 off DNA raises the possibility that other histone chaperones or chromatin remodelers are capable of carrying out the same activity. A recent screen of factors influencing repair of Cas9 breaks with a plasmid double-stranded donor DNA identified several components of the INO80 complex (Wienert et al., 2020). INO80 is a multi-subunit ATP-dependent chromatin remodeler with roles in DNA repair, transcription, and replication (Conaway and Conaway, 2009; Gospodinov et al., 2011; Morrison and Shen, 2009). One of the most significant hits was INO80B (Wienert et al., 2020). We thus asked whether depletion of INO80B similarly affected editing outcomes and the efficacy of dCas9-based transcriptional effectors. Depletion of INO80 (Figure 17A) did not alter indel rates in the absence of an ssODN donor (Figure 17B) or total editing rates in the presence of an ssODN donor (Figure 17C). However, INO80B depletion significantly decreased HDR rates and increased indel rates across several sites in the presence of an ssODN donor (Figures 17D and 17E).

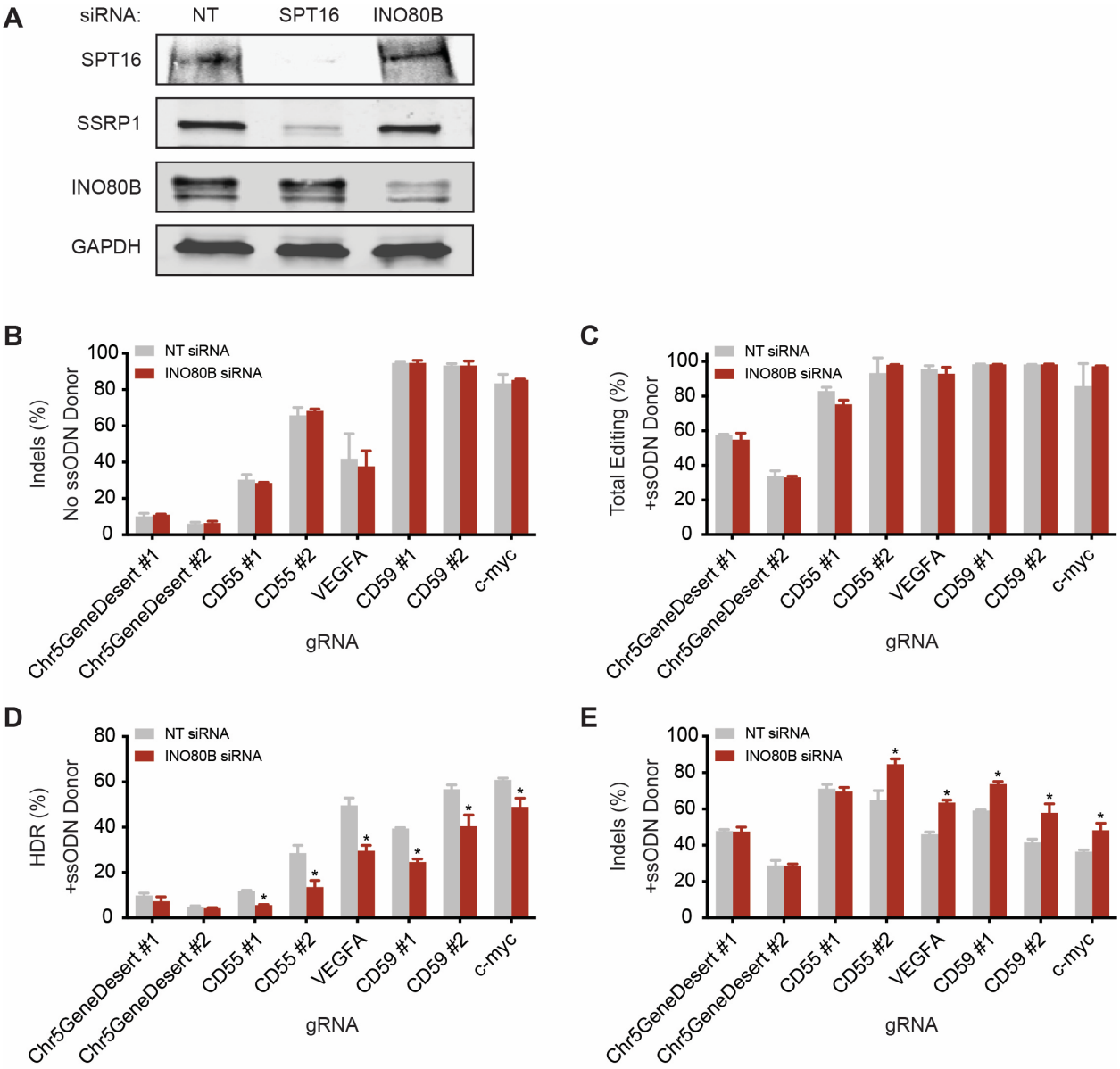

Figure 17: INO80B Alters Cas9 Genome Editing Outcomes in Human Cells
(A) Western blot of SPT16, SSRP1, INO80B, and GAPDH in K562 cells transfected with either NT, SPT16, or INO80B siRNAs. (B) Indel rates from amplicon-NGS sequencing of eight different loci after electroporation of Cas9 RNPs in the absence of an HDR donor (n = 3 biological replicates). Data are represented as mean ± standard deviation ($p < 0.05$). (C) Total editing rates from amplicon-NGS sequencing of eight different loci after electroporation of Cas9 RNPs in the presence of an HDR donor (n = 3 biological replicates). Data are represented as mean ± standard deviation ($p < 0.05$). (D) HDR rates from amplicon-NGS sequencing of eight different loci 48 h after electroporation of Cas9 RNPs in the presence of an HDR donor (n = 3 biological replicates). Data are represented as mean ± standard deviation ($p < 0.05$). (E) Indel rates from amplicon-

NGS sequencing of eight different loci 48 h after electroporation of Cas9 RNPs in the presence of an HDR donor (n = 3 biological replicates). Data are represented as mean ± standard deviation ($p < 0.05$).

We next interrogated whether INO80B knockdown also enhanced the potency of dCas9-based transcriptional effectors. Similar to FACT depletion, INO80B depletion induced a significant increase in H3K27ac levels in dCas9-p300 cells co-expressing *CD25* gRNAs according to qPCR primers amplifying a region either upstream (Figure 18A) or inclusive (Figure 18B) of the protospacer. INO80B depletion also increased H3K9me2 levels in dCas9-KRAB cells co-expressing *CD55* gRNAs according to qPCR primers amplifying a region either upstream (Figure 18C) or inclusive (Figure 18D) of the protospacer.

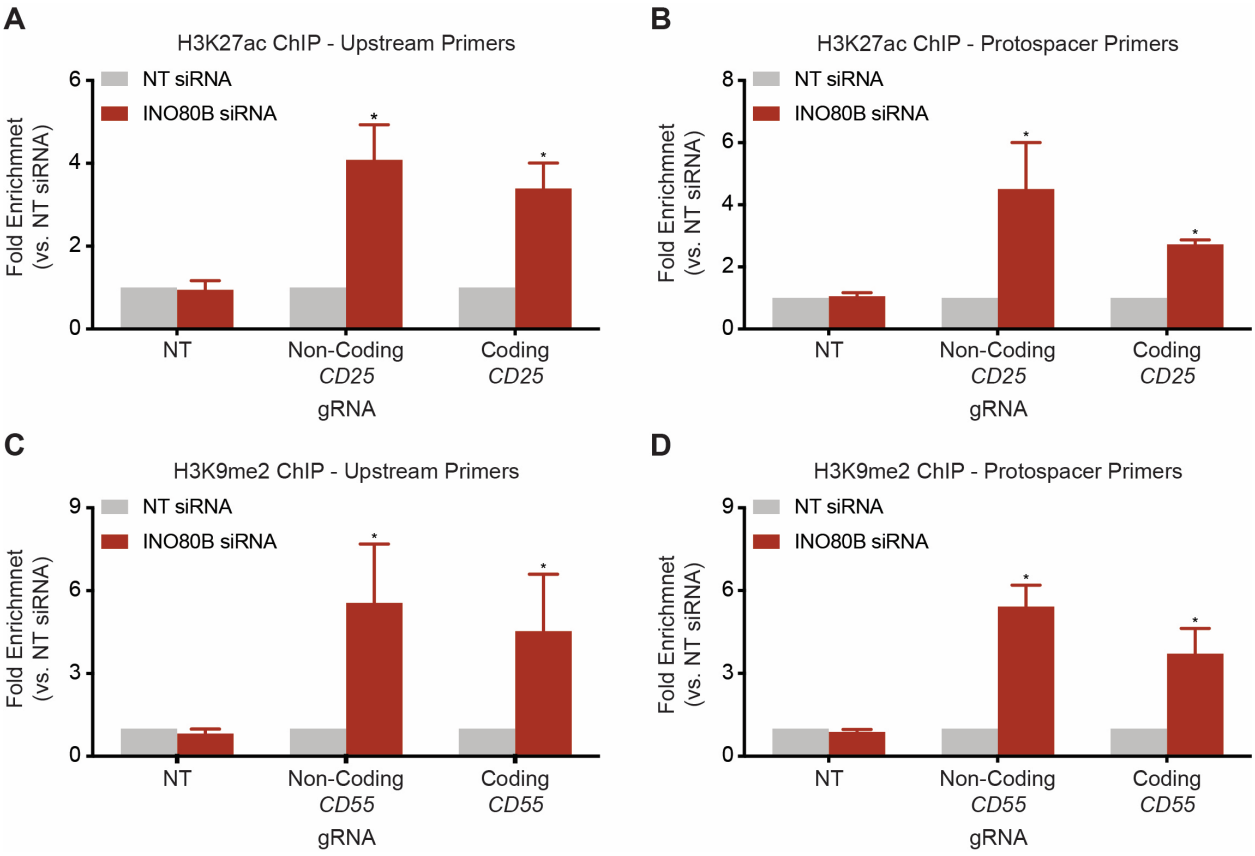

Figure 18: INO80B Depletion Increases Epigenetic Marking from dCas9-based Effectors in Human Cells
(A) Knockdown of INO80B increases H3K27 acetylation in HEK293T dCas9-p300 cells (n = 3 biological replicates). Fold enrichment is the amount of H3K27ac after INO80B depletion normalized to the amount of H3K27ac after treatment with a NT siRNA. qPCR primers amplified a region upstream of the protospacer. Data are represented as mean ± standard deviation ($p < 0.05$). (B) Knockdown of INO80B increases H3K27 acetylation in HEK293T dCas9-p300 cells (n = 3 biological replicates). Fold enrichment is the

amount of H3K27ac after INO80B depletion normalized to the amount of H3K27ac after treatment with a NT siRNA. qPCR primers amplified a region inclusive of the protospacer. Data are represented as mean ± standard deviation ($p < 0.05$). (C) Knockdown of INO80B increases H3K9 methylation in K562 dCas9-KRAB cells (n = 3 biological replicates). Fold enrichment is the amount of H3K9me2 after INO80B depletion normalized to the amount of H3K9me2 after treatment with a NT siRNA. qPCR primers amplified a region upstream of the protospacer. Data are represented as mean ± standard deviation ($p < 0.05$). (D) Knockdown of INO80B increases H3K9 methylation in K562 dCas9-KRAB cells (n = 3 biological replicates). Fold enrichment is the amount of H3K9me2 after INO80B depletion normalized to the amount of H3K9me2 after treatment with a NT siRNA. qPCR primers amplified a region inclusive of the protospacer. Data are represented as mean ± standard deviation ($p < 0.05$).

We also tested whether the increased epigenetic levels generated after INO80B knockdown translates into increased transcriptional phenotypes. In dCas9-KRAB cells co-expressing *CD55* gRNAs, INO80B depletion significantly potentiated CRISPRi phenotypes as measured by a decrease in CD55-positive cells (Figure 19A). The decreases in the percentage of CD55-positive cells were observed regardless of the strand to which the gRNA bound. Similar to FACT knockdown, INO80B knockdown did not affect CD55 levels in cells expressing dCas9 unattached to any effector. We observed a similar set of phenotypes in dCas9-KRAB (Figure 19C) and dCas9 (Figure 19D) cells expressing *CD59* gRNAs.

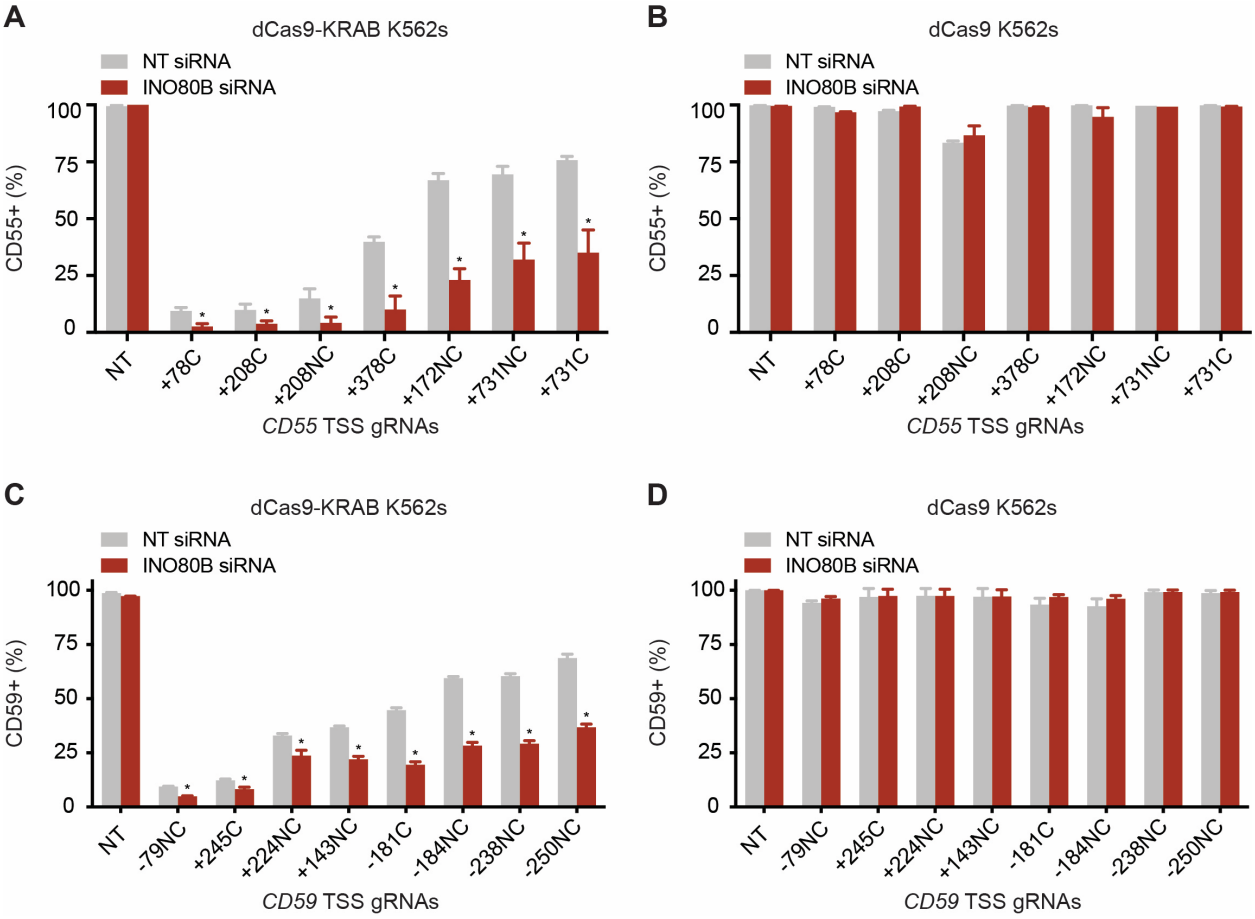

Figure 19: INO80B Depletion Increases Transcriptional Phenotypes From dCas9-based Effectors in Human Cells

(A) INO80B depletion enhances dCas9-KRAB-mediated knockdown of *CD55* in K562 cells expressing *CD55* TSS gRNAs (n = 3 biological replicates). CRISPRi cells were stained with FITC anti-CD55 after transfection of either NT or INO80B siRNAs. gRNAs are labeled as in Figure 14D. Data are represented as mean ± standard deviation ($p < 0.05$). (B) Knockdown of INO80B does not affect *CD55* expression in K562 dCas9 cells expressing *CD55* TSS gRNAs (n = 3 biological replicates). gRNAs are labeled as in Figure 14D. Data are represented as mean ± standard deviation ($p < 0.05$). (C) INO80B depletion enhances dCas9-KRAB-mediated knockdown of *CD59* in K562 cells expressing *CD59* TSS gRNAs (n = 3 biological replicates). CRISPRi cells were stained with FITC anti-CD59 after transfection of either NT or INO80B siRNAs. gRNAs are labeled as in Figure 14D. Data are represented as mean ± standard deviation ($p < 0.05$). (D) Knockdown of INO80B does not affect *CD59* expression in K562 dCas9 cells expressing *CD59* TSS gRNAs (n = 3 biological replicates). gRNAs are labeled as in Figure 14D. Data are represented as mean ± standard deviation ($p < 0.05$).

3.4 Discussion

Programmable prokaryotic nucleases, such as Cas9, are widely used for eukaryotic genome and transcriptome manipulation, but it is largely unclear how host cells interface with these foreign enzymes. Although several studies have uncovered how histones impede Cas9 target search and binding (Horlbeck et al., 2016b; Isaac et al., 2016; Kallimasioti-Pazi et al., 2018; Knight et al., 2015; Yarrington et al., 2018), none have described how proteins responsible for restructuring and remodeling nucleosomes might affect Cas9. We have found that the histone chaperone FACT is required for Cas9 unloading and multi-turnover activity in cell-free extract. In live human cells, direct observations of dCas9 turnover at a synthetic array revealed that FACT promoted displacement of dCas9. Knockdown of FACT also inhibited templated repair of Cas9-induced breaks, increased indel formation, and increased the efficacy of dCas9-based transcriptional effectors.

We observed similar editing and transcriptional phenotypes with knockdown of INO80B, one of the components of the ATP-dependent INO80 chromatin remodeler. Our data do not rule out the potential importance of other histone chaperones or chromatin remodelers in genome surveillance and Cas9 displacement but highlight prominent roles of FACT and INO80 in this process.

FACT not only maintains nucleosome integrity by tethering the H3-H4 tetramer to DNA and helping deposit H2A-H2B dimers after displacement but also promotes nucleosome disassembly by dislodging H2A-H2B dimers and uncoiling DNA (Chen et al., 2018b; Gurova et al., 2018; Hsieh et al., 2013; Kemble et al., 2015; Valieva et al., 2016; Winkler et al., 2011). Cas9 is a prokaryotic enzyme never before seen by eukaryotic histone chaperones, making it unlikely that FACT specifically recognizes Cas9. The simplest model is that FACT's nucleosome-displacing capabilities allow it to displace genomic roadblocks, such as Cas9. Indeed, a recent structure of FACT bound to a nucleosome reveals that FACT primarily contacts the double-stranded DNA and makes only peripheral interactions with histones (Liu et al., 2020). This finding could imply that FACT scans genomic DNA looking for impediments and helps resolve them when encountered.

Modulating the turnover of Cas9 from a eukaryotic genome could inform the extent to which genome editing and transcriptional regulation rely upon repeated rounds of Cas9 binding and eviction. Indeed, we found that knockdown of FACT had no effect on basal epigenetic marking when dCas9-p300 or dCas9-KRAB was paired with a NT gRNA but increased specific epigenetic marking when either effector was guided to multiple target sites. The situation of DNA double-strand break repair is more complex. Kinetic analysis of Cas9-induced break repair has suggested that cells primarily invoke error-prone pathways to slowly repair Cas9 damage in a single round (Brinkman et al., 2018). Conversely, experiments inducing adjacent Cas9 breaks or modulating DNA repair with non-homologous single-stranded DNA implied that cells invoke error-free repair pathways that enable repeated rounds of Cas9 binding and eviction preceding eventual end-point mutation (Guo et al., 2018; Richardson et al., 2016a; Wang et al., 2019). We

found that knockdown of FACT reduced Cas9-induced HDR and increased indels, which might imply that the balance between HDR and indels is influenced by multiple rounds of Cas9 cleavage and turnover. However, we note that histone chaperones and chromatin remodelers can also directly influence DNA repair through both direct and indirect mechanisms (Aleksandrov et al., 2018; Ayrapetov et al., 2014; Gospodinov et al., 2011; Lademann et al., 2017; Lans et al., 2012; Piquet et al., 2018; Price and D'Andrea, 2013). For example, FACT helps recruit DNA repair factors such as RNF20 (Oliveira et al., 2014). However, enforced chromatin relaxation and reduced nucleosome occupancy are sufficient to promote RNF20 localization, H2AX deposition, and end resection (Kari et al., 2011; Oliveira et al., 2014; Piquet et al., 2018). It is still unclear whether Cas9 owes its genome editing prowess to single-turnover or multi-turnover kinetics, but it is likely that the same nucleosome remodeling activity that promotes Cas9 displacement also promotes HDR.

Although Cas9 unloading within *X. laevis* egg extracts is ATP-dependent, FACT activity is ATP-independent (Orphanides et al., 1998). Notably, we found that depletion of ATP or immunodepletion of FACT are both sufficient to abrogate the multi-turnover behavior of Cas9 in *Xenopus* extract. It is possible that egg extracts actively recruit FACT to DNA-bound Cas9 and dCas9 in an ATP-dependent manner. We note that the most enriched factor in our proteomics data set is the lipid kinase PIP4K2C, and recent work has revealed that phosphoinositides localize around DNA lesions to recruit proteins through the lipids' associations with pleckstrin homology (PH) domains (Wang et al., 2017). Intriguingly, both SPT16 and SSRP1 contain PH domains (Kemble et al., 2013; Zhang et al., 2015), but a great deal of additional work is necessary to determine if lipid metabolism around the R-loop generated by Cas9 binding is responsible for recruitment of FACT to Cas9.

Although RNA polymerases are capable of dislodging Cas9 in a strand-specific manner *in vitro* (Clarke et al., 2018), our data argue that FACT plays a prominent role in Cas9 removal within eukaryotic systems. Although FACT is often associated with transcription (Mason and Struhl, 2003; Saunders et al., 2003), it possesses nucleosome remodeling activity separate from RNA polymerases. The egg extract we employed is transcriptionally silent and does not initiate DNA replication (Lebofsky et al., 2009), indicating that basal FACT activity decoupled from transcription or replication within egg extract may be sufficient to remove Cas9 from its substrate. Although previous studies have reported RNA polymerase-mediated displacement of Cas9 bound to the non-coding strand (Clarke et al., 2018), we and others have found no strand bias in dCas9-based epigenetic reprogramming (Gilbert et al., 2013; Hilton et al., 2015; Konermann et al., 2015; Qi et al., 2013).

Targeting dCas9 downstream of a TSS in *E. coli* effectively suppresses gene expression presumably because dCas9 acts as a potent transcriptional roadblock to the bacterial RNA polymerase (Qi et al., 2013). Transcriptional reprogramming in human cells is less effective with dCas9 alone and is greatly increased by recruitment of an epigenetic modifier (Gilbert et al., 2013; Qi et al., 2013), suggesting that dCas9 is not a major roadblock to human RNA polymerases. We found that depleting FACT increased

epigenetic marking and CRISPRi phenotypes for both coding and non-coding gRNAs across multiple loci. Notably, we also found that depleting FACT was insufficient to turn dCas9 alone into a transcriptional roadblock. These results indicate that either human RNA polymerases can displace Cas9 or dCas9 occupancy is so low to begin with that any small increase in dCas9 residence times after FACT depletion is not sufficient to generate a detectable effect on transcription. These results are consistent with Cas9's utility as a generalized genome editing tool effective at editing both highly transcribed genes and transcriptionally silent regions.

FACT's Cas9-displacing activity markedly influences epigenetic reprogramming by dCas9-fused effectors. Knockdown of FACT in dCas9-p300 cells induced an up to 7-fold increase in histone acetylation. However, FACT depletion did not increase CRISPRa transcriptional phenotypes in these cells, even though recruiting histone acetyltransferases, such as p300, has been previously shown to effectively upregulate transcription (Hilton et al., 2015). These results thus suggest that factors beyond histone acetylation are the critical bottlenecks to increased *CD25* expression. By contrast, increasing dCas9-KRAB's residence time by globally downregulating FACT potentiates both dCas9-based histone methylation and transcriptional downregulation. This downregulation was evident only when we localized the KRAB domain around TSSs. Together with prior observations that Cas9-effectors are ineffective as short-lived RNPs but potent when expressed through permanent lentiviral constructs, our data suggest that the effectiveness of CRISPRi depends upon dCas9's residence time at a TSS. Future approaches might specifically increase residence time without affecting other genome transactions.

3.5 Methods

3.5.1 Data and Code Availability

The accession number for the amplicon-NGS data reported in this paper is SRA:PRJNA634106. Code for amplicon sequencing data processing is available at https://github.com/staciawyman/cortado.

3.5.2 Experimental Model and Subject Details

HEK293T dCas9-p300 cells were a generous gift from Dr. Charles Gersbach. Parental K562 cells were acquired from the UC Berkeley Cell Culture Facility. K562 dCas9-KRAB were identical to those previously reported (Richardson et al., 2018). U2OS cells in which a cassette of *tetO* and *lacO* sequences had been integrated at high copy number at a single genomic locus (Janicki et al., 2004) were modified to stably express dCas9-HaloTag with a puromycin selection marker, and individual clones were isolated by limiting dilution. All cells were regularly tested for mycoplasma contamination. HEK293T and U2OS cells were maintained in DMEM with glutamax (GIBCO) supplemented with 10% fetal bovine serum, 1% sodium pyruvate (GIBCO), and 100 U/ml penicillin-streptomycin (GIBCO). dCas9-HaloTag expressing cells were also maintained in 0.5 μg/ml puromycin and 50 μg/ml hygromycin. K562 cells were

maintained in RPMI (GIBCO) supplemented with 10% fetal bovine serum, 1% sodium pyruvate, and 100 U/ml penicillin-streptomycin. All cells were maintained at 37°C with 5% CO_2.

3.5.3 X. laevis HSS

X. laevis HSS was prepared as previously described (Lebofsky et al., 2009). Aliquots were snap frozen and thawed as necessary. To immunodeplete SSRP1, HSS diluted 1:10 in Unloading Buffer (20 mM Tris pH 7.5, 100 mM KCl, 5 mM $MgCl_2$, 1 mM DTT, 0.01% Tween) was exposed to two rounds of SSRP1 antibody. For each round, 150 μl of Dynabeads™ Protein G (Thermo Fisher Scientific) was washed three times in PBS, resuspended in 35 μg of SSRP1 antibody (Santa Cruz Biotechnology # sc-74536) and 825 μl of PBS, incubated with rotation for 90 min at room temperature, washed three times with PBST, resuspended in 2.4 μl of HSS diluted 1:10 in Unloading Buffer to 24 μl, and mixed for 45 min at room temperature. SPT16 antibody was generously provided by Dr. Hasan Yardimci. To immunodeplete SPT16, HSS was incubated with two rounds of 200 μl SPT16 antibody conjugated to 150 μl of Dynabeads™ Protein G. Mock depletions were conducted with the same amount of IgG antibody (BioLegend #400101).

3.5.4 Cas9, FACT, RNA, and Donor DNA Preparation

Streptococcus pyogenes Cas9 (pMJ915, Addgene #69090) with two nuclear localization signal sequences and an HA tag at the C-terminus (Lin et al., 2014) was expressed in Rosetta2 DE3 (QB3-Berkeley Macrolab) cells. Cell pellets were sonicated, clarified, Ni^{2+}-affinity purified (HisTraps, GE Life Sciences), TEV cleaved, cation-exchanged (HiTrap SP HP, GE Life Sciences), size excluded (Sephacryl S-200, GE Life Sciences) and eluted at 40 μM in 20 mM HEPES KOH pH 7.5, 5% glycerol, 150 mM KCl, and 1 mM DTT. dCas9, Cas9-BirA*, and dCas9-BirA* were similarly expressed and purified. Recombinant human FACT was generously provided by Dr. Danny Reinberg. gRNAs were generated by HiScribe™ (New England Biolabs) T7 *in vitro* transcription using PCR-generated DNA as a template and purified using RNeasy Mini columns (QIAGEN) (dx.doi.org/10.17504/protocols.io.dm749m). ssODN donor DNA was obtained by ordering unmodified ultramer oligonucleotides (Integrated DNA Technologies). For generation of stable cell lines, gRNAs were cloned into the lentiviral pLG1-library vector (Addgene #84832) as previously described (Horlbeck et al., 2016a).

3.5.5 Multi-Turnover Cas9 Activity

84 fmol of Cas9 diluted in Unloading Buffer to a volume of 1 μl was added to 504 fmol of gRNA diluted in Unloading Buffer to a volume of 0.5 μl. Cas9 and gRNA were incubated for 15 min at room temperature. 168 fmol of either linear or plasmid substrate was then added to the RNPs, and reaction mixtures were incubated for 45 min at room temperature. Next, either 3 μl of Unloading Buffer and 1 μl of 100 mM ATP, 3 μl of

diluted HSS (1:8 in Unloading Buffer) and 1 μl of 100 mM ATP, 3 μl of mock-depleted and diluted HSS (1:8 in Unloading Buffer) and 1 μl of 100 mM ATP, 3 μl of SSRP1-depleted and diluted HSS (1:8 in Unloading Buffer) and 1 μl of 100 mM ATP, or 3 μl of diluted HSS (1:8 in Unloading Buffer) supplemented with CIP, ATPγS, and 1 μl of Unloading Buffer were added. 0.5 μl of CIP (New England Biolabs) and 0.6 μl of 34 mM ATPγS (Sigma-Aldrich) was added to every 18 μl of diluted HSS for the final condition. An additional 3 μl of Unloading Buffer and 1 μl of 100 mM ATP, 3 μl of diluted HSS (1:8 in Unloading Buffer) and 1 μl of 100 mM ATP, 3 μl of mock-depleted and diluted HSS (1:8 in Unloading Buffer) and 1 μl of 100 mM ATP, 3 μl of SSRP1-depleted and diluted HSS (1:8 in Unloading Buffer) and 1 μl of 100 mM ATP, or 3 μl of diluted HSS (1:8 in Unloading Buffer) supplemented with CIP and ATPγS and 1 μl of Unloading Buffer were added to the corresponding samples after 5, 10, 30, 60, 90, 120, and 150 min. Samples were mixed with Proteinase K (Sigma), incubated at 50°C for 30 min, and run on an agarose gel.

3.5.6 Plasmid Protection in HSS

504 fmol of the on-target gRNA diluted in 0.5 μl of Unloading Buffer was added to either 0.5 μl of Unloading Buffer, 420 fmol of dCas9 diluted in 0.5 μl of Unloading Buffer, or 420 fmol of BirA*-dCas9 diluted in 0.5 μl of Unloading Buffer. Samples were incubated at room temperature for 15 min, added to 84 fmol of plasmid DNA diluted in 2.0 μl of Unloading Buffer, and incubated for 45 min at room temperature. Either 18 μl of Unloading Buffer, 18 μl of HSS supplemented with 0.55 μl of ARS, or 18 μl of HSS supplemented with 0.5 μl of CIP (New England Biolabs) and 0.6 μl of 34 mM ATPγS (Sigma-Aldrich) was added to the reaction mixtures. A stock solution of ARS was generated by mixing 10 μl of 100 mM ATP (VWR), 5 μl of 2 M phosphocreatine (Sigma-Aldrich), and 0.5 μl of 5 mg/ml creatine phosphokinase (Sigma-Aldrich). Samples were incubated for 15 min at room temperature. Next, either 1 μl of Unloading Buffer or 4.2 pmol of Cas9 diluted in 0.5 μl of Unloading Buffer pre-complexed with 5.04 pmol of the on-target gRNA diluted in 0.5 μl of Unloading Buffer was added to the reaction mixtures and incubated for 30 min. Samples were incubated with Proteinase K (Sigma-Aldrich) at 50°C for 30 minutes and then run on an agarose gel. The percentage of linear DNA was quantified through ImageJ. For the single-turnover protection assay using immunodepleted extracts, either 18 μl of diluted HSS (1:10 in Unloading Buffer) that was mock-depleted, 18 μl of diluted HSS (1:10 in Unloading Buffer) depleted of SSRP1, or 18 μl of diluted HSS (1:10 in Unloading Buffer) depleted of SPT16 was added to the RNPs after the 45 min incubation with the plasmid.

For FACT add-back experiments, 2 μg of recombinant human FACT was added to 18 μl of diluted HSS (1:10 in Unloading Buffer) immunodepleted of SSRP1 or SPT16 and incubated with pre-formed dCas9 RNP-plasmid complexes for 4 hours at room temperature prior to addition of Cas9 RNPs.

3.5.7 Mass Spectrometry

5.04 pmol of the on-target gRNA diluted in 14 μl of Unloading Buffer was added to 4.2 pmol of either Cas9-BirA* or dCas9-BirA*. As a reference sample, 5.04 pmol of a non-targeting gRNA diluted in 14 μl of Unloading Buffer was added to 4.2 pmol of dCas9-BirA*. RNPs were incubated at room temperature for 15 min. Samples were then added to 52.4 pmol of plasmid DNA, and reaction mixtures were incubated for 45 min at room temperature. 45 μl of HSS supplemented with 1.36 μl of ARS and biotin at a final concentration at 5 μM was added to these samples, and the resulting solutions were incubated for 60 min at room temperature. 405 μl of Unloading Buffer, 2.5 μl of Apyrase (New England Biolabs), and 56.25 μl of Apyrase Buffer was added to samples, which were incubated at 30°C for 15 minutes. 25 μl of DNase I (New England Biolabs) and 56.26 μl of DNase I Buffer were then added to samples, which were incubated at 37°C for 15 minutes. Samples were diluted 1:2 in Unloading Buffer and then mixed with 250 μl of MyOne™ Streptavidin C1 Dynabeads™ (Thermo Fisher Scientific) that had been washed three times in 50 mM Tris pH 7.4, 500 mM NaCl, 0.4% SDS, 5 mM EDTA, and 1 mM DTT. Samples were incubated overnight at 4°C with rotation.

Beads were washed once with 1 ml of 0.1% sodium deoxycholate, 1% Triton X-100, 500 mM NaCl, 1 mM EDTA, and 50 mM HEPES pH 7.5, once with 1 ml of 250 mM LiCl, 0.5% NP-40, 0.5% sodium deoxycholate, 1 mM EDTA, 10 mM Tris pH 8.1, and twice with 1 ml of 50 mM Tris pH 7.4, 50 mM NaCl. Beads were then washed five times with 1 ml of 50 mM ammonium bicarbonate and then resuspended in 100 μl of 50 mM ammonium bicarbonate containing 0.01% ProteaseMAX (Promega) and 3 μg of sequencing-grade trypsin (Promega). Samples were incubated with mixing at 37°C for 4 hours after which the supernatant was collected and transferred to a new tube. Beads were washed again with 50 μl of 50 mM ammonium bicarbonate, and supernatants were pooled. 2 μl of formic acid (Fisher Scientific) was added to acidify the samples to a pH of ~3.0. Samples were then spun down to dryness in a speedvac and submitted to the University of California, Davis Proteomics Core for Multi-Dimension Protein Identification Technology mass spectrometry. Trypsinized peptides were mapped to the *X. laevis* proteome using the PHROG database (Wuhr et al., 2014). Protein enrichment levels were analyzed by the Limma Bioconductor package.

3.5.8 Western Blots

For *X. laevis* HSS, samples of equal volumes were incubated with Laemmli Buffer (Bio-Rad) at 95°C for 5 min. For human tissue culture, cells were washed in PBS and then lysed in 1X RIPA Buffer (Millipore Sigma) supplemented with Halt™ Protease Inhibitors (Thermo Fisher Scientific) at 4°C for 60 min. Samples were spun down at 15,000 g for 15 min, and the protein concentrations of the cleared lysates were measured using a BCA Protein Assay Kit (Thermo Fisher Scientific). 30 ug of lysate was denatured by incubation with Laemmli Buffer at 95°C for 5 min.

Both *X. laevis* and mammalian protein samples were resolved on Mini-PROTEAN® TGX™ 4-20% gels (Bio-Rad), and resolved proteins were transferred (TransBlot Turbo, Bio-Rad) to nitrocellulose membranes. Membranes were blocked in 5% milk in TBST for 30 min at room temperature and incubated with primary antibodies in 5% milk in TBST overnight at 4°C. Membranes were washed three times in TBST, incubated with secondary antibodies (LI-COR Biosciences) in 5% milk in TBST for 45 min, and then exposed on an Odyssey® CLx Imaging System (LI-COR Biosciences). *X. laevis* protein levels were probed using the following antibodies: GAPDH (Cell Signaling Technology #2118 1:5000), SPT16 (Cell Signaling Technology #12191 1:1000), SSRP1 (Santa Cruz Biotechnology #sc-74536 1:1000), and Cas9 (Novus Biologicals #7A9-3A3 1:1000). Human cell protein levels were probed using the following antibodies: GAPDH (Cell Signaling Technology #2118 1:5000), SPT16 (Cell Signaling Technology #12191 1:1000), SSRP1 (BioLegend #609701 1:100), INO80B (Thermo Fisher Scientific #PA5-24764 1:1000), and Cas9 (Novus Biologicals #7A9-3A3 1:1000).

3.5.9 Lentiviral Packaging and Transduction

Lentiviral packaging of all constructs was performed in HEK293T cells. Plasmids were transfected using TransIT®-LT1 Transfection Reagent (Mirus) at a ratio of 1 μg of total DNA to 3 μl of the transfection reagent. The plasmid mixture consisted of 50% lentiviral transfer plasmid, 40% ΔVPR plasmid, and 10% VSVG plasmid. Virus was harvested at 48 and 72 hours after transfection, passed through a 0.45 μM filter, and added to target cells for transduction. 48 hours after transduction, both K562 and HEK293T cells were exposed to puromycin at 1 μg/ml. Cells were maintained in media containing puromycin for at least two passages to ensure complete selection.

3.5.10 siRNA Transfection

For FRAP imaging, 150,000 cells were co-transfected with 1 μg of the *tetO* gRNA plasmid and 30 pmol of siRNA complexed with 4 μl of Lipofectamine™ 2000 (Thermo Fisher Scientific) in Opti-MEM (Gibco). For Western blots and flow cytometry, 50,000 cells were transfected with 7.5 pmol of siRNA complexed with 2.25 μl of Lipofectamine™ RNAiMAX (Thermo Fisher Scientific) in Opti-MEM (Gibco). For editing experiments, 1,200,000 K562 cells were transfected 180 pmol of siRNA complexed with 54 μl of Lipofectamine™ RNAiMAX in Opti-MEM (Gibco). Cells were transfected in the absence of penicillin-streptomycin. 12 hours after transfection, cells were transferred to fresh media containing penicillin-streptomycin. For ChIP experiments, 5,000,000 HEK293T or K562 cells were transfected with 750 pmol of siRNA complexed with 225 μl of Lipofectamine™ RNAiMAX in Opti-MEM (Gibco). The following siRNAs were used: SMARTpool ON-TARGETplus SUPT16H siRNA (Horizon Discovery #L-009517-00), ON-TARGETplus SSRP1 siRNA (Horizon Discovery #J-011783-07), ON-TARGETplus INO80B siRNA (Horizon Discovery #L-009848-02), and ON-TARGETplus Nontargeting Pool (Horizon Discovery #D-001810-10).

3.5.11 Fluorescence Recovery After Photobleaching

dCas9-HaloTag was stably expressed in a previously reported U2OS cell line containing arrays of *lacO* and *tetO* (Janicki et al., 2004). Targeting of dCas9-HaloTag to the arrays was confirmed by expressing mOrange-LacI-NLS to mark the array and labeling the HaloTag with the JF_{646} dye (Chong et al., 2018). For FRAP, forty-eight hours after co-transection of the gRNA plasmid and siRNA, cells were seeded onto glass bottom microwell dishes (MatTek Corporation) and labeled with 100 nm of JF_{549}. Cells were imaged on an inverted Zeiss LSM 710 AxioObserver confocal microscope equipped with a 40x/NA 1.4 oil immersion objective and an incubation chamber at 37°C and 5% CO_2. For each experiment, the FRAP spot was bleached with a 561 nm laser set to maximum power. Recovery was monitored by a time-lapse of Z-stacks at 10-20 second intervals with a 0.68 μm step size. Due to the long interval between Z-stacks, the fast mode of recovery immediately after photobleaching cannot be measured.

FRAP images were analyzed as previously described (Hansen et al., 2017). Briefly, for each FRAP movie, the XY position of the array was manually annotated, its Z position was inferred by the maximum intensity pixel in the XY annotated column, and the fluorescence intensity around the spot was integrated. An unbleached control spot was used to normalize for loss of fluorescence due to bleaching during recovery, and the FRAP curves were normalized so that the pre-bleach intensity was 1.

3.5.12 Flow Cytometry

Sixty hours after transfection of siRNAs, cells were washed once in 1% BSA in PBS and then stained on ice for 1 hour. Cells were stained in 50 □l of either a PE CD25 antibody (BioLegend #302606 1:100), FITC CD55 antibody (BioLegend #311306 1:100), or FITC CD59 antibody BioLegend #304706). Samples were also stained with PE Mouse IgG1 κ antibody (BioLegend #400112 1:100), FITC Mouse IgG1, κ antibody (BioLegend #400108 1:100), or FITC Mouse IgG2a, κ antibody (BioLegend #400208 1:100) as an isotype control. Cells were washed three times in 1% BSA in PBS. Fluorescence was measured using the Attune NxT Flow Cytometer (Thermo Fisher Scientific).

3.5.13 Chromatin Immunoprecipitation

Sixty hours after transfections, cells were trypsinized if necessary, washed once in PBS, and then incubated in 10 ml of 1% formaldehyde in PBS for 15 min at room temperature. Reactions were quenched with 1.54 ml of 1.5 M glycine. Samples were spun down, resuspended in 1 ml of ice-cold PBS, spun down again, and snap-frozen in liquid nitrogen.

Cell pellets were lysed after thawing on ice by incubation first in 10 ml of 50 mM HEPES, 140 mM NaCl, 1 mM EDTA, 10% glycerol, 0.5% NP-40, 0.25% Triton X-100, and Halt™ Protease Inhibitors at 4°C for 10 min. Samples were spun down, the supernatant was aspirated, and the pellet was resuspended in 10 ml of 200 mM NaCl, 1 mM EDTA, 0.5 mM EGTA, 10 mM Tris, and Halt™ Protease Inhibitors at 4°C for 10 min.

Samples were spun down again, the supernatant was aspirated, and the pellets were resuspended in 900 μl of 10 mM Tris, 1 mM EDTA, 0.5 mM EGTA, 100 mM NaCl, 0.1% sodium deoxycholate, 0.5% sarcosine, and Halt™ Protease Inhibitors. Resuspended samples were sonicated with a Sartorius probe sonicator with three 1-minute intervals with an amplitude of 70% and a cycle of 0.9. Sonicated samples were added to 5.1 ml of 10 mM Tris, 1 mM EDTA, 0.5 mM EGTA, 100 mM NaCl, 0.1% sodium deoxycholate, 0.5% sarcosine, and Halt™ Protease Inhibitors, and 600 μl of 10% Triton X-100. Solutions were centrifuged at 4°C at max speed for 20 minutes. 150 μl of the supernatant was retained as input. 6 ml of supernatant was used for immunoprecipitation.

8 μg of H3K9me2 (Abcam ab1220), H3K27ac (Abcam ab4729), or IgG antibody (BioLegend #400101) was incubated with 100 μl of Protein G Dynabeads™ (Thermo Fisher Scientific) at room temperature for 2 hours, washed three times with 0.5% BSA in PBS, resuspended in 100 μl of 0.5% BSA in PBS, and added to 3 ml of cell lysate. Samples were incubated overnight at 4°C with rotation. Beads were then washed four times with 1 ml of 10 mM HEPES, 500 mM LiCl, 1 mM EDTA, 1% NP-40, and 0.7% sodium deoxycholate, washed once in 1 ml of TBS, resuspended in 200 μl of 50 mM Tris, 10 mM EDTA, and 1% SDS, and incubated at 65°C overnight. Supernatants were collected and added to 200 μl of TE. 100 μl of input lysate was added to 300 μl of TE. 1 μl of RNAse A (New England Biolabs) was added to the samples, which were incubated at 37°C for 1 hour. 4 μl of Proteinase K (Thermo Fisher Scientific) was added to the samples, which were incubated at 57°C for 1 hour. 2 ml of Buffer PB (Qiagen) was added to the samples, which were flowed over MinElute columns (Qiagen). Columns were washed with Buffer PE (Qiagen) and eluted in 30 μl of Buffer EB (Qiagen). Immunoprecipitation samples were diluted 1:3 in distilled water while input samples were diluted 1:49 in distilled water.

qPCR reactions were performed in a total volume of 10 μl containing 2 μl of diluted samples, 5 ul of 2X ssoFast™ EvaGreen Supermix with Low ROX (Bio-Rad), and primers (Table S5) each at a final concentration of 500 nM. Samples were run on an Applied Biosystems™ StepOne™ Real-Time PCR System (Fisher Scientific). The thermocycler was set for 95°C for 2 minutes and 40 cycles of 95°C for 5 seconds and 55°C for 10 seconds. Fold enrichment of the assayed genes over a control locus were calculated using the $2^{-\Delta\Delta Ct}$ method.

3.5.14 Cas9 Electroporation

Cells were electroporated with Cas9 RNPs 60 hours after transfection of siRNAs. For each electroporation, 30 pmol of Cas9 was diluted to a final volume of 3.5 μl with Cas9 Buffer (20 mM HEPES pH 7.5, 150 mM KCl, 1 mM $MgCl_2$, 10% glycerol, and 1 mM TCEP). Cas9 was incubated with 36 pmol of gRNA diluted to a final volume of 3.5 μl in Cas9 Buffer. The resulting mixture was incubated for 10 min at room temperature. For HDR experiments, 1 μl of 100 μM ssODN donor was then added to the RNPs. 200,000 cells were washed once in PBS, resuspended in 16 μl of

Buffer SF (Lonza), added to the RNP complexes, and electroporated using the FF120 program on the 4D-Nucleofector™ (Lonza). Reaction mixtures were incubated at room temperature for 10 min after electroporation and then transferred to pre-warmed media.

3.5.15 Next-Generation Sequencing

Either 0, 1, 2, 3, 6, 9, 12, 24 or 48 hours after electroporation, genomic DNA was harvested cells using QuickExtract™ DNA Extraction Solution (Lucigen). 200 ng of genomic DNA from edited cells was amplified using primer pairs from primer set 1 in a 30-cycle PCR reaction (Table S4). PCR products were SPRI cleaned, and 25 ng of SPRI-cleaned amplicons were amplified again using primer pairs from primer set 2 (Table S4) in a 12-cycle PCR reaction. Amplicons from the second PCR were SPRI cleaned, and 10 ng of SPRI-cleaned amplicons were used in a 9-cycle PCR reaction with Illumina compatible primers. All PCRs were conducted with PrimeSTAR® GXL DNA Polymerase (Takara) according to the manufacturer's instructions. Libraries were pooled and submitted to the Vincent J. Coates Genomics Sequencing Laboratory at the University of California, Berkeley for 300 bp paired-end cycle processing using an Illumina MiSeq sequencing Kit (Illumina Inc., San Diego, CA).

Samples were deep sequenced to a depth of at least 10,000 reads. Reads were trimmed of adapters and low quality bases. Paired reads were joined into a single read and aligned to the input reference and donor sequences using NEEDLE (Li et al., 2015). Editing outcomes were determined and quantified using a modified version (https://github.com/staciawyman/cortado) of CRISPResso (Pinello et al., 2016). Reads were classified as NHEJ if an insertion or deletion in the alignment overlapped a 6 bp window around the cut site. Reads were classified as HDR if they were not NHEJ and contained the primary edit specified in the donor sequence. Percent NHEJ and HDR are calculated as the number of reads divided by the number of aligned reads. Indel size distributions were visualized through CRISPResso2 (Clement et al., 2019).

3.5.16 Quantification and Statistical Analysis

All analysis was performed using data from three biological replicates. Data are presented as mean ± standard deviation. Statistical analyses were performed in the PRISM software using a Student's t-test. FRAP data was analyzed using a Mann-Whitney U Test. Statistical details can be found in figures and the corresponding figure legends. Significance was defined as $p < 0.05$.

3.6 Acknowledgements

A.S.W. is supported by the National Science Foundation Graduate Research Fellowships Program and the Li Ka Shing Foundation. R.A.W. is supported by postdoctoral fellowship 131415-PF-17-168-01-DMC from the American Cancer Society. Y.H., D.T.W., A.B.H., and X.D. are supported by NIH grants UO1-497 EB021236 and U54-DK107980. A.B.H. and X.D. are supported by California Institute for Regenerative

Medicine grant LA1-08013. A.B.H is supported by the NIH predoctoral fellowship T32 GM098218. C.D.R., B.G.G., K.R.K., J.T.V., S.K.W., J.J.S., and J.E.C. are supported by the Li Ka Shing Foundation and Heritage Medical Research Institute. J.T.V. is supported by CIRM TRAN1-09292. J.C.W. is supported by NIH grant HL098316. J.C.W. is a Howard Hughes Medical Institute Investigator and an American Cancer Society Research Professor. This work used the Vincent J. Coates Genomics Sequencing Laboratory at UC Berkeley, supported by NIH S10 OD018174 Instrumentation Grant. We would like to thank Dr. Danny Reinberg for generously providing recombinant FACT and Dr. Hasan Yardimci for generously providing the SPT16 antibody.

3.7 Author Contributions

Conceptualization, A.S.W., R.A.W., Y.H., D.T.M., A.B.H., C.D.R., J.C.W. and J.E.C.; Methodology, A.S.W., R.A.W., Y.H., D.T.M., A.B.H., C.D.R., B.G.G., J.J.S., J.C.W. and J.E.C.; Software, Y.H., A.B.H. and S.K.W.; Formal Analysis, J.E.C.; Investigation, A.S.W., L.C., R.A.W., Y.H., A.B.H., C.D.R., B.G.G., K.R.K., J.T.V. and S.K.W.; Writing – Original Draft, A.S.W. and J.E.C.; Writing – Review & Editing, A.S.W., Y.H., A.B.H. and J.E.C.; Visualization, A.S.W., Y.H. and A.B.H.; Supervision, X.D., J.C.W. and J.E.C.; Funding Acquisition, X.D., J.C.W. and J.E.C.

3.8 Data S1: Amino Acid Sequences of Cas9-BirA* and dCas9-BirA*

Cas9-BirA*:

MDYKDHDGDYKDHDIDYKDDDDKMAPKKKRKVGIHGVPAADKKYSIGLDIGTNSVGW
AVITDEYKVPSKKFKVLGNTDRHSIKKNLIGALLFDSGETAEATRLKRTARRRYTRRKN
RICYLQEIFSNEMAKVDDSFFHRLEESFLVEEDKKHERHPIFGNIVDEVAYHEKYPTIYH
LRKKLVDSTDKADLRLIYLALAHMIKFRGHFLIEGDLNPDNSDVDKLFIQLVQTYNQLFE
ENPINASGVDAKAILSARLSKSRRLENLIAQLPGEKKNGLFGNLIALSLGLTPNFKSNFD
LAEDAKLQLSKDTYDDDLDNLLAQIGDQYADLFLAAKNLSDAILLSDILRVNTEITKAPLS
ASMIKRYDEHHQDLTLLKALVRQQLPEKYKEIFFDQSKNGYAGYIDGGASQEEFYKFIK
PILEKMDGTEELLVKLNREDLLRKQRTFDNGSIPHQIHLGELHAILRRQEDFYPFLKDNR
EKIEKILTFRIPYYVGPLARGNSRFAWMTRKSEETITPWNFEEVVDKGASAQSFIERMT
NFDKNLPNEKVLPKHSLLYEYFTVYNELTKVKYVTEGMRKPAFLSGEQKKAIVDLLFKT
NRKVTVKQLKEDYFKKIECFDSVEISGVEDRFNASLGTYHDLLKIIKDKDFLDNEENEDIL
EDIVLTLTLFEDREMIEERLKTYAHLFDDKVMKQLKRRRYTGWGRLSRKLINGIRDKQS
GKTILDFLKSDGFANRNFMQLIHDDSLTFKEDIQKAQVSGQGDSLHEHIANLAGSPAIKK
GILQTVKVVDELVKVMGRHKPENIVIEMARENQTTQKGQKNSRERMKRIEEGIKELGS
QILKEHPVENTQLQNEKLYLYYLQNGRDMYVDQELDINRLSDYDVDHIVPQSFLKDDSI
DNKVLTRSDKNRGKSDNVPSEEVVKKMKNYWRQLLNAKLITQRKFDNLTKAERGGLS
ELDKAGFIKRQLVETRQITKHVAQILDSRMNTKYDENDKLIREVKVITLKSKLVSDFRKD
FQFYKVREINNYHHAHDAYLNAVVGTALIKKYPKLESEFVYGDYKVYDVRKMIAKSEQE
IGKATAKYFFYSNIMNFFKTEITLANGEIRKRPLIETNGETGEIVWDKGRDFATVRKVLS
MPQVNIVKKTEVQTGGFSKESILPKRNSDKLIARKKDWDPKKYGGFDSPTVAYSVLVV
AKVEKGKSKKLKSVKELLGITIMERSSFEKNPIDFLEAKGYKEVKKDLIIKLPKYSLFELE
NGRKRMLASAGELQKGNELALPSKYVNFLYLASHYEKLKGSPEDNEQKQLFVEQHKH

YLDEIIEQISEFSKRVILADANLDKVLSAYNKHRDKPIREQAENIIHLFTLTNLGAPAAFKY
FDTTIDRKRYTSTKEVLDATLIHQSITGLYETRIDLSQLGGDKRPAATKKAGQAKKKKGG
GSGGGSGGGSKDNTVPLKLIALLANGEFHSGEQLGETLGMSRAAINKHIQTLRDWGV
DVFTVPGKGYSLPEPIQLLNAKQILGQLDGGSVAVLPVIDSTNQYLLDRIGELKSGDACI
AEYQQAGRGGRGRKWFSPFGANLYLSMFWRLEQGPAAAIGLSLVIGIVMAEVLRKLG
ADKVRVKWPNDLYLQDRKLAGILVELTGKTGDAAQIVIGAGINMAMRRVEESVVNQGW
ITLQEAGINLDRNTLAAMLIRELRAALELFEQEGLAPYLSRWEKLDNFINRPVKLIIGDKEI
FGISRGIDKQGALLLEQDGIIKPWMGGEISLRSAEKAYPYDVPDYA*

dCas9-BIrA*:

MDYKDHDGDYKDHDIDYKDDDDKMAPKKKRKVGIHGVPAADKKYSIGLAIGTNSVGW
AVITDEYKVPSKKFKVLGNTDRHSIKKNLIGALLFDSGETAEATRLKRTARRRYTRRKN
RICYLQEIFSNEMAKVDDSFFHRLEESFLVEEDKKHERHPIFGNIVDEVAYHEKYPTIYH
LRKKLVDSTDKADLRLIYLALAHMIKFRGHFLIEGDLNPDNSDVDKLFIQLVQTYNQLFE
ENPINASGVDAKAILSARLSKSRRLENLIAQLPGEKKNGLFGNLIALSLGLTPNFKSNFD
LAEDAKLQLSKDTYDDDLDNLLAQIGDQYADLFLAAKNLSDAILLSDILRVNTEITKAPLS
ASMIKRYDEHHQDLTLLKALVRQQLPEKYKEIFFDQSKNGYAGYIDGGASQEEFYKFIK
PILEKMDGTEELLVKLNREDLLRKQRTFDNGSIPHQIHLGELHAILRRQEDFYPFLKDNR
EKIEKILTFRIPYYVGPLARGNSRFAWMTRKSEETITPWNFEEVVDKGASAQSFIERMT
NFDKNLPNEKVLPKHSLLYEYFTVYNELTKVKYVTEGMRKPAFLSGEQKKAIVDLLFKT
NRKVTVKQLKEDYFKKIECFDSVEISGVEDRFNASLGTYHDLLKIIKDKDFLDNEENEDIL
EDIVLTLTLFEDREMIEERLKTYAHLFDDKVMKQLKRRRYTGWGRLSRKLINGIRDKQS
GKTILDFLKSDGFANRNFMQLIHDDSLTFKEDIQKAQVSGQGDSLHEHIANLAGSPAIKK
GILQTVKVVDELVKVMGRHKPENIVIEMARENQTTQKGQKNSRERMKRIEEGIKELGS
QILKEHPVENTQLQNEKLYLYYLQNGRDMYVDQELDINRLSDYDVDAIVPQSFLKDDSI
DNKVLTRSDKNRGKSDNVPSEEVVKKMKNYWRQLLNAKLITQRKFDNLTKAERGGLS
ELDKAGFIKRQLVETRQITKHVAQILDSRMNTKYDENDKLIREVKVITLKSKLVSDFRKD
FQFYKVREINNYHHAHDAYLNAVVGTALIKKYPKLESEFVYGDYKVYDVRKMIAKSEQE
IGKATAKYFFYSNIMNFFKTEITLANGEIRKRPLIETNGETGEIVWDKGRDFATVRKVLS
MPQVNIVKKTEVQTGGFSKESILPKRNSDKLIARKKDWDPKKYGGFDSPTVAYSVLVV
AKVEKGKSKKLKSVKELLGITIMERSSFEKNPIDFLEAKGYKEVKKDLIIKLPKYSLFELE
NGRKRMLASAGELQKGNELALPSKYVNFLYLASHYEKLKGSPEDNEQKQLFVEQHKH
YLDEIIEQISEFSKRVILADANLDKVLSAYNKHRDKPIREQAENIIHLFTLTNLGAPAAFKY
FDTTIDRKRYTSTKEVLDATLIHQSITGLYETRIDLSQLGGDKRPAATKKAGQAKKKKGG
GSGGGSGGGSKDNTVPLKLIALLANGEFHSGEQLGETLGMSRAAINKHIQTLRDWGV
DVFTVPGKGYSLPEPIQLLNAKQILGQLDGGSVAVLPVIDSTNQYLLDRIGELKSGDACI
AEYQQAGRGGRGRKWFSPFGANLYLSMFWRLEQGPAAAIGLSLVIGIVMAEVLRKLG
ADKVRVKWPNDLYLQDRKLAGILVELTGKTGDAAQIVIGAGINMAMRRVEESVVNQGW
ITLQEAGINLDRNTLAAMLIRELRAALELFEQEGLAPYLSRWEKLDNFINRPVKLIIGDKEI
FGISRGIDKQGALLLEQDGIIKPWMGGEISLRSAEKAYPYDVPDYA*

3.9 Table S1: *X. laevis* Proteomics Enrichment Comparisons

Cas9-BirA* + On-Target gRNA vs. dCas9-BirA* + NT gRNA

Significant	-Log (p-value)	Log_2 (Fold Change)	Protein IDs	Majority protein IDs
+	4.955	9.492	PIP4K2C	PIP4K2C
+	3.984	4.362	DKC1	DKC1
	0.000	4.079	NHP2	NHP2
+	3.195	3.986	NOLC1	NOLC1
	1.456	3.924	SFI1	SFI1
	0.000	3.174	GAR1	GAR1
	1.727	2.767	FBL	FBL
+	2.858	2.583	SSRP1	SSRP1
+	3.526	2.428	SUPT16H	SUPT16H
	0.000	2.410	CETN2	CETN2
	1.190	2.204	H1F0	H1F0
+	2.986	2.026	SUB1	SUB1
	1.767	1.990	TPR	TPR
	0.993	1.945	ALDOA; ALDOC	ALDOA; ALDOC
	1.155	1.895	HIST1H1D	HIST1H1D
+	1.997	1.797	TRPM7	TRPM7
+	2.501	1.784	NOP2	NOP2
	0.000	1.612	SPTAN1	SPTAN1
	1.026	1.353	CAND1	CAND1
	0.669	1.351	HIST1H1D; HIST1H1B	HIST1H1D; HIST1H1B
+	2.193	1.344	H1FOO	H1FOO
	0.000	1.342	TPI1	TPI1
	1.290	1.314	NHP2L1	NHP2L1
	0.816	1.304	CIRBP	CIRBP
	1.206	1.301	PPP2R1A	PPP2R1A
	0.000	1.256	NPM2	NPM2
	0.894	1.243	ACRC; HDLBP	HDLBP
	0.000	1.102	FKBP3	FKBP3
	1.481	1.033	MSH6	MSH6
	1.540	1.014	NOP56; DDX27	NOP56
	0.000	0.933	CFL1	CFL1

	0.774	0.919	IPO5	IPO5
	0.426	0.888	HLCS	HLCS
	0.674	0.887	AP3D1	AP3D1
	1.660	0.878	EIF5B	EIF5B
	0.700	0.858	PKM	PKM
	0.917	0.809	MAP4K4	MAP4K4
	0.803	0.808	LDHB	LDHB
	0.369	0.806	RNASEH2B	RNASEH2B
	0.604	0.798	NPM2	NPM2
	0.449	0.729	KPNA6; KPNA1	KPNA6; KPNA1
	0.924	0.724	MCCC1; ACACB	ACACB
	0.442	0.721	RAN	RAN
	0.000	0.714	MAP4	MAP4
	0.384	0.675	GEMIN5	GEMIN5
	0.700	0.639	MCM2	MCM2
	0.000	0.635	PPM1H	PPM1H
	0.972	0.633	NUP107	NUP107
	1.207	0.595	CKM;CKB	CKB
	0.289	0.594	MCM4	MCM4
	0.418	0.591	KRT19; KRT18	KRT19; KRT18
	0.000	0.579	LAMB4	LAMB4
	0.346	0.563	GSTM1	GSTM1
	0.543	0.545	HSP90AB1	HSP90AB1
	0.310	0.542	NOP58	NOP58
	0.602	0.538	HCFC1	HCFC1
	0.165	0.538	PRMT1	PRMT1
	0.409	0.530	RANBP2	RANBP2
	0.164	0.529	NLRX1	NLRX1
	0.972	0.516	ACACA	ACACA
	0.609	0.514	UMPS	UMPS
	0.220	0.501	MDN1	MDN1
	0.304	0.494	C8ORF59	C8ORF59
	1.299	0.490	CCT6A	CCT6A
	0.494	0.490	DNAJC13	DNAJC13

	1.737	0.477	ARF3; ARF1	ARF3; ARF1
	0.466	0.477	MGC4836	MGC4836
	0.836	0.464	ATP6V1A	ATP6V1A
	0.207	0.457	APOB	APOB
	0.250	0.432		
	0.420	0.431	EIF4A1; EIF4A3; EIF4A2	EIF4A1; EIF4A2
	0.565	0.413	TUBA1A	TUBA1A
	0.328	0.404	CAB39L; CAB39	CAB39L; CAB39
	0.145	0.389	RBBP6	RBBP6
	0.476	0.381	YWHAB	YWHAB
	0.295	0.375	NAP1L1; NAP1L4B; NAP1L4	NAP1L1; NAP1L4B; NAP1L4
	0.424	0.374	GSTT1	GSTT1
	0.131	0.357	KARS	KARS
	0.330	0.355	MDH1	MDH1
	0.407	0.355	POLR2M	POLR2M
	0.536	0.353	TUBB6; TUBB4B; TUBB3; TUBB; TUBB2A; TUBB2C; TUBB2B	TUBB4B; TUBB; TUBB2B
	1.253	0.348	PGK1	PGK1
	0.221	0.346	CLTCL1; CLTC	CLTCL1; CLTC
	0.153	0.335	C10ORF71	C10ORF71
	0.414	0.334	CSNK2A1	CSNK2A1
	0.318	0.330	RPS6	RPS6
	0.000	0.328	TXNDC9	TXNDC9
	0.556	0.328	DDX39B; BAT1; DDX39A	DDX39B; BAT1; DDX39A

	0.191	0.324	FLNA	FLNA
	0.000	0.322	RFC2	RFC2
	0.262	0.321		
	0.108	0.318	C2CD2L	C2CD2L
	0.000	0.311	RPS26	RPS26
	0.409	0.310	H1FOO	H1FOO
	0.404	0.301	LYPLA2	LYPLA2
	0.199	0.300	MGC4836	MGC4836
	0.346	0.292	SFRS2	SFRS2
	0.139	0.290	KIF5B	KIF5B
	0.828	0.279	TUBA1C; TUBA4A; TUBA1B	TUBA4A
	0.782	0.267	ACACA	ACACA
	0.043	0.259	RFC5	RFC5
	0.158	0.258	IMPDH2	IMPDH2
	0.335	0.246	TCEB3	TCEB3
	0.903	0.245	ACTA2; ACTA1; ACTG1; ACTG2; ACTC1; ACTB	ACTB; ACTG1
	0.191	0.241	RPS11	RPS11
	0.339	0.241	ITLN2; ITLN1	ITLN2; ITLN1
	0.823	0.240	PRSS1	PRSS1
	0.261	0.239	ANXA11; ANXA7	ANXA11; ANXA7
	1.734	0.234	GAPDH	GAPDH
	0.000	0.234	XAB2	XAB2
	0.194	0.234	DHFR	DHFR
	0.119	0.233	MYH10; MYH9; MYH14	MYH10; MYH9; MYH14
	0.223	0.233	CCT7	CCT7
	0.182	0.230	ACACA	ACACA
	0.179	0.229	EEF2	EEF2

	0.983	0.228		
	0.573	0.225	ZCCHC17	ZCCHC17
	0.341	0.215	ACACB	ACACB
	0.000	0.210	DHRS12	DHRS12
	0.000	0.202	PGAM2; PGAM1	PGAM2; PGAM1
	0.000	0.194	HNRNPU	HNRNPU
	0.127	0.182	HBZ	HBZ
	0.160	0.178	PSMD3	PSMD3
	0.000	0.177	RPS15A	RPS15A
	0.097	0.175	RANGAP1	RANGAP1
	0.196	0.173	PSMC2	PSMC2
	0.157	0.173	SRP72	SRP72
	0.103	0.171	IPO7	IPO7
	0.203	0.168	DYNLT1	DYNLT1
	0.141	0.165	DPCD	DPCD
	0.250	0.160	CCT3	CCT3
	0.196	0.160	PRDX2	PRDX2
	0.000	0.158	EIF4G1	EIF4G1
	0.366	0.151	MAP2K1	MAP2K1
	0.148	0.149	UGDH	UGDH
	0.000	0.139	CAD	CAD
	0.301	0.139	ACACA	ACACA
	0.134	0.139	PCNA	PCNA
	0.074	0.138	CKM;CKB	CKM;CKB
	0.274	0.135	KPNB1	KPNB1
	0.171	0.135	ENO1;ENO3	ENO1;ENO3
	0.133	0.126	PSMD6	PSMD6
	0.091	0.124	CCT2	CCT2
	0.076	0.123	RPL29; RP11-632C17__A.1-001	RPL29; RP11-632C17__A.1-001
	0.198	0.122	MCM3	MCM3
	0.095	0.118	SNRPD2	SNRPD2
	0.206	0.116	PRPF8	PRPF8
	0.134	0.112	PPIF	PPIF
	0.000	0.112	PRPF40A	PRPF40A
	0.162	0.111	PSMD12	PSMD12

	0.153	0.106	EEF1A1; EEF1A2; TYW5	EEF1A1; EEF1A2
	0.000	0.104	CSNK2A1	CSNK2A1
	0.148	0.103	PFN1	PFN1
	0.048	0.101	PGK1	PGK1
	0.074	0.098	CSNK2B	CSNK2B
	0.280	0.097	GRHPR	GRHPR
	0.111	0.096	YARS	YARS
	0.116	0.092	RP11-632C17__A.1-001	RP11-632C17__A.1-001
	0.125	0.089	CFL1	CFL1
	0.097	0.085	TCP1	TCP1
	0.098	0.084	POLD1	POLD1
	0.068	0.079	ACACA	ACACA
	0.200	0.077	CKB	CKB
	0.109	0.074	GPI	GPI
	0.121	0.074	PSMC1	PSMC1
	0.081	0.073	YWHAZ; YWHAH; YWHAQ; YWHAG; YWHAE	YWHAQ
	0.135	0.068	PSMD7	PSMD7
	0.180	0.057	FEN1	FEN1
	0.000	0.054	GEMIN4	GEMIN4
	0.025	0.047	EPRS	EPRS
	0.073	0.045	TUBA1C	TUBA1C
	0.042	0.045	VPS4A; VPS4B	VPS4B
	0.053	0.045	CCT2	CCT2
	0.023	0.037	IPO4	IPO4
	0.022	0.035	EEF1A1; EEF1A2	EEF1A1
	0.035	0.035	CTPS1	CTPS1
	0.016	0.032	DNAJC2	DNAJC2
	0.197	0.026	IARS	IARS
	0.009	0.019	CKB	CKB
	0.007	0.017	CSNK2A2	CSNK2A2

	0.005	0.009	BAZ1A	BAZ1A
	0.010	0.008	PSMC3	PSMC3
	0.004	0.007	DNAJA1; DNAJA4	DNAJA1; DNAJA4
	0.002	0.001	HBA1; HBZ	HBZ
	0.000	0.000	DDX1	DDX1
	0.002	-0.001	TUBA1C	TUBA1C
	0.002	-0.002	TUBA1C; TUBA4A; TUBA3C; TUBA1B	TUBA4A
	0.005	-0.005	VTA1	VTA1
	0.004	-0.007	CLIC1	CLIC1
	0.021	-0.013	CCT6A	CCT6A
	0.011	-0.015	EEF1G	EEF1G
	0.007	-0.016	MTA2	MTA2
	0.000	-0.017	TUBA4A	TUBA4A
	0.008	-0.018	EPB41L2	EPB41L2
	0.006	-0.026	PDPR	PDPR
	0.026	-0.030	RPL23A	RPL23A
	0.050	-0.040	TPI1	TPI1
	0.060	-0.041	RRM1	RRM1
	0.037	-0.044	CAPN1	CAPN1
	0.023	-0.044	NARS	NARS
	0.000	-0.045	TCEB1	TCEB1
	0.038	-0.047	G6PD; H6PD	G6PD
	0.250	-0.050	TUBA1B	TUBA1B
	0.350	-0.050	FARSB	FARSB
	0.054	-0.055	CAP1	CAP1
	0.000	-0.062	TYMS	TYMS
	0.043	-0.063	DRIP4	DRIP4
	0.094	-0.064	FAM115C	FAM115C
	0.046	-0.071	GPD1	GPD1
	0.068	-0.073	NANS	NANS

	0.103	-0.073	ACLY; ACLY VARIANT PROTEIN	ACLY; ACLY VARIANT PROTEIN
	0.115	-0.078	TCOF1	TCOF1
	0.052	-0.084	DCTN1	DCTN1
	0.157	-0.084	RPS6KA1; RPS6KA3; RPS6KA6	RPS6KA1; RPS6KA3
	0.033	-0.086	EPRS	EPRS
	0.021	-0.086	IPO7	IPO7
	0.077	-0.093	TUBB4B; TUBB4A; TUBB2B	TUBB4B; TUBB2B
	0.157	-0.096	CAMK2D; CAMK2G; CAMK2A; CAMK2B	CAMK2D; CAMK2G; CAMK2B
	0.097	-0.103	HIST2H2BF	HIST2H2BF
	0.041	-0.107	MARS	MARS
	0.000	-0.109	ST13	ST13
	0.151	-0.117	ACTB	ACTB
	0.084	-0.120	HDAC1; HDAC2	HDAC1
	0.117	-0.121	GSTO2; GSTO1	GSTO1
	0.041	-0.122	TUBA1C; TUBA1B; TUBA3C; TUBA1A	TUBA3C
	0.175	-0.124	CCT8	CCT8
	0.057	-0.125	TBCB	TBCB
	0.073	-0.132	VARS2; VARS	VARS2; VARS
	0.436	-0.135	DYNC1H1	DYNC1H1
	0.197	-0.136	PSMD2	PSMD2
	0.297	-0.141	CCT5	CCT5
	0.095	-0.143	IPO7	IPO7
	0.194	-0.143	YWHAQ	YWHAQ

	0.093	-0.146	CKAP5	CKAP5
	0.117	-0.154	ABCE1	ABCE1
	0.203	-0.158	PSMD11	PSMD11
	0.102	-0.161		
	0.165	-0.164	LIG1	LIG1
	0.086	-0.173	NASP	NASP
	0.102	-0.177	PCM1	PCM1
	0.093	-0.177	MCM7	MCM7
	0.251	-0.180	RPS8	RPS8
	0.589	-0.190	HSP90AB1; HSP90B1	HSP90AB1
	0.206	-0.195	COPG1	COPG1
	0.436	-0.196	HMGB2; HMGB1	HMGB2; HMGB1
	0.130	-0.200	GAPDH	GAPDH
	0.130	-0.207	MCM5	MCM5
	0.260	-0.217	PRIC295; GCN1L1	PRIC295
	0.459	-0.218	LRRC40	LRRC40
	0.182	-0.233	POLD3	POLD3
	0.248	-0.237	RHEB	RHEB
	0.151	-0.237	NSF	NSF
	0.393	-0.241	AKR1B1	AKR1B1
	0.119	-0.251	RFC3	RFC3
	0.213	-0.251	EPRS	EPRS
	0.056	-0.253	CSE1L	CSE1L
	0.303	-0.255	MCM6	MCM6
	0.195	-0.262	GART	GART
	0.204	-0.265	UBA1	UBA1
	0.295	-0.271	OLA1	OLA1
	0.363	-0.273	NANS	NANS
	0.918	-0.287	PSMD13	PSMD13
	0.224	-0.290	PSMC4	PSMC4
	0.070	-0.290	KRT75; KRT8; KRT7	KRT75; KRT8; KRT7
	0.268	-0.290	EXOC1	EXOC1
	0.000	-0.299	TRIM69	TRIM69

	0.986	-0.302	HBZ	HBZ
	0.099	-0.304	ACTA2; ACTA1; ACTG1; ACTG2; ACTC1; ACTB	ACTA2; ACTA1; ACTG1; ACTG2; ACTC1; ACTB
	0.382	-0.308	LOC392793; EEF1B2	EEF1B2
	0.247	-0.315	RAD50	RAD50
	0.382	-0.317	ST13	ST13
	0.404	-0.327	UBE2O	UBE2O
	0.342	-0.331	TBC1D24	TBC1D24
	1.124	-0.335	QARS	QARS
	0.631	-0.336	KPNA7; KPNA2	KPNA7; KPNA2
	0.549	-0.339	FARSA	FARSA
	0.464	-0.342	GBE1	GBE1
	0.966	-0.343	GART	GART
	0.397	-0.348	MYBBP1A	MYBBP1A
	1.309	-0.349		
	1.037	-0.350	DRG2	DRG2
	0.349	-0.351	LARS	LARS
	0.659	-0.357		
	0.448	-0.357	PSMC5; SPATA5	PSMC5
	0.128	-0.371	PSMD10	PSMD10
	0.499	-0.372	ARCN1	ARCN1
	0.334	-0.372	UBA2	UBA2
	0.370	-0.378	HPGDS	HPGDS
	1.025	-0.381	CSE1L	CSE1L
	0.234	-0.387	PROSC	PROSC
	0.000	-0.387	ECD	ECD
	0.612	-0.388	MYO5C; MYO5B; MYO5A	MYO5A
	0.163	-0.394	PTGR1	PTGR1
	0.286	-0.395	HMGB3	HMGB3

	0.609	-0.395	NMRAL1	NMRAL1
	1.921	-0.398	HSPA2; HSPA1A; HSPA8; HSPA5	HSPA8
	0.286	-0.402	CCT4	CCT4
	0.481	-0.405	DARS	DARS
	0.370	-0.405	EIF2S3	EIF2S3
	0.291	-0.406	GSTA1	GSTA1
	0.000	-0.410	EEF1G	EEF1G
	0.578	-0.443	PSMD2	PSMD2
	0.462	-0.455	PSMC6	PSMC6
	0.000	-0.458	DKFZP781K0743	DKFZP781K0743
	0.248	-0.458	KAT8; TRIM69	KAT8; TRIM69
	0.455	-0.459	CSE1L	CSE1L
	1.790	-0.471	RBM14; CCT4; RBM14/RBM4 FUSION	CCT4
	0.351	-0.479	EIF3F	EIF3F
	0.000	-0.486	DNAJB7; DNAJB6	DNAJB7; DNAJB6
	1.113	-0.486	EEF1G	EEF1G
	0.582	-0.486	EEF1G	EEF1G
	0.605	-0.496	EEF1D; EEF1B2	EEF1D
	0.238	-0.503	SNRPD1	SNRPD1

	0.743	-0.511	CDK18; NEK5; CDK12; CDK13; CDK16; CDK17; CDK14; CDK15; CDK1; CDK2; CDK4; CDK5; CDK9	CDK1
	0.447	-0.514	GBP1; GBP4	GBP1
	0.098	-0.515	KIF27	KIF27
	0.516	-0.518	UBA6	UBA6
	1.024	-0.539	DNAJC9	DNAJC9
	0.346	-0.541	NCCRP1	NCCRP1
	0.986	-0.559	RARS	RARS
	0.000	-0.564	PARP4	PARP4
	0.723	-0.586	RPS9	RPS9
	0.348	-0.589	RPS23	RPS23
	0.920	-0.592	NACA	NACA
	0.000	-0.594	NOL9	NOL9
	0.772	-0.633	AQR	AQR
	1.179	-0.639	PSMD1	PSMD1
	0.000	-0.643	TRIP13	TRIP13
	2.123	-0.644	ANXA1	ANXA1
	0.771	-0.646	DNM1L	DNM1L
	0.000	-0.647	PRIM1	PRIM1
	0.694	-0.647	APAF1	APAF1
	0.815	-0.680	HSPA8	HSPA8
	1.207	-0.687	AP2M1	AP2M1
	0.000	-0.689	NASP	NASP
	0.346	-0.693	TTLL7	TTLL7

	1.449	-0.702	CENPA; H3F3A; HIST2H3A; H3F3B	H3F3A; HIST2H3A; H3F3B
	0.708	-0.750	HMGB1	HMGB1
	0.000	-0.785	IPO9	IPO9
+	2.641	-0.800	COPA	COPA
	2.090	-0.816	PSMD4	PSMD4
	1.159	-0.817	COPB1	COPB1
	1.177	-0.847	RPL31	RPL31
	0.000	-0.853	PRMT5	PRMT5
	0.628	-0.863	TEX10	TEX10
	0.954	-0.890	HIST1H4A	HIST1H4A
	1.167	-0.900	CHMP5	CHMP5
	0.155	-0.901	SEC23B	SEC23B
	0.779	-0.913	CHTF18	CHTF18
	1.520	-0.941	TSG101	TSG101
	0.610	-0.958	SSB	SSB
	0.202	-1.022	DLGAP5	DLGAP5
	0.794	-1.026	GBP2; GBP1; GBP7; GBP5; GBP4	GBP1; GBP4
+	2.308	-1.060	RPL17	RPL17
	0.978	-1.111	ABCF1	ABCF1
	0.995	-1.125	PFKM	PFKM
	0.281	-1.140	CCT6A	CCT6A
	0.624	-1.175	FNTA	FNTA
+	2.411	-1.190	CHMP2A	CHMP2A
	1.094	-1.226	COPE	COPE
	0.000	-1.420	THYN1	THYN1
	1.591	-1.421	CHMP2A	CHMP2A
	1.869	-1.476	CHMP1A	CHMP1A
	1.013	-1.493	HIST2H2AB	HIST2H2AB
	0.000	-1.501	COPA	COPA
	0.937	-1.507	RPS3A	RPS3A
+	2.200	-1.521	HIST1H2BJ	HIST1H2BJ

	1.482	-1.562	CHD3; CHD5; CHD4	CHD3; CHD4
	1.649	-1.596	HIST1H4A	HIST1H4A
	1.309	-1.611	RPL23	RPL23
	1.372	-1.715	CHMP4B	CHMP4B
+	2.441	-1.750	CHMP1B	CHMP1B
	1.377	-1.901	H2AFX; H2AFV; HIST2H2AB; H2AFZ; H2AFJ	H2AFX; HIST2H2AB; H2AFJ
+	4.054	-2.935	UBA52; RPS27A; UBBP4; UBB; UBC	UBA52; RPS27A; UBB; UBC
+	2.539	-2.961	CHMP2B	CHMP2B
+	1.729	-3.946	UBB	UBB
	0.000	NaN	HIST2H2BF; HIST1H2BJ; HIST1H2BA	HIST2H2BF; HIST1H2BJ
	0.000	NaN	AHNAK	AHNAK
	0.000	NaN	HSD17B6	HSD17B6
	0.000	NaN	RFC4	RFC4
	0.000	NaN	MSH2	MSH2
	0.000	NaN	HMGA2	HMGA2
	0.000	NaN	CCDC176	CCDC176
	0.000	NaN	TAF6	TAF6
	0.000	NaN	U2AF1; U2AF1L4	U2AF1; U2AF1L4
	0.000	NaN	CBR1	CBR1
	0.000	NaN	RAPGEF3	RAPGEF3
	0.000	NaN	COPB2	COPB2
	0.000	NaN	SMARCAD1	SMARCAD1
	0.000	NaN	DKC1	DKC1
	0.000	NaN	PIP4K2C	PIP4K2C
	0.000	NaN	RPL10A	RPL10A

	0.000	NaN	TLN1	TLN1
	0.000	NaN	RPL3	RPL3
	0.000	NaN	ANXA1	ANXA1
	0.000	NaN	RRAGC	RRAGC
	0.000	NaN	UBE2N	UBE2N
	0.000	NaN		
	0.000	NaN	NOP10	NOP10
	0.000	NaN	AKR1B1; AKR1B15	AKR1B1; AKR1B15
	0.000	NaN	HSPA8	HSPA8

Cas9-BirA* + On-Target gRNA vs. dCas9-BirA* + On-Target gRNA

Significant	-Log (p-value)	Log_2 (Fold Change)	Protein IDs	Majority protein IDs
	0.724	2.697	C10ORF71	C10ORF71
	0.304	2.602	PIP4K2C	PIP4K2C
	0.360	2.252	DKC1	DKC1
	0.482	1.848	NLRX1	NLRX1
	0.407	1.556	POLR2M	POLR2M
	1.023	1.464	KPNA6; KPNA1	KPNA6; KPNA1
	0.538	1.456	C2CD2L	C2CD2L
	0.896	1.238	SUPT16H	SUPT16H
	0.854	1.207	SSRP1	SSRP1
	0.295	1.132	CSE1L	CSE1L
	0.000	1.104	TRPM7	TRPM7
	0.000	1.064	RPS15A	RPS15A
	1.429	1.038	KRT19; KRT18	KRT19; KRT18
	0.337	1.014	HIST1H1D	HIST1H1D
	0.657	0.984	NOP10	NOP10
	0.755	0.981	SUB1	SUB1
	0.243	0.949	MGC4836	MGC4836
	0.532	0.930	KRT75; KRT8; KRT7	KRT75; KRT8; KRT7
	1.175	0.904	NHP2L1	NHP2L1

	0.616	0.841	PPM1H	PPM1H
	0.401	0.838	HLCS	HLCS
	0.189	0.813	NOLC1	NOLC1
	1.310	0.809	GSTT1	GSTT1
	0.101	0.768	RFC5	RFC5
	0.329	0.756	CIRBP	CIRBP
	0.668	0.745	GSTM1	GSTM1
	0.153	0.674	ALDOA; ALDOC	ALDOA; ALDOC
	0.319	0.670	APOB	APOB
	0.000	0.667	LAMB4	LAMB4
	1.478	0.662	GAR1	GAR1
	0.562	0.659	ENO1; ENO3	ENO1; ENO3
	0.371	0.641	LDHB	LDHB
	0.465	0.641	CLIC1	CLIC1
	0.861	0.641	MSH6	MSH6
	0.407	0.614	CKB	CKB
	0.212	0.612	SNRPD1	SNRPD1
	0.207	0.612	HIST1H1D; HIST1H1B	HIST1H1D; HIST1H1B
	0.275	0.611		
	0.338	0.607	IPO7	IPO7
	0.567	0.600	DYNLT1	DYNLT1
	0.554	0.582	OLA1	OLA1
	0.323	0.581	NARS	NARS
	0.606	0.560	CSNK2A1	CSNK2A1
	0.450	0.509	CSNK2B	CSNK2B
	0.685	0.509	RHEB	RHEB
	0.374	0.508	DHFR	DHFR
	0.464	0.503	CLTCL1; CLTC	CLTCL1; CLTC
	0.000	0.499	TXNDC9	TXNDC9
	0.198	0.490	PIP4K2C	PIP4K2C
	0.475	0.489	NAP1L1; NAP1L4B; NAP1L4	NAP1L1; NAP1L4B; NAP1L4

	0.505	0.489	EIF4A1; EIF4A3; EIF4A2	EIF4A1; EIF4A2
	0.377	0.483	TUBA1A	TUBA1A
	0.581	0.459	NUP107	NUP107
	0.000	0.443	RPS26	RPS26
	0.724	0.441	ATP6V1A	ATP6V1A
	0.365	0.427	HBZ	HBZ
	0.544	0.414	CCT7	CCT7
	0.506	0.405	EIF5B	EIF5B
	0.259	0.385	MAP4	MAP4
	0.200	0.378	HMGB3	HMGB3
	0.000	0.371	XAB2	XAB2
	0.119	0.365	EEF1G	EEF1G
	0.167	0.365	PPP2R1A	PPP2R1A
	0.144	0.360	TUBA1C; TUBA1B; TUBA3C; TUBA1A	TUBA3C
	0.195	0.347	HDAC1; HDAC2	HDAC1
	0.309	0.331	FLNA	FLNA
	0.444	0.324	MCCC1; ACACB	ACACB
	0.181	0.322	GAPDH	GAPDH
	0.275	0.316	MAP4K4	MAP4K4
	0.129	0.311	CAND1	CAND1
	0.000	0.305	PRMT5	PRMT5
	0.157	0.304	CAP1	CAP1
	0.126	0.304	CKM; CKB	CKM; CKB
	0.000	0.299	CKB	CKB
	0.759	0.292	PGK1	PGK1
	0.000	0.289	ZCCHC17	ZCCHC17
	0.204	0.276	NOP2	NOP2
	0.097	0.271	TPR	TPR
	0.142	0.257	PGK1	PGK1
	0.414	0.252	FAM115C	FAM115C

	0.102	0.239	FBL	FBL
	0.419	0.233	KPNA7; KPNA2	KPNA7; KPNA2
	0.189	0.230	DRIP4	DRIP4
	0.196	0.223	CCT5	CCT5
	0.000	0.216	C8ORF59	C8ORF59
	0.235	0.215	PPIF	PPIF
	0.900	0.213	ACACA	ACACA
	0.529	0.208		
	0.000	0.207	NASP	NASP
	0.148	0.206	NANS	NANS
	0.101	0.192	HSD17B6	HSD17B6
	0.079	0.186	PTGR1	PTGR1
	0.000	0.184	HNRNPU	HNRNPU
	0.091	0.183	MCM7	MCM7
	0.273	0.180	CCT6A	CCT6A
	0.113	0.179	MDH1	MDH1
	0.181	0.178	ACACA	ACACA
	0.237	0.177	ITLN2; ITLN1	ITLN2; ITLN1
	0.468	0.175	HMGB2; HMGB1	HMGB2; HMGB1
	0.451	0.174	IARS	IARS
	0.275	0.171	GAPDH	GAPDH
	0.461	0.170	GPI	GPI
	0.260	0.163	TUBA1C	TUBA1C
	0.240	0.158	ACACB	ACACB
	0.153	0.154	PRIM1	PRIM1
	0.239	0.154	CCT2	CCT2
	0.209	0.145	NOP56; DDX27	NOP56
	0.229	0.142	TUBB6; TUBB4B; TUBB3; TUBB; TUBB2A; TUBB2C; TUBB2B	TUBB4B; TUBB; TUBB2B

	0.051	0.128	TSG101	TSG101
	0.248	0.128	DDX39B; BAT1; DDX39A	DDX39B; BAT1; DDX39A
	0.053	0.126	PKM	PKM
	0.194	0.125	HBZ	HBZ
	0.086	0.123	DNM1L	DNM1L
	0.056	0.122	CCDC176	CCDC176
	0.160	0.119	EEF1A1; EEF1A2; TYW5	EEF1A1; EEF1A2
	0.147	0.118	ST13	ST13
	0.073	0.117	H1FOO	H1FOO
	0.156	0.114	PSMD6	PSMD6
	0.000	0.110	PDPR	PDPR
	0.000	0.106	AP2M1	AP2M1
	0.064	0.104	UBA6	UBA6
	0.267	0.103	MAP2K1	MAP2K1
	0.152	0.103	TUBA1C; TUBA4A; TUBA3C; TUBA1B	TUBA4A
	0.191	0.103	RPS6KA1; RPS6KA3; RPS6KA6	RPS6KA1; RPS6KA3
	0.109	0.101	LOC392793; EEF1B2	EEF1B2
	0.098	0.097	UBE2O	UBE2O
	0.051	0.095	ACRC; HDLBP	HDLBP
	0.151	0.094	ACACA	ACACA
	0.070	0.085	PSMD2	PSMD2
	0.000	0.081	PRPF40A	PRPF40A
	0.084	0.072	ACTB	ACTB
	0.055	0.068	ANXA1	ANXA1
	0.000	0.066	ST13	ST13

	0.237	0.065	TUBA1C; TUBA4A; TUBA1B	TUBA4A
	0.043	0.060	DARS	DARS
	0.043	0.059	CDK18; NEK5; CDK12; CDK13; CDK16; CDK17; CDK14; CDK15; CDK1; CDK2; CDK4; CDK5; CDK9	CDK1
	0.042	0.055	TUBB4B; TUBB4A; TUBB2B	TUBB4B; TUBB2B
	0.135	0.053	MGC4836	MGC4836
	0.114	0.048	FARSB	FARSB
	0.035	0.040	NMRAL1	NMRAL1
	0.033	0.040	ACACA	ACACA
	0.035	0.035	CKM; CKB	CKB
	0.160	0.034	PRPF8	PRPF8
	0.063	0.032	CAPN1	CAPN1
	0.041	0.031	MCM4	MCM4
	0.000	0.030	EEF1G	EEF1G
	0.062	0.027	ARF3; ARF1	ARF3; ARF1
	0.034	0.024	TUBA4A	TUBA4A
	0.008	0.017	RARS	RARS
	0.002	0.004	VTA1	VTA1
	0.000	0.000	YARS	YARS
	0.002	-0.002	RRM1	RRM1
	0.013	-0.006	CCT6A	CCT6A

	0.013	-0.012	HPGDS	HPGDS
	0.000	-0.014	U2AF1; U2AF1L4	U2AF1; U2AF1L4
	0.017	-0.015	RPS8	RPS8
	0.014	-0.016	GSTO2; GSTO1	GSTO1
	0.047	-0.017	PRSS1	PRSS1
	0.010	-0.020	IPO7	IPO7
	0.039	-0.021	ACTA2; ACTA1; ACTG1; ACTG2; ACTC1; ACTB	ACTB; ACTG1
	0.032	-0.026	TPI1	TPI1
	0.028	-0.027	TUBA1C	TUBA1C
	0.037	-0.030	TCOF1	TCOF1
	0.010	-0.034	NPM2	NPM2
	0.015	-0.046	NPM2	NPM2
	0.090	-0.051	UGDH	UGDH
	0.028	-0.061	RPL31	RPL31
	0.029	-0.070	GEMIN5	GEMIN5
	0.021	-0.082	H1F0	H1F0
	0.046	-0.088	RPS6	RPS6
	0.239	-0.089	HSP90AB1; HSP90B1	HSP90AB1
	0.048	-0.091	IMPDH2	IMPDH2
	0.124	-0.094	ACACA	ACACA
	0.063	-0.100	MCM6	MCM6
	0.095	-0.102	UBA1	UBA1
	0.082	-0.105	CFL1	CFL1
	0.000	-0.113	SSB	SSB
	0.055	-0.113	UMPS	UMPS
	0.128	-0.116	RP11-632C17__A.1-001	RP11-632C17__A.1-001
	0.055	-0.118	DCTN1	DCTN1
	0.224	-0.119	MCM3	MCM3
	0.101	-0.122	PSMD1	PSMD1
	0.062	-0.123	HSP90AB1	HSP90AB1

	0.064	-0.128	CSE1L	CSE1L
	0.089	-0.128	DKC1	DKC1
	0.145	-0.132	MYBBP1A	MYBBP1A
	0.098	-0.134	TAF6	TAF6
	0.128	-0.136	RPS9	RPS9
	0.136	-0.138	H1FOO	H1FOO
	0.071	-0.148	MDN1	MDN1
	0.089	-0.151	CCT2	CCT2
	0.184	-0.152	QARS	QARS
	0.203	-0.158	PSMD11	PSMD11
	0.331	-0.160	RBM14; CCT4; RBM14/RBM4 FUSION	CCT4
	0.126	-0.162	VPS4A; VPS4B	VPS4B
	0.269	-0.167	PSMD12	PSMD12
	0.141	-0.170	DDX1	DDX1
	0.375	-0.171	HBA1; HBZ	HBZ
	0.052	-0.172	PSMD4	PSMD4
	0.307	-0.175	CSE1L	CSE1L
	0.139	-0.176	GBP1; GBP4	GBP1
	0.083	-0.177	RPS23	RPS23
	0.159	-0.178	ARCN1	ARCN1
	0.471	-0.184	GART	GART
	0.056	-0.184	RAN	RAN
	0.076	-0.185	EEF2	EEF2
	0.401	-0.187	PFN1	PFN1
	0.269	-0.188	PSMD2	PSMD2
	0.000	-0.190	ECD	ECD
	0.218	-0.194	YWHAQ	YWHAQ
	0.286	-0.194	PRIC295; GCN1L1	PRIC295
	0.088	-0.202	HCFC1	HCFC1
	0.424	-0.203	EEF1G	EEF1G
	0.232	-0.206	TCP1	TCP1

	0.159	-0.209	LYPLA2	LYPLA2
	0.352	-0.210	GRHPR	GRHPR
	0.103	-0.210	CAB39L; CAB39	CAB39L; CAB39
	0.095	-0.221	DNAJB7; DNAJB6	DNAJB7; DNAJB6
	0.888	-0.225	PSMD3	PSMD3
	0.047	-0.230	KIF27	KIF27
	0.802	-0.231	HSPA2; HSPA1A; HSPA8; HSPA5	HSPA8
	0.222	-0.232	YWHAZ; YWHAH; YWHAQ; YWHAG; YWHAE	YWHAQ
	0.108	-0.234	BAZ1A	BAZ1A
	0.360	-0.236	LRRC40	LRRC40
	0.287	-0.237	UBA2	UBA2
	0.202	-0.239	AQR	AQR
	0.000	-0.239	TCEB1	TCEB1
	0.214	-0.248	NANS	NANS
	0.321	-0.251	CCT8	CCT8
	0.097	-0.253	NOP58	NOP58
	0.168	-0.259		
	0.233	-0.259	SFRS2	SFRS2
	0.471	-0.263	EIF2S3	EIF2S3
	0.226	-0.265	RPL23A	RPL23A
	0.307	-0.266	PSMC1	PSMC1
	0.284	-0.267	DRG2	DRG2
	0.875	-0.273	PSMD13	PSMD13
	0.076	-0.274	CETN2	CETN2
	0.133	-0.281	CSNK2A2	CSNK2A2
	0.169	-0.284	IPO4	IPO4
	0.303	-0.284	COPA	COPA
	0.091	-0.291	IPO5	IPO5
	1.110	-0.293	DYNC1H1	DYNC1H1

	0.695	-0.293	KPNB1	KPNB1
	1.288	-0.302		
	0.132	-0.311	TBCB	TBCB
	0.087	-0.313	ACTA2; ACTA1; ACTG1; ACTG2; ACTC1; ACTB	ACTA2; ACTA1; ACTG1; ACTG2; ACTC1; ACTB
	0.233	-0.314	HIST2H2BF	HIST2H2BF
	0.314	-0.321	CCT3	CCT3
	1.718	-0.323	TUBA1B	TUBA1B
	0.000	-0.324	CAD	CAD
	0.290	-0.334	TCEB3	TCEB3
	0.379	-0.335	EEF1D; EEF1B2	EEF1D
	0.258	-0.343	DPCD	DPCD
	0.454	-0.350	AKR1B1	AKR1B1
	0.764	-0.356	PSMD7	PSMD7
	0.810	-0.356	MYO5C; MYO5B; MYO5A	MYO5A
	0.512	-0.360	CAMK2D; CAMK2G; CAMK2A; CAMK2B	CAMK2D; CAMK2G; CAMK2B
	0.537	-0.371	CTPS1	CTPS1
	0.337	-0.374	TPI1	TPI1
	0.214	-0.379	DNAJC2	DNAJC2
	0.307	-0.390	RPS11	RPS11
	0.303	-0.390	TEX10	TEX10
	0.263	-0.395	MCM2	MCM2
	0.250	-0.408	SRP72	SRP72
	0.344	-0.409	GSTA1	GSTA1
	0.299	-0.411	EEF1G	EEF1G
	0.383	-0.415	PSMC6	PSMC6
	0.397	-0.420	PSMC2	PSMC2
	0.571	-0.429	HSPA8	HSPA8

	0.396	-0.438	PSMC3	PSMC3
	0.285	-0.447	CHMP1A	CHMP1A
	0.362	-0.448	DNAJA1; DNAJA4	DNAJA1; DNAJA4
	0.493	-0.456	POLD1	POLD1
	0.335	-0.461	CHMP2A	CHMP2A
	0.273	-0.470	CHMP1B	CHMP1B
	0.433	-0.479	EPRS	EPRS
	0.360	-0.483	POLD3	POLD3
	0.343	-0.483	G6PD; H6PD	G6PD
	0.445	-0.484	HMGB1	HMGB1
	0.209	-0.485	HIST1H4A	HIST1H4A
	0.000	-0.487	NOL9	NOL9
	0.340	-0.489	COPG1	COPG1
	0.425	-0.498	ABCE1	ABCE1
	0.485	-0.501	EXOC1	EXOC1
	0.321	-0.508	YWHAB	YWHAB
	0.281	-0.509	KIF5B	KIF5B
	0.179	-0.515	RBBP6	RBBP6
	0.225	-0.524	MTA2	MTA2
	0.816	-0.526	CENPA; H3F3A; HIST2H3A; H3F3B	H3F3A; HIST2H3A; H3F3B
	0.477	-0.527	GBE1	GBE1
	0.388	-0.534	PSMC4	PSMC4
	0.340	-0.538	VARS2; VARS	VARS2; VARS
	0.709	-0.538	PSMC5; SPATA5	PSMC5
	0.312	-0.539	RAD50	RAD50
	0.294	-0.542	RPL29; RP11-632C17__A.1-001	RPL29; RP11-632C17__A.1-001
	0.315	-0.548	SNRPD2	SNRPD2
	0.314	-0.549	NSF	NSF
	0.159	-0.555	COPE	COPE

	0.385	-0.556	CCT4	CCT4
	1.792	-0.560	FEN1	FEN1
	0.000	-0.567	DKFZP781K0743	DKFZP781K0743
	0.000	-0.578	CBR1	CBR1
	0.000	-0.601		
	0.339	-0.607	AP3D1	AP3D1
	0.301	-0.608	CHMP2A	CHMP2A
	0.450	-0.613	ACLY; ACLY VARIANT PROTEIN	ACLY; ACLY VARIANT PROTEIN
	0.584	-0.621	LIG1	LIG1
	0.310	-0.627	CKAP5	CKAP5
	0.252	-0.632	RANBP2	RANBP2
	0.000	-0.632	TYMS	TYMS
	0.338	-0.635	PCM1	PCM1
	0.463	-0.635	GBP2; GBP1; GBP7; GBP5; GBP4	GBP1; GBP4
	0.438	-0.655	EEF1A1; EEF1A2	EEF1A1
	0.807	-0.657	CHMP5	CHMP5
	0.377	-0.660	KAT8; TRIM69	KAT8; TRIM69
	0.416	-0.674	DHRS12	DHRS12
	0.000	-0.680	FNTA	FNTA
	0.000	-0.682	CSNK2A1	CSNK2A1
	0.000	-0.683	IPO7	IPO7
	0.901	-0.686		
	0.000	-0.691	FKBP3	FKBP3
	0.221	-0.715	KARS	KARS
	0.000	-0.720	PGAM2; PGAM1	PGAM2; PGAM1
	0.507	-0.730	TRIM69	TRIM69
	0.554	-0.744	RPS3A	RPS3A
	0.332	-0.744	MARS	MARS
	0.771	-0.751	LARS	LARS

	0.000	-0.751	TRIP13	TRIP13
	1.190	-0.754	FARSA	FARSA
	0.365	-0.756	RANGAP1	RANGAP1
	0.902	-0.766	DNAJC9	DNAJC9
	0.673	-0.793	GART	GART
	0.472	-0.799	EPRS	EPRS
	0.909	-0.801	TBC1D24	TBC1D24
	0.369	-0.805	RNASEH2B	RNASEH2B
	0.356	-0.807	NASP	NASP
	0.528	-0.812	MCM5	MCM5
	0.841	-0.816	GEMIN4	GEMIN4
	0.897	-0.826	HIST1H4A	HIST1H4A
	0.589	-0.835	RFC3	RFC3
	0.832	-0.838	ABCF1	ABCF1
	0.291	-0.864	UBA52; RPS27A; UBBP4; UBB; UBC	UBA52; RPS27A; UBB; UBC
	0.554	-0.873	CHMP4B	CHMP4B
	0.703	-0.881	PFKM	PFKM
	0.378	-0.882	HIST2H2AB	HIST2H2AB
	0.000	-0.898	IPO9	IPO9
	0.405	-0.906	EPRS	EPRS
	0.472	-0.906	PCNA	PCNA
	0.796	-0.923	RPL23	RPL23
	0.702	-0.972	EIF3F	EIF3F
	0.931	-0.974	COPB1	COPB1
	1.225	-0.974	HIST1H2BJ	HIST1H2BJ
	0.686	-0.993	NCCRP1	NCCRP1
	1.205	-1.005	GPD1	GPD1
	1.105	-1.022	NACA	NACA
	0.723	-1.036	H2AFX; H2AFV; HIST2H2AB; H2AFZ; H2AFJ	H2AFX; HIST2H2AB; H2AFJ
	0.401	-1.070	PSMD10	PSMD10

	0.880	-1.102	CHTF18	CHTF18
	0.000	-1.115	CHD3; CHD5; CHD4	CHD3; CHD4
	0.703	-1.139	PROSC	PROSC
	0.634	-1.151	PRDX2	PRDX2
	0.000	-1.154	SMARCAD1	SMARCAD1
	0.540	-1.160	EPB41L2	EPB41L2
	0.759	-1.175	NHP2	NHP2
	0.000	-1.193	UBE2N	UBE2N
	1.400	-1.205		
	1.123	-1.213	RPL17	RPL17
	0.000	-1.275	THYN1	THYN1
	0.334	-1.369	SEC23B	SEC23B
	0.000	-1.380	EIF4G1	EIF4G1
	0.742	-1.401	CHMP2B	CHMP2B
	0.545	-1.409	SFI1	SFI1
	0.381	-1.412	DLGAP5	DLGAP5
	0.000	-1.474	HMGA2	HMGA2
	1.328	-1.559	DNAJC13	DNAJC13
	0.661	-1.596	PRMT1	PRMT1
	0.000	-1.628	COPA	COPA
	0.709	-1.780	MYH10; MYH9; MYH14	MYH10; MYH9; MYH14
	0.491	-1.847	UBB	UBB
	0.400	-1.936	APAF1	APAF1
	0.000	-1.995	CFL1	CFL1
	0.000	-2.162	CCT6A	CCT6A
	1.620	-2.411	TTLL7	TTLL7
	0.000	-2.870	ANXA11; ANXA7	ANXA11; ANXA7
	0.000	NaN	HIST2H2BF; HIST1H2BJ; HIST1H2BA	HIST2H2BF; HIST1H2BJ
	0.000	NaN	AHNAK	AHNAK
	0.000	NaN	RFC4	RFC4
	0.000	NaN	MSH2	MSH2

	0.000	NaN	SPTAN1	SPTAN1
	0.000	NaN	PARP4	PARP4
	0.000	NaN	RAPGEF3	RAPGEF3
	0.000	NaN	COPB2	COPB2
	0.000	NaN	RPL10A	RPL10A
	0.000	NaN	TLN1	TLN1
	0.000	NaN	RPL3	RPL3
	0.000	NaN	ANXA1	ANXA1
	0.000	NaN	RRAGC	RRAGC
	0.000	NaN	RFC2	RFC2
	0.000	NaN	AKR1B1; AKR1B15	AKR1B1; AKR1B15
	0.000	NaN	HSPA8	HSPA8

dCas9-BirA* + On-Target gRNA vs. dCas9-BirA* + NT gRNA

Significant	-Log (p-value)	Log_2 (Fold Change)	Protein IDs	Majority protein IDs
	0.926	6.890	PIP4K2C	PIP4K2C
	2.465	5.333	SFI1	SFI1
	0.000	5.254	NHP2	NHP2
	0.924	3.173	NOLC1	NOLC1
	0.000	3.109	ANXA11; ANXA7	ANXA11; ANXA7
	0.000	2.928	CFL1	CFL1
	0.000	2.684	CETN2	CETN2
	1.234	2.528	FBL	FBL
	0.000	2.512	GAR1	GAR1
	0.639	2.285	H1F0	H1F0
	0.750	2.134	PRMT1	PRMT1
	0.332	2.110	DKC1	DKC1
	1.947	2.049	DNAJC13	DNAJC13
	0.769	2.013	MYH10; MYH9; MYH14	MYH10; MYH9; MYH14
	0.000	1.794	FKBP3	FKBP3
	0.834	1.719	TPR	TPR
	0.901	1.718	TTLL7	TTLL7

	1.017	1.611	RNASEH2B	RNASEH2B
	0.800	1.539	EIF4G1	EIF4G1
	1.249	1.508	NOP2	NOP2
	1.297	1.494	AP3D1	AP3D1
	1.099	1.376	SSRP1	SSRP1
	0.000	1.369	TPI1	TPI1
	0.496	1.311	PRDX2	PRDX2
	0.000	1.291	NPM2	NPM2
	0.394	1.289	APAF1	APAF1
	0.299	1.271	ALDOA ;ALDOC	ALDOA; ALDOC
	1.156	1.228	H1FOO	H1FOO
	0.508	1.209	IPO5	IPO5
	0.845	1.189	SUPT16H	SUPT16H
	0.648	1.161	RANBP2	CH
	0.850	1.148	ACRC; HDLBP	HDLBP
	1.045	1.142	EPB41L2	EPB41L2
	0.398	1.073	KARS	KARS
	0.547	1.045	PCNA	PCNA
	0.872	1.044	SUB1	SUB1
	0.966	1.044		
	0.703	1.042	CAND1	CAND1
	0.755	1.034	MCM2	MCM2
	0.000	1.022	CCT6A	CCT6A
	0.490	0.937	PPP2R1A	PPP2R1A
	1.005	0.934	GPD1	GPD1
	0.643	0.931	RANGAP1	RANGAP1
	0.000	0.922	PGAM2; PGAM1	PGAM2; PGAM1
	0.356	0.905	RAN	RAN
	0.725	0.904	RBBP6	RBBP6
	0.655	0.889	YWHAB	YWHAB
	0.000	0.885	DHRS12	DHRS12
	0.305	0.880	HIST1H1D	HIST1H1D
	0.000	0.871	GEMIN4	GEMIN4
	1.172	0.869	NOP56; DDX27	NOP56

	0.719	0.847	EPRS	EPRS
	0.399	0.843	NPM2	NPM2
	0.380	0.820	EPRS	EPRS
	0.404	0.798	KIF5B	KIF5B
	0.416	0.795	NOP58	NOP58
	0.000	0.786	CSNK2A1	CSNK2A1
	0.577	0.752	PROSC	PROSC
	0.502	0.745	GEMIN5	GEMIN5
	0.518	0.740	HCFC1	HCFC1
	0.212	0.739	HIST1H1D; HIST1H1B	HIST1H1D; HIST1H1B
	0.377	0.732	PKM	PKM
	0.319	0.699	PSMD10	PSMD10
	0.000	0.693	TRPM7	TRPM7
	0.405	0.690	EEF1A1; EEF1A2	EEF1A1
	0.435	0.668	HSP90AB1	HSP90AB1
	0.328	0.666	SNRPD2	SNRPD2
	0.515	0.665	RPL29; RP11-632C17__A.1-001	RPL29; RP11-632C17__A.1-001
	0.000	0.658	RAPGEF3	RAPGEF3
	0.324	0.649	MDN1	MDN1
	0.355	0.637	MARS	MARS
	0.274	0.634	NASP	NASP
	0.699	0.631	RPS11	RPS11
	0.414	0.628	UMPS	UMPS
	1.873	0.617	FEN1	FEN1
	0.397	0.614	CAB39L; CAB39	CAB39L; CAB39
	0.773	0.610	ACACA	ACACA
	0.459	0.606	MCM5	MCM5
	0.000	0.597	IPO7	IPO7
	0.774	0.593	PSMC2	PSMC2
	0.385	0.584	RFC3	RFC3
	0.441	0.581	SRP72	SRP72
	0.501	0.581		
	0.711	0.580	TCEB3	TCEB3

	0.858	0.570	TYMS	TYMS
	0.261	0.563	MCM4	MCM4
	0.623	0.560	CKM; CKB	CKB
	0.722	0.552	SFRS2	SFRS2
	0.207	0.548	CIRBP	CIRBP
	0.516	0.540	POLD1	POLD1
	0.418	0.540	ACLY; ACLY VARIANT PROTEIN	ACLY; ACLY VARIANT PROTEIN
	0.359	0.531	GART	GART
	0.517	0.511	LYPLA2	LYPLA2
	0.328	0.508	MTA2	MTA2
	0.460	0.508	DPCD	DPCD
	0.394	0.494	EIF3F	EIF3F
	0.625	0.493	MAP4K4	MAP4K4
	0.580	0.481	CCT3	CCT3
	0.283	0.481	CKAP5	CKAP5
	0.000	0.475	RPL10A	RPL10A
	0.723	0.472	EIF5B	EIF5B
	0.446	0.470	TBC1D24	TBC1D24
	0.201	0.468	SEC23B	SEC23B
	0.813	0.463	CAD	CAD
	0.351	0.458	PCM1	PCM1
	0.429	0.457	LIG1	LIG1
	0.288	0.455	DNAJA1; DNAJA4	DNAJA1; DNAJA4
	0.381	0.452	NCCRP1	NCCRP1
	1.180	0.450	ARF3; ARF1	ARF3; ARF1
	0.000	0.449	ANXA1	ANXA1
	0.952	0.447	H1FOO	H1FOO
	0.475	0.445	PSMC3	PSMC3
	0.264	0.437	G6PD; H6PD	G6PD
	0.000	0.432	TRIM69	TRIM69
	1.270	0.430	NACA	NACA
	0.833	0.429	KPNB1	KPNB1

	0.427	0.424	MGC4836	MGC4836
	1.747	0.424	PSMD7	PSMD7
	0.321	0.418	RPS6	RPS6
	0.998	0.414	FARSA	FARSA
	0.187	0.414	EEF2	EEF2
	0.623	0.411	DNAJC2	DNAJC2
	0.834	0.410	NHP2L1	NHP2L1
	0.413	0.406	VARS2; VARS	VARS2; VARS
	0.570	0.405	CTPS1	CTPS1
	0.428	0.403	PSMD3	PSMD3
	0.551	0.400	MCCC1; ACACB	ACACB
	0.603	0.399	LARS	LARS
	0.441	0.396	EEF1G	EEF1G
	0.597	0.392	MSH6	MSH6
	0.168	0.390	DLGAP5	DLGAP5
	0.000	0.387	MSH2	MSH2
	0.519	0.349	IMPDH2	IMPDH2
	0.418	0.343	ABCE1	ABCE1
	0.366	0.340	PSMC1	PSMC1
	0.298	0.334	TPI1	TPI1
	0.000	0.329	MAP4	MAP4
	0.461	0.329		
	0.309	0.320	IPO4	IPO4
	0.184	0.311	NSF	NSF
	0.659	0.310	CCT6A	CCT6A
	0.515	0.307	GRHPR	GRHPR
	0.501	0.305	YWHAZ; YWHAH; YWHAQ; YWHAG; YWHAE	YWHAQ
	0.159	0.298	CSNK2A2	CSNK2A2
	0.229	0.294	COPG1	COPG1
	0.477	0.291	TCP1	TCP1
	0.634	0.290	PFN1	PFN1
	0.000	0.279	C8ORF59	C8ORF59

	0.416	0.277	PSMD12	PSMD12
	0.151	0.275	CCT2	CCT2
	2.060	0.273	TUBA1B	TUBA1B
	0.659	0.266	ACTA2; ACTA1; ACTG1; ACTG2; ACTC1; ACTB	ACTB; ACTG1
	0.385	0.264	CAMK2D; CAMK2G; CAMK2A; CAMK2B	CAMK2D; CAMK2G; CAMK2B
	0.937	0.257	PRSS1	PRSS1
	0.000	0.256	RRAGC	RRAGC
	0.159	0.250	POLD3	POLD3
	0.303	0.244	PSMC4	PSMC4
	0.153	0.242	BAZ1A	BAZ1A
	0.641	0.241	MCM3	MCM3
	0.329	0.235	RPL23A	RPL23A
	0.238	0.228	DNAJC9	DNAJC9
	0.270	0.227	EPRS	EPRS
	0.099	0.223	RAD50	RAD50
	0.813	0.214	TUBA1C; TUBA4A; TUBA1B	TUBA4A
	0.320	0.211	TUBB6; TUBB4B; TUBB3; TUBB; TUBB2A; TUBB2C; TUBB2B	TUBB4B; TUBB; TUBB2B
	0.245	0.211	EXOC1	EXOC1
	0.196	0.210	HIST2H2BF	HIST2H2BF
	0.384	0.208	RP11-632C17__A.1-001	RP11-632C17__A.1-001

	0.199	0.207	VPS4A; VPS4B	VPS4B
	0.115	0.202	KAT8; TRIM69	KAT8; TRIM69
	0.225	0.200	UGDH	UGDH
	0.276	0.200	DDX39B; BAT1; DDX39A	DDX39B; BAT1; DDX39A
	0.000	0.194	TCEB1	TCEB1
	0.167	0.194	CFL1	CFL1
	0.168	0.188	CHTF18	CHTF18
	0.119	0.186	TBCB	TBCB
	0.128	0.185	GBE1	GBE1
	0.247	0.181	PSMC5; SPATA5	PSMC5
	0.102	0.176	MDH1	MDH1
	0.194	0.175	NANS	NANS
	0.330	0.174	NUP107	NUP107
	0.467	0.171	HBA1; HBZ	HBZ
	0.112	0.170	DDX1	DDX1
	0.060	0.167	LDHB	LDHB
	0.617	0.158	DYNC1H1	DYNC1H1
	0.096	0.157	COPB1	COPB1
	0.101	0.154	CCT4	CCT4
	0.110	0.153	RPL17	RPL17
	0.000	0.128	COPA	COPA
	0.147	0.127	CCT8	CCT8
	0.000	0.113	IPO9	IPO9
	0.133	0.109	DKFZP781K0743	DKFZP781K0743
	0.110	0.109	AKR1B1	AKR1B1
	0.000	0.108	TRIP13	TRIP13
	0.079	0.095	YARS	YARS
	0.133	0.082	PRPF8	PRPF8
	0.073	0.073	TUBA1C	TUBA1C
	0.127	0.064	ITLN2; ITLN1	ITLN2; ITLN1
	0.088	0.063	GAPDH	GAPDH

	0.074	0.058	ACACB	ACACB
	0.101	0.056	PGK1	PGK1
	0.107	0.054	ACACA	ACACA
	0.050	0.052	ACACA	ACACA
	0.059	0.052	PSMD2	PSMD2
	0.057	0.051	YWHAQ	YWHAQ
	1.245	0.050	HLCS	HLCS
	0.122	0.048	MAP2K1	MAP2K1
	0.065	0.044	ACACA	ACACA
	0.042	0.040	ACACA	ACACA
	0.090	0.034	DCTN1	DCTN1
	0.000	0.030	PRPF40A	PRPF40A
	0.063	0.023	ATP6V1A	ATP6V1A
	0.048	0.020		
	0.020	0.018	LRRC40	LRRC40
	0.011	0.012	PSMD6	PSMD6
	0.008	0.010	HNRNPU	HNRNPU
	0.003	0.009	ACTA2; ACTA1; ACTG1; ACTG2; ACTC1; ACTB	ACTA2; ACTA1; ACTG1; ACTG2; ACTC1; ACTB
	0.002	0.003	GSTA1	GSTA1
	0.000	0.000	PSMD11	PSMD11
	0.013	-0.007	CCT6A	CCT6A
	0.005	-0.008	FLNA	FLNA
	0.005	-0.009	VTA1	VTA1
	0.018	-0.013	EEF1A1; EEF1A2; TYW5	EEF1A1; EEF1A2
	0.047	-0.015	PSMD13	PSMD13
	0.031	-0.022	PRIC295; GCN1L1	PRIC295
	0.051	-0.032	MYO5C; MYO5B; MYO5A	MYO5A
	0.103	-0.040	RRM1	RRM1

	0.058	-0.040	PSMC6	PSMC6
	0.000	-0.041	TUBA4A	TUBA4A
	0.169	-0.047		
	0.093	-0.048	TCOF1	TCOF1
	0.052	-0.058	EIF4A1; EIF4A3; EIF4A2	EIF4A1; EIF4A2
	0.000	-0.064	ZCCHC17	ZCCHC17
	0.090	-0.064	HIST1H4A	HIST1H4A
	0.049	-0.070	TUBA1A	TUBA1A
	0.065	-0.076	CAPN1	CAPN1
	0.076	-0.083	DRG2	DRG2
	0.000	-0.089	LAMB4	LAMB4
	0.154	-0.096	GPI	GPI
	0.240	-0.099	FARSB	FARSB
	1.229	-0.101	HSP90AB1; HSP90B1	HSP90AB1
	0.161	-0.103	PPIF	PPIF
	0.129	-0.105	TUBA1C; TUBA4A; TUBA3C; TUBA1B	TUBA4A
	0.355	-0.105	GSTO2; GSTO1	GSTO1
	0.068	-0.107	NOL9	NOL9
	0.134	-0.109	CCT2	CCT2
	0.064	-0.114	NAP1L1; NAP1L4B; NAP1L4	NAP1L1; NAP1L4B; NAP1L4
	0.073	-0.122	IPO7	IPO7
	0.000	-0.133	RPS26	RPS26
	0.141	-0.135	UBA2	UBA2
	0.000	-0.136	PDPR	PDPR
	0.068	-0.137	XAB2	XAB2
	0.183	-0.142	EIF2S3	EIF2S3
	0.058	-0.145	THYN1	THYN1
	0.366	-0.148	IARS	IARS

	0.149	-0.148	TUBB4B; TUBB4A; TUBB2B	TUBB4B; TUBB2B
	0.097	-0.154	MCM6	MCM6
	0.062	-0.156	PGK1	PGK1
	0.120	-0.157	CLTCL1; CLTC	CLTCL1; CLTC
	0.319	-0.160	GART	GART
	0.481	-0.161	EEF1D; EEF1B2	EEF1D
	0.129	-0.162	UBA1	UBA1
	0.248	-0.164	TUBA1C	TUBA1C
	0.254	-0.165	RPS8	RPS8
	0.089	-0.166	CKM; CKB	CKM; CKB
	0.463	-0.167	HSPA2; HSPA1A; HSPA8; HSPA5	HSPA8
	0.000	-0.170	TXNDC9	TXNDC9
	0.000	-0.175	ST13	ST13
	0.313	-0.176	CENPA; H3F3A; HIST2H3A; H3F3B	H3F3A; HIST2H3A; H3F3B
	0.151	-0.179		
	0.201	-0.181	CCT7	CCT7
	0.101	-0.182	GSTM1	GSTM1
	0.212	-0.183	QARS	QARS
	0.326	-0.187	RPS6KA1; RPS6KA3; RPS6KA6	RPS6KA1; RPS6KA3
	0.278	-0.189	ACTB	ACTB
	0.182	-0.194	ARCN1	ARCN1
	0.178	-0.198	ECD	ECD
	0.361	-0.205	CSE1L	CSE1L
	0.000	-0.206	PPM1H	PPM1H
	1.071	-0.213	APOB	APOB

	0.294	-0.216	MYBBP1A	MYBBP1A
	0.000	-0.222	CKB	CKB
	0.179	-0.226	CSNK2A1	CSNK2A1
	0.956	-0.243	CHMP5	CHMP5
	0.142	-0.245	PFKM	PFKM
	0.186	-0.246	HBZ	HBZ
	0.391	-0.251	HSPA8	HSPA8
	0.000	-0.265	DNAJB7; DNAJB6	DNAJB7; DNAJB6
	0.323	-0.265	HMGB1	HMGB1
	0.376	-0.274	ABCF1	ABCF1
	0.161	-0.274	DHFR	DHFR
	0.559	-0.283	EEF1G	EEF1G
	0.100	-0.285	KIF27	KIF27
	0.264	-0.293	DRIP4	DRIP4
	0.624	-0.310	RBM14; CCT4; RBM14/RBM4 FUSION	CCT4
	0.545	-0.317	FAM115C	FAM115C
	0.157	-0.332	CSE1L	CSE1L
	0.247	-0.338	GBP1; GBP4	GBP1
	0.182	-0.359	CAP1	CAP1
	0.181	-0.360	MCM7	MCM7
	0.347	-0.365	CCT5	CCT5
	0.350	-0.366	HPGDS	HPGDS
	0.812	-0.372	HMGB2; HMGB1	HMGB2; HMGB1
	0.325	-0.391	GBP2; GBP1; GBP7; GBP5; GBP4	GBP1; GBP4
	0.415	-0.394	AQR	AQR
	0.421	-0.409	LOC392793; EEF1B2	EEF1B2
	0.394	-0.411	CSNK2B	CSNK2B

	0.369	-0.412	RPS23	RPS23
	0.412	-0.424	UBE2O	UBE2O
	0.692	-0.428	HBZ	HBZ
	0.387	-0.432	DYNLT1	DYNLT1
	0.455	-0.435	ST13	ST13
	0.428	-0.435	NMRAL1	NMRAL1
	0.590	-0.435	GSTT1	GSTT1
	0.211	-0.436	IPO7	IPO7
	0.667	-0.440	EEF1G	EEF1G
	0.476	-0.447	KRT19; KRT18	KRT19; KRT18
	0.000	-0.447	CHD3; CHD5; CHD4	CHD3; CHD4
	0.898	-0.450	RPS9	RPS9
	0.404	-0.465	DARS	DARS
	0.308	-0.467	HDAC1; HDAC2	HDAC1
	0.281	-0.473	TEX10	TEX10
	0.395	-0.479	NANS	NANS
	0.211	-0.482	TUBA1C; TUBA1B; TUBA3C; TUBA1A	TUBA3C
	0.000	-0.495	FNTA	FNTA
	0.067	-0.509	RFC5	RFC5
	0.595	-0.516	COPA	COPA
	0.467	-0.517	PSMD1	PSMD1
	0.325	-0.521	GAPDH	GAPDH
	0.541	-0.525	ENO1; ENO3	ENO1; ENO3
	0.569	-0.529	PSMD2	PSMD2
	0.851	-0.547	HIST1H2BJ	HIST1H2BJ
	2.287	-0.570	KPNA7; KPNA2	KPNA7; KPNA2

	0.578	-0.570	CDK18; NEK5; CDK12; CDK13; CDK16; CDK17; CDK14; CDK15; CDK1; CDK2; CDK4; CDK5; CDK9	CDK1
	0.345	-0.576	RARS	RARS
	0.284	-0.580	PTGR1	PTGR1
	0.501	-0.595	CKB	CKB
	0.225	-0.611	HIST2H2AB	HIST2H2AB
	0.597	-0.622	UBA6	UBA6
	0.332	-0.626	NARS	NARS
	0.217	-0.644	PSMD4	PSMD4
	0.440	-0.648	CLIC1	CLIC1
	0.000	-0.648	AKR1B1; AKR1B15	AKR1B1; AKR1B15
	0.205	-0.649	MGC4836	MGC4836
	0.202	-0.671	COPE	COPE
	0.455	-0.687	RPL23	RPL23
	0.730	-0.712	ANXA1	ANXA1
	0.820	-0.730	CHMP2A	CHMP2A
	0.584	-0.735	KPNA6; KPNA1	KPNA6; KPNA1
	0.999	-0.746	RHEB	RHEB
	0.740	-0.764	RPS3A	RPS3A
	0.706	-0.769	DNM1L	DNM1L
	0.531	-0.772	HMGB3	HMGB3
	0.419	-0.786	RPL31	RPL31
	0.000	-0.794	AP2M1	AP2M1
	0.000	-0.801	PRIM1	PRIM1
	0.373	-0.813	CHMP2A	CHMP2A

	0.941	-0.843	CHMP4B	CHMP4B
	0.000	-0.844	SSB	SSB
	0.310	-0.851	EEF1G	EEF1G
	1.009	-0.854	OLA1	OLA1
	1.065	-0.865	H2AFX; H2AFV; HIST2H2AB; H2AFZ; H2AFJ	H2AFX; HIST2H2AB; H2AFJ
	0.000	-0.887	RPS15A	RPS15A
	0.000	-0.896	NASP	NASP
	0.000	-0.974	COPB2	COPB2
	0.910	-1.029	CHMP1A	CHMP1A
	0.708	-1.069	TSG101	TSG101
	0.498	-1.111	HIST1H4A	HIST1H4A
	0.417	-1.115	SNRPD1	SNRPD1
	0.326	-1.138	C2CD2L	C2CD2L
	1.598	-1.158	PRMT5	PRMT5
	0.305	-1.202	POLR2M	POLR2M
	0.524	-1.208	HIST2H2BF; HIST1H2BJ; HIST1H2BA	HIST2H2BF; HIST1H2BJ
	0.450	-1.220	KRT75; KRT8; KRT7	KRT75; KRT8; KRT7
	0.955	-1.281	CHMP1B	CHMP1B
	0.373	-1.320	NLRX1	NLRX1
	0.308	-1.385	CSE1L	CSE1L
	0.991	-1.559	CHMP2B	CHMP2B
	0.801	-2.072	UBA52; RPS27A; UBBP4; UBB; UBC	UBA52; RPS27A; UBB; UBC
	0.806	-2.099	UBB	UBB
	0.575	-2.362	C10ORF71	C10ORF71
	0.000	NaN	AHNAK	AHNAK
	0.000	NaN	HSD17B6	HSD17B6

	0.000	NaN	RFC4	RFC4
	0.000	NaN	HMGA2	HMGA2
	0.000	NaN	CCDC176	CCDC176
	0.000	NaN	SPTAN1	SPTAN1
	0.000	NaN	TAF6	TAF6
	0.000	NaN	U2AF1; U2AF1L4	U2AF1; U2AF1L4
	0.000	NaN	PARP4	PARP4
	0.000	NaN	CBR1	CBR1
	0.000	NaN	SMARCAD1	SMARCAD1
	0.000	NaN	DKC1	DKC1
	0.000	NaN	PIP4K2C	PIP4K2C
	0.000	NaN	TLN1	TLN1
	0.000	NaN	RPL3	RPL3
	0.000	NaN	RFC2	RFC2
	0.000	NaN	UBE2N	UBE2N
	0.000	NaN		
	0.000	NaN	NOP10	NOP10
	0.000	NaN	HSPA8	HSPA8

3.10 Table S2: Sequences of gRNAs

gRNA	Sequence
TetO	TCTCTATCACTGATAGGGAG
Chr5 Gene Desert #1	CCAGAAATTAACTGTACCTG
Chr5 Gene Desert #2	GAAGGTCAGACATTAATGTG
CD55 #1	GCTGACTTGGCTTTAGGGGT
CD55 #2	AATGCCCAGCCAGCTTTGGA
VEGFA	GACCCCCTCCACCCCGCCTC
CD59 #1	TTCTCAGAACCTGGGCCAGG
CD59 #2	GGCCCAGGTTCTGAGAAGGC
c-myc	GCGTCCTGGGAAGGGAGATC
Non-coding CD25	TTGGGCTGGCGTGTTCAGCC
Coding CD25	CACAAGGGTGACAGCCCAGG
Non-coding CD55	TCCAAAGCTGGCTGGGCATT
Coding CD55	AATGCCCAGCCAGCTTTGGA
Non-targeting	ACGGAGGCTAAGCGTCGCAA
CD25 -48NC	TTGGGCTGGCGTGTTCAGCC
CD25 -203NC	GTGGGCTGGGGTTGATGAGA

CD25 +17C	CACAAGGGTGACAGCCCAGG
CD25 -249C	TTATGGGCGTAGCTGAAGAA
CD25 -287C	CACCCTACCTTCAACGGCAG
CD25 +0NC	TGGGTCCATCCAGTCTCTAT
CD25 -80C	AGATGAGAGAAGAGAGTGCT
CD55 +78C	GGCGCGCCATGACCGTCGCG
CD55 +208C	GGGAAGCCCCTGGGCTGGGT
CD55 +208NC	GGGAAGCCCCTGGGCTGGGT
CD55 +378C	GCTGACTTGGCTTTAGGGGT
CD55 +172NC	ACTCACCCCACACGGCCGGC
CD55 +731NC	TCCAAAGCTGGCTGGGCATT
CD55 +731C	AATGCCCAGCCAGCTTTGGA
CD55 +3541C	GCTTCTTGGAAGGCTGAGGC
CD55 +3541NC	GCCTCAGCCTTCCAAGAAGC
CD55 +8044NC	GCTACAAGGGAGGCTGAGGT
CD59 -79NC	CAGGATGCCCTTGCCCTCCC
CD59 +245C	TATCTACGAGGAAGGAGAAA
CD59 +224NC	AATGAAGCCAGCGTTCGGCT
CD59 +143NC	GGTCGAGTGGAAAGCGAGGA
CD59 -181C	TTCTCAGAACCTGGGCCAGG
CD59 -184NC	GGCCCAGGTTCTGAGAAGGC
CD59 -238NC	CCCAGGGAACTGAAAGTTTG
CD59 -250NC	AAAGTTTGGGGCGTCCTCCT
CD59 +13564C	TCAGACCAAAGGGGTGACTC
CD59 +13643C	GTTCCCACTCTACTGGCCCC
CD59 +13744NC	CAGTGTGGTAGTACACACTG

3.11 Table S3: Sequences of ssODN HDR Donors

Chr5 Gene Desert #1	CATTTAAATCTCTCTACATGAAAAGATAATTGCTCCAGA AATTAACTGTACCTGGAATTCATTCATTTGGTCATGGCT AGTTTCTTATGTAGTGATGATTTGATATCAGAGCTAA
Chr5 Gene Desert #2	TATCAGAGCTAATTAAGATCGGGTCAGAGTTGGTGAAG GTCAGACATTAATGTGTAAGATCATTGAAATGATAATTAT AAACAGATTAGGAAGCCACGGTCCTTTATAAGGGGTT
CD55 #1	CCAGCATTTGGGGCTCCTGCTGTGTCGGCCCCCAGCT GACTTGGCTTTAGGGGTAGACGTGGAGGGTTAAAGAG GCCCCGGCTGGGTTTGCGGAGCAGCCAAGCCTGGCAA AATC

CD55 #2	CCTAGGTGACTGTGGCCTTCCCCCAGATGTACCTAATG CCCAGCCAGCTTTGGAAAGCCGTACAAGTTTTCCCGAG GATACTGTAATAACGTACAAATGTGAAGAAAGCTTTGTG
VEGFA	GGACGAAAAGTTTCAGTGCGACGCCGCGAGCCCCGAC CCCCTCCACCCCGCCACCTGGCGCGGGCTCCGGCCCC TGCCCGCGGCTCGCCGCCGCGTCCACTGTCCGCCGCC GGCC
CD59 #1	TTGAAGGTGCTCATTGGGTCCTGGCCACCCGGCCTTCT CAGAACCTGGGCCAGGATTCTGAGCTCCGCGCGGGGG TGGAGGGAGAGGAGGAGGTTCCTGCCGAGGTGCGGCT GCG
CD59 #2	TCTCCCTCCACCCCCGCGCGGAGCTCAGCCTCCTGGC CCAGGTTCTGAGAAGGCCTTGTGGCCAGGACCCAATGA GCACCTTCAAAACCCCAGGGAACTGAAAGTTTGGGGCG TC
c-myc	GTGGAAGAGCCGGGCGAGCAGAGCTGCGCTGCGGGC GTCCTGGGAAGGGAGATCCAAAGCGAATAGGGGGCTT CGCCTCTGGCCCAGCCCTCCCGCTGATCCCCCAGCCA GCGGT

3.12 Table S4: Sequences of Amplicon-NGS PCR Primers

Chr5 Gene Desert gRNA #1	
PCR #1 - Forward Primer	GACTACCTGCCCACATCGTTAC
PCR #1 - Reverse Primer	GAGGAAGGAATACACTCTCACC
PCR #2 - Forward Primer	gctcttccgatctGACTGTGGAGCCCTGCCTTTG
PCR #2 - Reverse Primer	gctcttccgatctCCCCTTATAAAGGACCGTGGC
Chr5 Gene Desert gRNA #2	
PCR #1 - Forward Primer	GACTGTGGAGCCCTGCCTTTG
PCR #1 - Reverse Primer	CCATCATTGTCCACAGGACAGC
PCR #2 - Forward Primer	gctcttccgatctGGGTTCATTCATTTGGTCATGGC
PCR #2 - Reverse Primer	gctcttccgatctGGGCTGGAGCTACCATTCTAC
CD55 gRNA #1	
PCR #1 - Forward Primer	AGGTCCAAGTCGGTCTCTGAG
PCR #1 - Reverse Primer	GGAGACAAAAGCAGAACTGAAGG
PCR #2 - Forward Primer	gctcttccgatctCCGCCGTCCTGTGCCTTTAAG
PCR #2 - Reverse Primer	gctcttccgatctCCACACGGCTGGACTCTGTC
CD55 gRNA #2	
PCR #1 - Forward Primer	CCACTCTCGACAGAGTCCAGC
PCR #1 - Reverse Primer	GTGACGTGCCAACAGGGTATAC
PCR #2 - Forward Primer	gctcttccgatctGCAACTGTGAGGACACTTGATAG
PCR #2 - Reverse Primer	gctcttccgatctCAATATCTGACCATTGACTGCCC

VEGFA	
PCR #1 - Forward Primer	GAGGTAGCAAGAGCTCCAGAGAG
PCR #1 - Reverse Primer	CTGGAGCACTGTCTGCGCACA
PCR #2 - Forward Primer	gctcttccgatctTGACGGACAGACAGACAGACAC
PCR #2 - Reverse Primer	gctcttccgatctGGCCCGAGCTAGCACTTCTC
CD59 gRNA #1	
PCR #1 - Forward Primer	GTAGGAAGCAGCTTCAGACTGC
PCR #1 - Reverse Primer	CTCGGCTCGGCTCACCCAAAC
PCR #2 - Forward Primer	gctcttccgatctGCAAATCCGAGGAGGACGCC
PCR #2 - Reverse Primer	gctcttccgatctCATTCTTTCGCTCCAGCCCGCA
CD59 gRNA #2	
PCR #1 - Forward Primer	GAAGCAGCTTCAGACTGCAGC
PCR #1 - Reverse Primer	GCCTTCGGGCCTTCTTACCTG
PCR #2 - Forward Primer	gctcttccgatctATGTCCCATAGCAAATCCGAGG
PCR #2 - Reverse Primer	gctcttccgatctCCCGCATTCTTTCGCTCCAGC
c-myc gRNA	
PCR #1 - Forward Primer	CCCTTTATAATGCGAGGGTCTG
PCR #1 - Reverse Primer	AATCCAGCGTCTAAGCAGCTGC
PCR #2 - Forward Primer	gctcttccgatctGGGCTTTATCTAACTCGCTGTAG
PCR #2 - Reverse Primer	gctcttccgatctTGCTATGGGCAAAGTTTCGTGG

3.13 Table S5: Sequences of qPCR Primers for ChIP

Template CD25 gRNA	
Upstream of Protospacer - Forward Primer	CTTCTCATCAACCCCAGCCC
Upstream of Protospacer - Reverse Primer	CCTAGCACTCTCTTCTCTCATCTC
Inclusive of Protospacer - Forward Primer	GAGATGAGAGAAGAGAGTGCTAG
Inclusive of Protospacer - Reverse Primer	ACCCTTGTGGGTCCATCCAG
Non-Template CD25 gRNA	
Upstream of Protospacer - Forward Primer	CTTCCCATCCCACATCCTCC
Upstream of Protospacer - Reverse Primer	CCCACATCAGCAGGTATGAATCC
Inclusive of Protospacer - Forward Primer	GAGAGCAACTCCTGACTCCG
Inclusive of Protospacer - Reverse Primer	CTTTCTCTGCAGAAGGCCCA
CD55 gRNAs	
Upstream of Protospacer - Forward Primer	CCACTCTCGACAGAGTCCAG
Upstream of Protospacer - Reverse Primer	CAAGTGTCCTCACAGTTGCTG
Inclusive of Protospacer - Forward Primer	CCTAGGTGACTGTGGCCTTC
Inclusive of Protospacer - Reverse Primer	GGCAGATCACTGAGTCCTTCTC
Reference (c-myc)	

Forward Primer	GCCGCATCCACGAAACTTTG
Reverse Primer	GCAAGGAGAGCCTTTCAGAGAAG

Chapter 4: Conclusions

Here, we deploy a dCas9-based proximity sensor in both live human cells and a cell-free *X. laevis* extract system to identify Cas9 displacement factors. While this dCas9-based proximity sensor effectively identified proteins known to bind to the highly repetitive alpha satellites and potential Cas9 displacement factors, we were unable to engineer this sensor to identify factors at non-repetitive genomic loci in live cells. With the *X. laevis* cell-free system, however, we identified the histone chaperone FACT as a Cas9 displacement factor.

Our results have generated several intriguing new lines of inquiry. For example, the mechanism by which FACT localizes to Cas9 requires further interrogation. One report suggests that DNA damage causes local accumulation of lipids that recruit DNA repair proteins through the lipids' interaction with the proteins' PH domains (Wang et al., 2017). It is possible that the R-loop that Cas9 generates attracts lipids that then interact with FACT, which possesses multiple PH domains (Kemble et al., 2013; Zhang et al., 2015) . Alternatively, FACT may displace Cas9 not because eukaryotic systems specifically recruit FACT to DNA-bound Cas9 but because FACT performs general genome surveillance. In addition, FACT may localize to Cas9 through different mechanisms in *X. laevis* extract and live human cells. Further experiments are thus necessary to interrogate how FACT makes its initial contact with genome-bound Cas9 in human cells.

Our results also highlight the need to further interrogate FACT's role in DNA repair. The editing results in cells with either wild-type or depleted levels of FACT indicate that FACT promotes HDR. However, it is unclear exactly what role FACT plays in repairing Cas9-induced breaks. Our observed phenotypes could be linked to FACT's ability to rapidly displace Cas9, thereby promoting multiple rounds of cleavage and turnover. Alternatively, these phenotypes may be connected to FACT's role in DSB repair completely independent of Cas9. Initial recruitment of repair factors to a DSB, RAD51-mediated homology search, and strand invasion may require proteins such as FACT to grant repair factors access to DNA.

Altogether, these results reveal an unexpected functional relationship between the eukaryotic cellular machinery and the prokaryotic Cas9. Several other such relationships likely exist, and our results highlight the need to better understand the nature of these interactions. We hope that our results here can serve as a foundation for further experiments that interrogate the unique ways in which different tissues and organisms engage with Cas9 in order to uncover possible strategies to improve the use of Cas9.

Chapter 5: References

Aldrup-Macdonald, M.E., and Sullivan, B.A. (2014). The past, present, and future of human centromere genomics. Genes (Basel) *5*, 33–50.

Aleksandrov, R., Dotchev, A., Poser, I., Krastev, D., Georgiev, G., Panova, G., Babukov, Y., Danovski, G., Dyankova, T., Hubatsch, L., et al. (2018). Protein Dynamics in Complex DNA Lesions. Mol Cell *69*, 1046–1061.e5.

Almouzni, G., and Wolffe, A.P. (1993). Nuclear assembly, structure, and function: the use of Xenopus in vitro systems. Exp Cell Res *205*, 1–15.

Arias, E.E., and Walter, J.C. (2004). Initiation of DNA replication in Xenopus egg extracts. Front Biosci *9*, 3029–3045.

Aymard, F., Bugler, B., Schmidt, C.K., Guillou, E., Caron, P., Briois, S., Iacovoni, J.S., Daburon, V., Miller, K.M., Jackson, S.P., et al. (2014). Transcriptionally active chromatin recruits homologous recombination at DNA double-strand breaks. Nat Struct Mol Biol *21*, 366–374.

Ayrapetov, M.K., Gursoy-Yuzugullu, O., Xu, C., Xu, Y., and Price, B.D. (2014). DNA double-strand breaks promote methylation of histone H3 on lysine 9 and transient formation of repressive chromatin. Proc Natl Acad Sci U S A *111*, 9169–9174.

Aze, A., Sannino, V., Soffientini, P., Bachi, A., and Costanzo, V. (2016). Centromeric DNA replication reconstitution reveals DNA loops and ATR checkpoint suppression. Nat Cell Biol *18*, 684–691.

Barkal, A.A., Srinivasan, S., Hashimoto, T., Gifford, D.K., and Sherwood, R.I. (2016). Cas9 Functionally Opens Chromatin. PLoS One *11*, e0152683.

Barrangou, R., Fremaux, C., Deveau, H., Richards, M., Boyaval, P., Moineau, S., Romero, D.A., and Horvath, P. (2007). CRISPR provides acquired resistance against viruses in prokaryotes. Science *315*, 1709–1712.

Bernstein, B.E., Meissner, A., and Lander, E.S. (2007). The mammalian epigenome. Cell *128*, 669–681.

Blow, J.J. (2001). Control of chromosomal DNA replication in the early Xenopus embryo. Embo J *20*, 3293–3297.

Blow, J.J., and Laskey, R.A. (2016). Xenopus cell-free extracts and their contribution to the study of DNA replication and other complex biological processes. Int J Dev Biol *60*, 201–207.

Bolotin, A., Quinquis, B., Sorokin, A., and Ehrlich, S.D. (2005). Clustered regularly interspaced short palindrome repeats (CRISPRs) have spacers of extrachromosomal origin. Microbiology *151*, 2551–2561.

Bothmer, A., Phadke, T., Barrera, L.A., Margulies, C.M., Lee, C.S., Buquicchio, F., Moss, S., Abdulkerim, H.S., Selleck, W., Jayaram, H., et al. (2017). Characterization of the interplay between DNA repair and CRISPR/Cas9-induced DNA lesions at an endogenous locus. Nat Commun *8*, 13905.

Brinkman, E.K., Chen, T., de Haas, M., Holland, H.A., Akhtar, W., and van Steensel, B. (2018). Kinetics and Fidelity of the Repair of Cas9-Induced Double-Strand DNA Breaks. Mol Cell *70*, 801–813.e806.

Brouns, S.J.J., Jore, M.M., Lundgren, M., Westra, E.R., Slijkhuis, R.J.H., Snijders, A.P.L., Dickman, M.J., Makarova, K.S., Koonin, E.V., and van der Oost, J. (2008). Small CRISPR RNAs guide antiviral defense in prokaryotes. Science *321*, 960–964.

Burman, B., Zhang, Z.Z., Pegoraro, G., Lieb, J.D., and Misteli, T. (2015). Histone modifications predispose genome regions to breakage and translocation. Genes Dev *29*, 1393–1402.

Byrum, S.D., Raman, A., Taverna, S.D., and Tackett, A.J. (2012). ChAP-MS: a method for identification of proteins and histone posttranslational modifications at a single genomic locus. Cell Rep *2*, 198–205.

Carte, J., Pfister, N.T., Compton, M.M., Terns, R.M., and Terns, M.P. (2010). Binding and cleavage of CRISPR RNA by Cas6. Rna *16*, 2181–2188.

Carte, J., Wang, R., Li, H., Terns, R.M., and Terns, M.P. (2008). Cas6 is an endoribonuclease that generates guide RNAs for invader defense in prokaryotes. Genes Dev *22*, 3489–3496.

Chari, R., Mali, P., Moosburner, M., and Church, G.M. (2015). Unraveling CRISPR-Cas9 genome engineering parameters via a library-on-library approach. Nat Methods *12*, 823–826.

Chen, B., Gilbert, L.A., Cimini, B.A., Schnitzbauer, J., Zhang, W., Li, G.-W., Park, J., Blackburn, E.H., Weissman, J.S., Qi, L.S., et al. (2013). Dynamic imaging of genomic loci in living human cells by an optimized CRISPR/Cas system. Cell *155*, 1479–1491.

Chen, C.-C., Feng, W., Lim, P.X., Kass, E.M., and Jasin, M. (2018a). Homology-Directed Repair and the Role of BRCA1, BRCA2, and Related Proteins in Genome Integrity and Cancer. Annu Rev Cancer Biol *2*, 313–336.

Chen, P., Dong, L., Hu, M., Wang, Y.-Z., Xiao, X., Zhao, Z., Yan, J., Wang, P.-Y., Reinberg, D., Li, M., et al. (2018b). Functions of FACT in Breaking the Nucleosome and Maintaining Its Integrity at the Single-Nucleosome Level. Mol Cell *71*, 284–293.e284.

Cho, K.F., Branon, T.C., Rajeev, S., Svinkina, T., Udeshi, N.D., Thoudam, T., Kwak, C., Rhee, H.-W., Lee, I.-K., Carr, S.A., et al. (2020). Split-TurboID enables contact-dependent proximity labeling in cells. Proc Natl Acad Sci U S A.

Chong, S., Dugast-Darzacq, C., Liu, Z., Dong, P., Dailey, G.M., Cattoglio, C., Heckert, A., Banala, S., Lavis, L., Darzacq, X., et al. (2018). Imaging dynamic and selective low-complexity domain interactions that control gene transcription. Science *361*.

Ciccia, A., and Elledge, S.J. (2010). The DNA damage response: making it safe to play with knives. Mol Cell *40*, 179–204.

Clarke, R., Heler, R., MacDougall, M.S., Yeo, N.C., Chavez, A., Regan, M., Hanakahi, L., Church, G.M., Marraffini, L.A., and Merrill, B.J. (2018). Enhanced Bacterial Immunity and Mammalian Genome Editing via RNA-Polymerase-Mediated Dislodging of Cas9 from Double-Strand DNA Breaks. Mol Cell *71*, 42–55.e48.

Clement, K., Rees, H., Canver, M.C., Gehrke, J.M., Farouni, R., Hsu, J.Y., Cole, M.A., Liu, D.R., Joung, J.K., Bauer, D.E., et al. (2019). CRISPResso2 provides accurate and rapid genome editing sequence analysis. Nat. Biotechnol. *37*, 224–226.

Clouaire, T., and Legube, G. (2015). DNA double strand break repair pathway choice: a chromatin based decision? Nucleus *6*, 107–113.

Conaway, R.C., and Conaway, J.W. (2009). The INO80 chromatin remodeling complex in transcription, replication and repair. Trends Biochem Sci *34*, 71–77.

Cong, L., Ran, F.A., Cox, D., Lin, S., Barretto, R., Habib, N., Hsu, P.D., Wu, X., Jiang, W., Marraffini, L.A., et al. (2013). Multiplex genome engineering using CRISPR/Cas systems. Science *339*, 819–823.

Costanzo, V., Robertson, K., and Gautier, J. (2004). Xenopus cell-free extracts to study the DNA damage response. Methods Mol Biol *280*, 213–227.

Cupello, S., Richardson, C., and Yan, S. (2016). Cell-free Xenopus egg extracts for studying DNA damage response pathways. Int J Dev Biol *60*, 229–236.

Daer, R.M., Cutts, J.P., Brafman, D.A., and Haynes, K.A. (2017). The Impact of Chromatin Dynamics on Cas9-Mediated Genome Editing in Human Cells. ACS Synth Biol *6*, 428–438.

Dejardin, J., and Kingston, R.E. (2009). Purification of proteins associated with specific genomic Loci. Cell *136*, 175–186.

Deltcheva, E., Chylinski, K., Sharma, C.M., Gonzales, K., Chao, Y., Pirzada, Z.A., Eckert, M.R., Vogel, J., and Charpentier, E. (2011). CRISPR RNA maturation by trans-encoded small RNA and host factor RNase III. Nature *471*, 602–607.

Deveau, H., Barrangou, R., Garneau, J.E., Labonté, J., Fremaux, C., Boyaval, P., Romero, D.A., Horvath, P., and Moineau, S. (2008). Phage response to CRISPR-encoded resistance in Streptococcus thermophilus. J Bacteriol *190*, 1390–1400.

Doudna, J.A., and Charpentier, E. (2014). Genome editing. The new frontier of genome engineering with CRISPR-Cas9. Science *346*, 1258096.

Earnshaw, W.C., Honda, B.M., Laskey, R.A., and Thomas, J.O. (1980). Assembly of nucleosomes: the reaction involving X. laevis nucleoplasmin. Cell *21*, 373–383.

Frock, R.L., Hu, J., Meyers, R.M., Ho, Y.-J., Kii, E., and Alt, F.W. (2015). Genome-wide detection of DNA double-stranded breaks induced by engineered nucleases. Nat. Biotechnol. *33*, 179–186.

Fujita, T., and Fujii, H. (2011). Direct identification of insulator components by insertional chromatin immunoprecipitation. PLoS One *6*, e26109.

Fujita, T., and Fujii, H. (2013). Efficient isolation of specific genomic regions and identification of associated proteins by engineered DNA-binding molecule-mediated chromatin immunoprecipitation (enChIP) using CRISPR. Biochem Biophys Res Commun *439*, 132–136.

Fujita, T., Asano, Y., Ohtsuka, J., Takada, Y., Saito, K., Ohki, R., and Fujii, H. (2013). Identification of telomere-associated molecules by engineered DNA-binding molecule-mediated chromatin immunoprecipitation (enChIP). Sci Rep *3*, 3171.

Fujita, T., Yuno, M., and Fujii, H. (2016). Allele-specific locus binding and genome editing by CRISPR at the p16INK4a locus. Sci Rep *6*, 30485.

Gao, X.D., Tu, L.-C., Mir, A., Rodriguez, T., Ding, Y., Leszyk, J., Dekker, J., Shaffer, S.A., Zhu, L.J., Wolfe, S.A., et al. (2018). C-BERST: defining subnuclear proteomic landscapes at genomic elements with dCas9-APEX2. Nat Methods *15*, 433–436.

Garcia, V., Phelps, S.E.L., Gray, S., and Neale, M.J. (2011). Bidirectional resection of DNA double-strand breaks by Mre11 and Exo1. Nature *479*, 241–244.

Garneau, J.E., Dupuis, M.-È., Villion, M., Romero, D.A., Barrangou, R., Boyaval, P., Fremaux, C., Horvath, P., Magadán, A.H., and Moineau, S. (2010). The CRISPR/Cas bacterial immune system cleaves bacteriophage and plasmid DNA. Nature *468*, 67–71.

Gasiunas, G., Barrangou, R., Horvath, P., and Siksnys, V. (2012). Cas9-crRNA ribonucleoprotein complex mediates specific DNA cleavage for adaptive immunity in bacteria. Proc Natl Acad Sci U S A *109*, E2579–E2586.

Gilbert, L.A., Larson, M.H., Morsut, L., Liu, Z., Brar, G.A., Torres, S.E., Stern-Ginossar, N., Brandman, O., Whitehead, E.H., Doudna, J.A., et al. (2013). CRISPR-mediated modular RNA-guided regulation of transcription in eukaryotes. Cell *154*, 442–451.

Goodarzi, A.A., Jeggo, P., and Lobrich, M. (2010). The influence of heterochromatin on DNA double strand break repair: Getting the strong, silent type to relax. DNA Repair (Amst) *9*, 1273–1282.

Gospodinov, A., Vaissiere, T., Krastev, D.B., Legube, G., Anachkova, B., and Herceg, Z. (2011). Mammalian Ino80 mediates double-strand break repair through its role in DNA end strand resection. Mol Cell Biol *31*, 4735–4745.

Guilinger, J.P., Thompson, D.B., and Liu, D.R. (2014). Fusion of catalytically inactive Cas9 to FokI nuclease improves the specificity of genome modification. Nat. Biotechnol. *32*, 577–582.

Guo, T., Feng, Y.-L., Xiao, J.-J., Liu, Q., Sun, X.-N., Xiang, J.-F., Kong, N., Liu, S.-C., Chen, G.-Q., Wang, Y., et al. (2018). Harnessing accurate non-homologous end joining for efficient precise deletion in CRISPR/Cas9-mediated genome editing. Genome Biol. *19*, 170.

Gurova, K., Chang, H.-W., Valieva, M.E., Sandlesh, P., and Studitsky, V.M. (2018). Structure and function of the histone chaperone FACT - Resolving FACTual issues. Biochim Biophys Acta Gene Regul Mech.

Haft, D.H., Selengut, J., Mongodin, E.F., and Nelson, K.E. (2005). A guild of 45 CRISPR-associated (Cas) protein families and multiple CRISPR/Cas subtypes exist in prokaryotic genomes. PLoS Comput Biol *1*, e60.

Hale, C.R., Zhao, P., Olson, S., Duff, M.O., Graveley, B.R., Wells, L., Terns, R.M., and Terns, M.P. (2009). RNA-guided RNA cleavage by a CRISPR RNA-Cas protein complex. Cell *139*, 945–956.

Hansen, A.S., Pustova, I., Cattoglio, C., Tjian, R., and Darzacq, X. (2017). CTCF and cohesin regulate chromatin loop stability with distinct dynamics. Elife *6*.

Haurwitz, R.E., Jinek, M., Wiedenheft, B., Zhou, K., and Doudna, J.A. (2010). Sequence- and structure-specific RNA processing by a CRISPR endonuclease. Science *329*, 1355–1358.

Heald, R., Tournebize, R., Blank, T., Sandaltzopoulos, R., Becker, P., Hyman, A., and Karsenti, E. (1996). Self-organization of microtubules into bipolar spindles around artificial chromosomes in Xenopus egg extracts. Nature *382*, 420–425.

Hilton, I.B., D'Ippolito, A.M., Vockley, C.M., Thakore, P.I., Crawford, G.E., Reddy, T.E., and Gersbach, C.A. (2015). Epigenome editing by a CRISPR-Cas9-based acetyltransferase activates genes from promoters and enhancers. Nat. Biotechnol. *33*, 510–517.

Hinz, J.M., Laughery, M.F., and Wyrick, J.J. (2015). Nucleosomes Inhibit Cas9 Endonuclease Activity in Vitro. Biochemistry *54*, 7063–7066.

Holden, P., and Horton, W.A. (2009). Crude subcellular fractionation of cultured mammalian cell lines. BMC Res Notes *2*, 243.

Hoogenboom, W.S., Klein Douwel, D., and Knipscheer, P. (2017). Xenopus egg extract: A powerful tool to study genome maintenance mechanisms. Dev Biol *428*, 300–309.

Horlbeck, M.A., Gilbert, L.A., Villalta, J.E., Adamson, B., Pak, R.A., Chen, Y., Fields, A.P., Park, C.Y., Corn, J.E., Kampmann, M., et al. (2016a). Compact and highly active next-generation libraries for CRISPR-mediated gene repression and activation. Elife *5*.

Horlbeck, M.A., Witkowsky, L.B., Guglielmi, B., Replogle, J.M., Gilbert, L.A., Villalta, J.E., Torigoe, S.E., Tjian, R., and Weissman, J.S. (2016b). Nucleosomes impede Cas9 access to DNA in vivo and in vitro. Elife *5*.

Hoshino, A., and Fujii, H. (2009). Insertional chromatin immunoprecipitation: a method for isolating specific genomic regions. J Biosci Bioeng *108*, 446–449.

Hsieh, F.-K., Kulaeva, O.I., Patel, S.S., Dyer, P.N., Luger, K., Reinberg, D., and Studitsky, V.M. (2013). Histone chaperone FACT action during transcription through chromatin by RNA polymerase II. Proc Natl Acad Sci U S A *110*, 7654–7659.

Hsu, P.D., Lander, E.S., and Zhang, F. (2014). Development and applications of CRISPR-Cas9 for genome engineering. Cell *157*, 1262–1278.

Isaac, R.S., Jiang, F., Doudna, J.A., Lim, W.A., Narlikar, G.J., and Almeida, R. (2016). Nucleosome breathing and remodeling constrain CRISPR-Cas9 function. Elife *5*.

Ishino, Y., Shinagawa, H., Makino, K., Amemura, M., and Nakata, A. (1987). Nucleotide sequence of the iap gene, responsible for alkaline phosphatase isozyme conversion in Escherichia coli, and identification of the gene product. J Bacteriol *169*, 5429–5433.

Janicki, S.M., Tsukamoto, T., Salghetti, S.E., Tansey, W.P., Sachidanandam, R., Prasanth, K.V., Ried, T., Shav-Tal, Y., Bertrand, E., Singer, R.H., et al. (2004). From silencing to gene expression: real-time analysis in single cells. Cell *116*, 683–698.

Jansen, R., Embden, J.D.A.V., Gaastra, W., and Schouls, L.M. (2002). Identification of genes that are associated with DNA repeats in prokaryotes. Mol Microbiol *43*, 1565–1575.

Jiang, F., and Doudna, J.A. (2017). CRISPR-Cas9 Structures and Mechanisms. Annu Rev Biophys *46*, 505–529.

Jinek, M., Chylinski, K., Fonfara, I., Hauer, M., Doudna, J.A., and Charpentier, E. (2012). A programmable dual-RNA-guided DNA endonuclease in adaptive bacterial immunity. Science *337*, 816–821.

Jinek, M., East, A., Cheng, A., Lin, S., Ma, E., and Doudna, J. (2013). RNA-programmed genome editing in human cells. Elife *2*, e00471.

Jinek, M., Jiang, F., Taylor, D.W., Sternberg, S.H., Kaya, E., Ma, E., Anders, C., Hauer, M., Zhou, K., Lin, S., et al. (2014). Structures of Cas9 endonucleases reveal RNA-mediated conformational activation. Science *343*, 1247997.

Joshi, H.K., Etzkorn, C., Chatwell, L., Bitinaite, J., and Horton, N.C. (2006). Alteration of sequence specificity of the type II restriction endonuclease HincII through an indirect readout mechanism. J Biol Chem *281*, 23852–23869.

Kalab, P., Pralle, A., Isacoff, E.Y., Heald, R., and Weis, K. (2006). Analysis of a RanGTP-regulated gradient in mitotic somatic cells. Nature *440*, 697–701.

Kallimasioti-Pazi, E.M., Thelakkad Chathoth, K., Taylor, G.C., Meynert, A., Ballinger, T., Kelder, M.J.E., Lalevee, S., Sanli, I., Feil, R., and Wood, A.J. (2018). Heterochromatin delays CRISPR-Cas9 mutagenesis but does not influence the outcome of mutagenic DNA repair. PLoS Biol *16*, e2005595.

Kari, V., Shchebet, A., Neumann, H., and Johnsen, S.A. (2011). The H2B ubiquitin ligase RNF40 cooperates with SUPT16H to induce dynamic changes in chromatin structure during DNA double-strand break repair. Cell Cycle *10*, 3495–3504.

Kemble, D.J., McCullough, L.L., Whitby, F.G., Formosa, T., and Hill, C.P. (2015). FACT Disrupts Nucleosome Structure by Binding H2A-H2B with Conserved Peptide Motifs. Mol Cell *60*, 294–306.

Kemble, D.J., Whitby, F.G., Robinson, H., McCullough, L.L., Formosa, T., and Hill, C.P. (2013). Structure of the Spt16 middle domain reveals functional features of the histone chaperone FACT. J Biol Chem *288*, 10188–10194.

Kim, S., Kim, D., Cho, S.W., Kim, J., and Kim, J.-S. (2014). Highly efficient RNA-guided genome editing in human cells via delivery of purified Cas9 ribonucleoproteins. Genome Res *24*, 1012–1019.

Kiss, T., Fayet-Lebaron, E., and Jady, B.E. (2010). Box H/ACA small ribonucleoproteins. Mol Cell *37*, 597–606.

Knight, S.C., Xie, L., Deng, W., Guglielmi, B., Witkowsky, L.B., Bosanac, L., Zhang, E.T., Beheiry, El, M., Masson, J.-B., Dahan, M., et al. (2015). Dynamics of CRISPR-Cas9 genome interrogation in living cells. Science *350*, 823–826.

Knipscheer, P., Raschle, M., Smogorzewska, A., Enoiu, M., Ho, T.V., Scharer, O.D., Elledge, S.J., and Walter, J.C. (2009). The Fanconi anemia pathway promotes replication-dependent DNA interstrand cross-link repair. Science *326*, 1698–1701.

Knott, G.J., and Doudna, J.A. (2018). CRISPR-Cas guides the future of genetic engineering. Science *361*, 866–869.

Konermann, S., Brigham, M.D., Trevino, A.E., Joung, J., Abudayyeh, O.O., Barcena, C., Hsu, P.D., Habib, N., Gootenberg, J.S., Nishimasu, H., et al. (2015). Genome-scale

transcriptional activation by an engineered CRISPR-Cas9 complex. Nature *517*, 583–588.

Koonin, E.V., Makarova, K.S., and Zhang, F. (2017). Diversity, classification and evolution of CRISPR-Cas systems. Curr Opin Microbiol *37*, 67–78.

Kuscu, C., Arslan, S., Singh, R., Thorpe, J., and Adli, M. (2014). Genome-wide analysis reveals characteristics of off-target sites bound by the Cas9 endonuclease. Nat. Biotechnol. *32*, 677–683.

Lademann, C.A., Renkawitz, J., Pfander, B., and Jentsch, S. (2017). The INO80 Complex Removes H2A.Z to Promote Presynaptic Filament Formation during Homologous Recombination. Cell Rep *19*, 1294–1303.

Lam, S.S., Martell, J.D., Kamer, K.J., Deerinck, T.J., Ellisman, M.H., Mootha, V.K., and Ting, A.Y. (2015). Directed evolution of APEX2 for electron microscopy and proximity labeling. Nat Methods *12*, 51–54.

Lans, H., Marteijn, J.A., and Vermeulen, W. (2012). ATP-dependent chromatin remodeling in the DNA-damage response. Epigenetics Chromatin *5*, 4.

Laskey, R.A., Honda, B.M., Mills, A.D., and Finch, J.T. (1978). Nucleosomes are assembled by an acidic protein which binds histones and transfers them to DNA. Nature *275*, 416–420.

Laskey, R.A., Mills, A.D., and Morris, N.R. (1977). Assembly of SV40 chromatin in a cell-free system from Xenopus eggs. Cell *10*, 237–243.

Lebofsky, R., Takahashi, T., and Walter, J.C. (2009). DNA replication in nucleus-free Xenopus egg extracts. Methods Mol Biol *521*, 229–252.

Lemaitre, C., Grabarz, A., Tsouroula, K., Andronov, L., Furst, A., Pankotai, T., Heyer, V., Rogier, M., Attwood, K.M., Kessler, P., et al. (2014). Nuclear position dictates DNA repair pathway choice. Genes Dev *28*, 2450–2463.

Li, W., Cowley, A., Uludag, M., Gur, T., McWilliam, H., Squizzato, S., Park, Y.M., Buso, N., and Lopez, R. (2015). The EMBL-EBI bioinformatics web and programmatic tools framework. Nucleic Acids Res *43*, W580–W584.

Lieber, M.R. (2010). The mechanism of double-strand DNA break repair by the nonhomologous DNA end-joining pathway. Annu Rev Biochem *79*, 181–211.

Lin, S., Staahl, B.T., Alla, R.K., and Doudna, J.A. (2014). Enhanced homology-directed human genome engineering by controlled timing of CRISPR/Cas9 delivery. Elife *3*, e04766.

Liu, X., Zhang, Y., Chen, Y., Li, M., Zhou, F., Li, K., Cao, H., Ni, M., Liu, Y., Gu, Z., et al. (2017). In Situ Capture of Chromatin Interactions by Biotinylated dCas9. Cell *170*, 1028–1043.e19.

Liu, Y., Zhou, K., Zhang, N., Wei, H., Tan, Y.Z., Zhang, Z., Carragher, B., Potter, C.S., D'Arcy, S., and Luger, K. (2020). FACT caught in the act of manipulating the nucleosome. Nature *577*, 426–431.

Ma, H., Tu, L.-C., Naseri, A., Huisman, M., Zhang, S., Grunwald, D., and Pederson, T. (2016). CRISPR-Cas9 nuclear dynamics and target recognition in living cells. J Cell Biol *214*, 529–537.

Maggio, I., and Goncalves, M.A.F.V. (2015). Genome editing at the crossroads of delivery, specificity, and fidelity. Trends Biotechnol *33*, 280–291.

Makarova, K.S., Grishin, N.V., Shabalina, S.A., Wolf, Y.I., and Koonin, E.V. (2006). A putative RNA-interference-based immune system in prokaryotes: computational analysis of the predicted enzymatic machinery, functional analogies with eukaryotic RNAi, and hypothetical mechanisms of action. Biol Direct *1*, 7.

Makarova, K.S., Wolf, Y.I., Alkhnbashi, O.S., Costa, F., Shah, S.A., Saunders, S.J., Barrangou, R., Brouns, S.J.J., Charpentier, E., Haft, D.H., et al. (2015). An updated evolutionary classification of CRISPR-Cas systems. Nat Rev Microbiol *13*, 722–736.

Mali, P., Yang, L., Esvelt, K.M., Aach, J., Guell, M., DiCarlo, J.E., Norville, J.E., and Church, G.M. (2013). RNA-guided human genome engineering via Cas9. Science *339*, 823–826.

Mao, Z., Bozzella, M., Seluanov, A., and Gorbunova, V. (2008). Comparison of nonhomologous end joining and homologous recombination in human cells. DNA Repair (Amst) *7*, 1765–1771.

Marraffini, L.A., and Sontheimer, E.J. (2008). CRISPR interference limits horizontal gene transfer in staphylococci by targeting DNA. Science *322*, 1843–1845.

Marraffini, L.A., and Sontheimer, E.J. (2010). Self versus non-self discrimination during CRISPR RNA-directed immunity. Nature *463*, 568–571.

Martell, J.D., Deerinck, T.J., Sancak, Y., Poulos, T.L., Mootha, V.K., Sosinsky, G.E., Ellisman, M.H., and Ting, A.Y. (2012). Engineered ascorbate peroxidase as a genetically encoded reporter for electron microscopy. Nat. Biotechnol. *30*, 1143–1148.

Mason, P.B., and Struhl, K. (2003). The FACT complex travels with elongating RNA polymerase II and is important for the fidelity of transcriptional initiation in vivo. Mol Cell Biol *23*, 8323–8333.

McCullagh, E., Seshan, A., El-Samad, H., and Madhani, H.D. (2010). Coordinate control of gene expression noise and interchromosomal interactions in a MAP kinase pathway. Nat Cell Biol *12*, 954–962.

Michael, W.M., Ott, R., Fanning, E., and Newport, J. (2000). Activation of the DNA replication checkpoint through RNA synthesis by primase. Science *289*, 2133–2137.

Mojica, F.J.M., Díez-Villaseñor, C., García-Martínez, J., and Almendros, C. (2009). Short motif sequences determine the targets of the prokaryotic CRISPR defence system. Microbiology *155*, 733–740.

Morrison, A.J., and Shen, X. (2009). Chromatin remodelling beyond transcription: the INO80 and SWR1 complexes. Nat Rev Mol Cell Biol *10*, 373–384.

Myers, S.A., Wright, J., Peckner, R., Kalish, B.T., Zhang, F., and Carr, S.A. (2018). Discovery of proteins associated with a predefined genomic locus via dCas9-APEX-mediated proximity labeling. Nat Methods *15*, 437–439.

Nelles, D.A., Fang, M.Y., O'Connell, M.R., Xu, J.L., Markmiller, S.J., Doudna, J.A., and Yeo, G.W. (2016). Programmable RNA Tracking in Live Cells with CRISPR/Cas9. Cell *165*, 488–496.

Nishimasu, H., Ran, F.A., Hsu, P.D., Konermann, S., Shehata, S.I., Dohmae, N., Ishitani, R., Zhang, F., and Nureki, O. (2014). Crystal structure of Cas9 in complex with guide RNA and target DNA. Cell *156*, 935–949.

Nishiyama, J., Mikuni, T., and Yasuda, R. (2017). Virus-Mediated Genome Editing via Homology-Directed Repair in Mitotic and Postmitotic Cells in Mammalian Brain. Neuron *96*, 755–768.e755.

O'Geen, H., Henry, I.M., Bhakta, M.S., Meckler, J.F., and Segal, D.J. (2015). A genome-wide analysis of Cas9 binding specificity using ChIP-seq and targeted sequence capture. Nucleic Acids Res *43*, 3389–3404.

Okuhara, K., Ohta, K., Seo, H., Shioda, M., Yamada, T., Tanaka, Y., Dohmae, N., Seyama, Y., Shibata, T., and Murofushi, H. (1999). A DNA unwinding factor involved in DNA replication in cell-free extracts of Xenopus eggs. Curr Biol *9*, 341–350.

Oliveira, D.V., Kato, A., Nakamura, K., Ikura, T., Okada, M., Kobayashi, J., Yanagihara, H., Saito, Y., Tauchi, H., and Komatsu, K. (2014). Histone chaperone FACT regulates homologous recombination by chromatin remodeling through interaction with RNF20. J Cell Sci *127*, 763–772.

Orphanides, G., LeRoy, G., Chang, C.H., Luse, D.S., and Reinberg, D. (1998). FACT, a factor that facilitates transcript elongation through nucleosomes. Cell *92*, 105–116.

Pattanayak, V., Lin, S., Guilinger, J.P., Ma, E., Doudna, J.A., and Liu, D.R. (2013). High-throughput profiling of off-target DNA cleavage reveals RNA-programmed Cas9 nuclease specificity. Nat. Biotechnol. *31*, 839–843.

Pawelczak, K.S., Gavande, N.S., VanderVere-Carozza, P.S., and Turchi, J.J. (2018). Modulating DNA Repair Pathways to Improve Precision Genome Engineering. ACS Chem Biol *13*, 389–396.

Pinello, L., Canver, M.C., Hoban, M.D., Orkin, S.H., Kohn, D.B., Bauer, D.E., and Yuan, G.-C. (2016). Analyzing CRISPR genome-editing experiments with CRISPResso. Nat. Biotechnol. *34*, 695–697.

Pingoud, A., and Jeltsch, A. (2001). Structure and function of type II restriction endonucleases. Nucleic Acids Res *29*, 3705–3727.

Piquet, S., Le Parc, F., Bai, S.-K., Chevallier, O., Adam, S., and Polo, S.E. (2018). The Histone Chaperone FACT Coordinates H2A.X-Dependent Signaling and Repair of DNA Damage. Mol Cell.

Pourcel, C., Salvignol, G., and Vergnaud, G. (2005). CRISPR elements in Yersinia pestis acquire new repeats by preferential uptake of bacteriophage DNA, and provide additional tools for evolutionary studies. Microbiology *151*, 653–663.

Pourfarzad, F., Aghajanirefah, A., de Boer, E., Have, Ten, S., Bryn van Dijk, T., Kheradmandkia, S., Stadhouders, R., Thongjuea, S., Soler, E., Gillemans, N., et al. (2013). Locus-specific proteomics by TChP: targeted chromatin purification. Cell Rep *4*, 589–600.

Price, B.D., and D'Andrea, A.D. (2013). Chromatin remodeling at DNA double-strand breaks. Cell *152*, 1344–1354.

Qi, L.S., Larson, M.H., Gilbert, L.A., Doudna, J.A., Weissman, J.S., Arkin, A.P., and Lim, W.A. (2013). Repurposing CRISPR as an RNA-guided platform for sequence-specific control of gene expression. Cell *152*, 1173–1183.

Qiu, W., Xu, Z., Zhang, M., Zhang, D., Fan, H., Li, T., Wang, Q., Liu, P., Zhu, Z., Du, D., et al. (2019). Determination of local chromatin interactions using a combined CRISPR and peroxidase APEX2 system. Nucleic Acids Res *47*, e52.

Raper, A.T., Stephenson, A.A., and Suo, Z. (2018). Functional Insights Revealed by the Kinetic Mechanism of CRISPR/Cas9. J. Am. Chem. Soc. *140*, 2971–2984.

Richardson, C.D., Ray, G.J., Bray, N.L., and Corn, J.E. (2016a). Non-homologous DNA increases gene disruption efficiency by altering DNA repair outcomes. Nat Commun *7*, 12463.

Richardson, C.D., Kazane, K.R., Feng, S.J., Zelin, E., Bray, N.L., Schafer, A.J., Floor, S.N., and Corn, J.E. (2018). CRISPR-Cas9 genome editing in human cells occurs via the Fanconi anemia pathway. Nat Genet *50*, 1132–1139.

Richardson, C.D., Ray, G.J., DeWitt, M.A., Curie, G.L., and Corn, J.E. (2016b). Enhancing homology-directed genome editing by catalytically active and inactive CRISPR-Cas9 using asymmetric donor DNA. Nat. Biotechnol. *34*, 339–344.

Robinson, C.R., and Sligar, S.G. (1998). Changes in solvation during DNA binding and cleavage are critical to altered specificity of the EcoRI endonuclease. Proc Natl Acad Sci U S A *95*, 2186–2191.

Romei, M.G., and Boxer, S.G. (2019). Split Green Fluorescent Proteins: Scope, Limitations, and Outlook. Annu Rev Biophys *48*, 19–44.

Roux, K.J., Kim, D.I., and Burke, B. (2013). BioID: a screen for protein-protein interactions. Curr Protoc Protein Sci *74*, Unit19.23.

Roux, K.J., Kim, D.I., Raida, M., and Burke, B. (2012). A promiscuous biotin ligase fusion protein identifies proximal and interacting proteins in mammalian cells. J Cell Biol *196*, 801–810.

Safina, A., Garcia, H., Commane, M., Guryanova, O., Degan, S., Kolesnikova, K., and Gurova, K.V. (2013). Complex mutual regulation of facilitates chromatin transcription (FACT) subunits on both mRNA and protein levels in human cells. Cell Cycle *12*, 2423–2434.

Saunders, A., Werner, J., Andrulis, E.D., Nakayama, T., Hirose, S., Reinberg, D., and Lis, J.T. (2003). Tracking FACT and the RNA polymerase II elongation complex through chromatin in vivo. Science *301*, 1094–1096.

Schmidtmann, E., Anton, T., Rombaut, P., Herzog, F., and Leonhardt, H. (2016). Determination of local chromatin composition by CasID. Nucleus *7*, 476–484.

Schopp, I.M., Amaya Ramirez, C.C., Debeljak, J., Kreibich, E., Skribbe, M., Wild, K., and Bethune, J. (2017). Split-BioID a conditional proteomics approach to monitor the composition of spatiotemporally defined protein complexes. Nat Commun *8*, 15690.

Semenova, E., Jore, M.M., Datsenko, K.A., Semenova, A., Westra, E.R., Wanner, B., van der Oost, J., Brouns, S.J.J., and Severinov, K. (2011). Interference by clustered regularly interspaced short palindromic repeat (CRISPR) RNA is governed by a seed sequence. Proc Natl Acad Sci U S A *108*, 10098–10103.

Shao, S., Zhang, W., Hu, H., Xue, B., Qin, J., Sun, C., Sun, Y., Wei, W., and Sun, Y. (2016). Long-term dual-color tracking of genomic loci by modified sgRNAs of the CRISPR/Cas9 system. Nucleic Acids Res *44*, e86.

Shibata, A., Moiani, D., Arvai, A.S., Perry, J., Harding, S.M., Genois, M.-M., Maity, R., van Rossum-Fikkert, S., Kertokalio, A., Romoli, F., et al. (2014). DNA double-strand break repair pathway choice is directed by distinct MRE11 nuclease activities. Mol Cell *53*, 7–18.

Shmakov, S., Abudayyeh, O.O., Makarova, K.S., Wolf, Y.I., Gootenberg, J.S., Semenova, E., Minakhin, L., Joung, J., Konermann, S., Severinov, K., et al. (2015). Discovery and Functional Characterization of Diverse Class 2 CRISPR-Cas Systems. Mol Cell *60*, 385–397.

Simeonov, D.R., Gowen, B.G., Boontanrart, M., Roth, T.L., Gagnon, J.D., Mumbach, M.R., Satpathy, A.T., Lee, Y., Bray, N.L., Chan, A.Y., et al. (2017). Discovery of stimulation-responsive immune enhancers with CRISPR activation. Nature *549*, 111–115.

Stark, J.M., and Jasin, M. (2003). Extensive loss of heterozygosity is suppressed during homologous repair of chromosomal breaks. Mol Cell Biol *23*, 733–743.

Sternberg, S.H., LaFrance, B., Kaplan, M., and Doudna, J.A. (2015). Conformational control of DNA target cleavage by CRISPR-Cas9. Nature *527*, 110–113.

Sternberg, S.H., Redding, S., Jinek, M., Greene, E.C., and Doudna, J.A. (2014). DNA interrogation by the CRISPR RNA-guided endonuclease Cas9. Nature *507*, 62–67.

Suzuki, K., Tsunekawa, Y., Hernandez-Benitez, R., Wu, J., Zhu, J., Kim, E.J., Hatanaka, F., Yamamoto, M., Araoka, T., Li, Z., et al. (2016). In vivo genome editing via CRISPR/Cas9 mediated homology-independent targeted integration. Nature *540*, 144–149.

Tsai, S.Q., Zheng, Z., Nguyen, N.T., Liebers, M., Topkar, V.V., Thapar, V., Wyvekens, N., Khayter, C., Iafrate, A.J., Le, L.P., et al. (2015). GUIDE-seq enables genome-wide profiling of off-target cleavage by CRISPR-Cas nucleases. Nat. Biotechnol. *33*, 187–197.

Uhlen, M., Fagerberg, L., Hallstrom, B.M., Lindskog, C., Oksvold, P., Mardinoglu, A., Sivertsson, A., Kampf, C., Sjostedt, E., Asplund, A., et al. (2015). Proteomics. Tissue-based map of the human proteome. Science *347*, 1260419.

Uusi-Makela, M.I.E., Barker, H.R., Bauerlein, C.A., Hakkinen, T., Nykter, M., and Ramet, M. (2018). Chromatin accessibility is associated with CRISPR-Cas9 efficiency in the zebrafish (Danio rerio). PLoS One *13*, e0196238.

Valieva, M.E., Armeev, G.A., Kudryashova, K.S., Gerasimova, N.S., Shaytan, A.K., Kulaeva, O.I., McCullough, L.L., Formosa, T., Georgiev, P.G., Kirpichnikov, M.P., et al. (2016). Large-scale ATP-independent nucleosome unfolding by a histone chaperone. Nat Struct Mol Biol *23*, 1111–1116.

Van, C., Yan, S., Michael, W.M., Waga, S., and Cimprich, K.A. (2010). Continued primer synthesis at stalled replication forks contributes to checkpoint activation. J Cell Biol *189*, 233–246.

Verkuijl, S.A., and Rots, M.G. (2019). The influence of eukaryotic chromatin state on CRISPR-Cas9 editing efficiencies. Curr Opin Biotechnol *55*, 68–73.

Waldrip, Z.J., Byrum, S.D., Storey, A.J., Gao, J., Byrd, A.K., Mackintosh, S.G., Wahls, W.P., Taverna, S.D., Raney, K.D., and Tackett, A.J. (2014). A CRISPR-based approach for proteomic analysis of a single genomic locus. Epigenetics *9*, 1207–1211.

Wang, H., Nakamura, M., Abbott, T.R., Zhao, D., Luo, K., Yu, C., Nguyen, C.M., Lo, A., Daley, T.P., La Russa, M., et al. (2019). CRISPR-mediated live imaging of genome editing and transcription. Science *365*, 1301–1305.

Wang, H., Xu, X., Nguyen, C.M., Liu, Y., Gao, Y., Lin, X., Daley, T., Kipniss, N.H., La Russa, M., and Qi, L.S. (2018). CRISPR-Mediated Programmable 3D Genome Positioning and Nuclear Organization. Cell *175*, 1405–1417.e1414.

Wang, Y.-H., Hariharan, A., Bastianello, G., Toyama, Y., Shivashankar, G.V., Foiani, M., and Sheetz, M.P. (2017). DNA damage causes rapid accumulation of phosphoinositides for ATR signaling. Nat Commun *8*, 2118.

Weaver, L.H., Kwon, K., Beckett, D., and Matthews, B.W. (2001). Corepressor-induced organization and assembly of the biotin repressor: a model for allosteric activation of a transcriptional regulator. Proc Natl Acad Sci U S A *98*, 6045–6050.

Wiedenheft, B., van Duijn, E., Bultema, J.B., Waghmare, S.P., Zhou, K., Barendregt, A., Westphal, W., Heck, A.J.R., Boekema, E.J., Dickman, M.J., et al. (2011). RNA-guided complex from a bacterial immune system enhances target recognition through seed sequence interactions. Proc Natl Acad Sci U S A *108*, 10092–10097.

Wienert, B., Nguyen, D.N., Guenther, A., Feng, S.J., Locke, M.N., Wyman, S.K., Shin, J., Kazane, K.R., Gregory, G.L., Carter, M.A.M., et al. (2020). Timed inhibition of CDC7 increases CRISPR-Cas9 mediated templated repair. Nat Commun *11*, 2109.

Winkler, D.D., and Luger, K. (2011). The histone chaperone FACT: structural insights and mechanisms for nucleosome reorganization. J Biol Chem *286*, 18369–18374.

Winkler, D.D., Muthurajan, U.M., Hieb, A.R., and Luger, K. (2011). Histone chaperone FACT coordinates nucleosome interaction through multiple synergistic binding events. J Biol Chem *286*, 41883–41892.

Wu, X., Scott, D.A., Kriz, A.J., Chiu, A.C., Hsu, P.D., Dadon, D.B., Cheng, A.W., Trevino, A.E., Konermann, S., Chen, S., et al. (2014). Genome-wide binding of the CRISPR endonuclease Cas9 in mammalian cells. Nat. Biotechnol. *32*, 670–676.

Wuhr, M., Freeman, R.M.J., Presler, M., Horb, M.E., Peshkin, L., Gygi, S., and Kirschner, M.W. (2014). Deep proteomics of the Xenopus laevis egg using an mRNA-derived reference database. Curr Biol *24*, 1467–1475.

Yarrington, R.M., Verma, S., Schwartz, S., Trautman, J.K., and Carroll, D. (2018). Nucleosomes inhibit target cleavage by CRISPR-Cas9 in vivo. Proc Natl Acad Sci U S A *115*, 9351–9358.

Yeh, C.D., Richardson, C.D., and Corn, J.E. (2019). Advances in genome editing through control of DNA repair pathways. Nat Cell Biol *21*, 1468–1478.

Yourik, P., Fuchs, R.T., Mabuchi, M., Curcuru, J.L., and Robb, G.B. (2019). Staphylococcus aureus Cas9 is a multiple-turnover enzyme. Rna *25*, 35–44.

Zhang, W., Zeng, F., Liu, Y., Shao, C., Li, S., Lv, H., Shi, Y., Niu, L., Teng, M., and Li, X. (2015). Crystal Structure of Human SSRP1 Middle Domain Reveals a Role in DNA Binding. Sci Rep *5*, 18688.

Zhu, Z., Chung, W.-H., Shim, E.Y., Lee, S.E., and Ira, G. (2008). Sgs1 helicase and two nucleases Dna2 and Exo1 resect DNA double-strand break ends. Cell *134*, 981–994.